NASA CONTRACTOR REPORT

NASA CR-1642

PRECIPITATION STRENGTHENED TANTALUM BASE ALLOYS

by R. W. Buckman, Jr., and R. C. Goodspeed

Prepared by
WESTINGHOUSE ASTRONUCLEAR LABORATORY
Pittsburgh, Pa. 15236
for Lewis Research Center

NATIONAL AERONAUTICS AND SPACE ADMINISTRATION • WASHINGTON, D. C. • MAY 1971

1. Report No.	2. Government Accession No.	3. Recipient's Catalog No.
NASA CR-1642		

4. Title and Subtitle	5. Report Date
PRECIPITATION STRENGTHENED TANTALUM BASE ALLOYS	May 1971
	6. Performing Organization Code
7. Author(s)	8. Performing Organization Report No.
R. W. Buckman, Jr., and R. C. Goodspeed	WANL-PR-(Q)-017
	10. Work Unit No.
9. Performing Organization Name and Address	
Westinghouse Astronuclear Laboratory Pittsburgh, Pennsylvania 15236	11. Contract or Grant No. NAS 3-2542
	13. Type of Report and Period Covered
12. Sponsoring Agency Name and Address	Contractor Report
National Aeronautics and Space Administration Washington, D. C. 20546	14. Sponsoring Agency Code

15. Supplementary Notes

16. Abstract

Precipitation strengthened tantalum base alloys were developed for application as sheet and tubing in Advanced Rankine Cycle Space Nuclear Power Systems. The Ta-W-Hf-C alloy system with additions of Re, Mo, Zr, and N was studied. Alloy compositions were selected to provide the best high temperature creep properties and still maintain good fabricating and welding characteristics. Screening studies were made on nonconsumable electrode melted ingots weighing $1\frac{3}{4}$ lb. and consumable electrode melted 2 inch diameter ingots weighing 7 lbs. All evaluations were made on 0.04 inch thick sheet. The results of the initial investigations led to the development of ASTAR-811C (Ta-8W-1Re-0.7Hf-0.025C) which exhibited creep strength at 2400° F approximately double that of T-111 (Ta-8W-2Hf). The ductility and fabricating characteristics of ASTAR-811C are similar to T-111. The ASTAR-811C composition was scaled up to 4 inch diameter ingot and processed to sheet and evaluated in detail. Short time tensile properties, recrystallization and grain growth behavior, weldability, and creep properties were determined.

17. Key Words (Suggested by Author(s))	18. Distribution Statement
Refractory metal alloys Tantalum Tantalum alloys Mechanical properties Welding Alloy development	Unclassified - unlimited

19. Security Classif. (of this report)	20. Security Classif. (of this page)	21. No. of Pages	22. Price*
Unclassified	Unclassified	190	$3.00

*For sale by the National Technical Information Service, Springfield, Virginia 22151

TABLE OF CONTENTS

LIST OF FIGURES (CONTINUED)

LIST OF FIGURES (CONTINUED)

LIST OF TABLES (CONTINUED)

I. INTRODUCTION

This report "Development of Precipitation Strengthened Tantalum Base Alloys" describes the work performed under Contract NAS 3-2542 during the period of June 19, 1963 to August 20, 1967. The prime objective of this work was the development of a tantalum base alloy(s) for use in advanced space nuclear power conversion systems which will operate in the 2000°F to 3000°F temperature range. The extended operational life, (> 10,000 hours) dictates resistance to creep deformation as the primary strength criterion. The principal shapes in which the alloy will be used are sheet and tubing, so in addition to creep resistance, good fabricating and welding characteristics are also essential.

The research program was conducted in two phases: Phase I, Screening Investigation, and Phase II, Scale-Up Investigation. Experimental investigations during the Phase I screening portion were conducted on compositions prepared by non-consumable and consumable electrode melting techniques. Non-consumable electrode melted ingots weighing 1-3/4 pounds and consumable electrode melted two inch diameter ingots weighing 7 pounds were prepared. The most promising compositions were then consumable electrode melted as 4 inch diameter ingots weighing 80 pounds during the Phase II scale-up portion of the investigation.

Alloy compositions were developed from the Ta-W-Hf-C system with minor additions and/or substitution of rhenium, molybdenum, zirconium and nitrogen. Experimental work was planned, using as a guide, theoretical models for dispersed phase strengthening that have been proposed for explaining creep deformation.

Because of the extensive amount of data generated during the performance of this work, a summary of the principal results and accomplishments are under a separate cover[1] and is recommended for those readers not vitally interested in all the experimental details.

II. PHASE I - SCREENING INVESTIGATION

A. EXPERIMENTAL PROGRAM

1. Background. Before discussing the design of the experimental program and the basis for selecting the Ta-W-Hf-C system for detailed investigation, some of the theoretical considerations involved in high temperature strengthening will be reviewed.

At approximately one-half the absolute melting temperature ($0.5\ T_M$) dislocation climb becomes the rate controlling deformation mechanism in creep. In pure metals, where self-diffusion occurs by a vacancy mechanism, the activation energy for creep should be equal to the activation energy for self-diffusion. It has been shown experimentally for pure metals that the activation energy for self-diffusion is approximately equal to that for creep above one-half the absolute melting temperature.[2,3] Creep strength is thus strongly controlled by atomic diffusion processes, hence the matrix element strongly limits strength improvements to be achieved by alloying.

Recently Sherby [4] reviewed high temperature creep data for pure metals to quantitatively assess factors which promote high temperature creep resistance. Sherby concluded that high temperature strength is favored by (1) high elastic modulus; (2) favorable crystal structure, the best being the diamond cubic followed in order by the close packed fcc and hcp structures with bcc being the poorest; (3) high melting temperature; (4) valence, the larger the number of bonding electrons the slower the diffusion rate, hence dislocation climb is decreased.

Obviously with any given base element the above factors are fixed. However, alloying elements should be selected which would tend to increase the elastic modulus, melting point, and/or electron to atom ratio. Changing the crystal structure of tantalum to fcc or hcp is obviously not feasible. Grain size is an additional factor which also appears to exert a significant effect on high temperature creep, but a complete understanding is not

yet available. There is, however, evidence to indicate that an optimum grain size for maximum creep strength exists.[5]

In recent years considerable research has been devoted to understanding the role of stable precipitates and the high temperature creep strength of materials. Attempts to duplicate the excellent high temperature strength characteristics of SAP and other alloy systems have provided much of the impetus for this work. Although a number of theoretical treatments of dispersion strengthening have been published, no completely satisfactory theory is available at present. Weertman[6] and Ansell[7] have developed a theory of dispersion strengthened alloys which appears to agree fairly well with experimental results. This treatment shows that the only property of either the matrix or the dispersed phase which significantly affects creep rate at all stress levels is the coefficient of self diffusion of the matrix. Also this treatment shows that the creep rate is inversely proportional to the cube of the shear modulus at high stresses. In addition, it can be shown that the stress level which separates the low stress behavior from the high stress behavior is directly proportional to the shear modulus of the matrix. Since the stress level defines the transition between the creep rate which is proportional to the applied stress and one which is proportional to some power of the applied stress, the importance of having a high matrix shear modulus is clearly shown. At high stresses the creep rate is proportional to the square of the dispersion spacing while it is independent of interparticle spacing at low stress levels. Thus, the interparticle spacing should be as small as possible. At low stress levels, the creep rate is inversely proportional to the square of the height of the particles. At high stress levels, the creep rate is inversely proportional to the height of the particle. These considerations of dispersed phase morphology indicate that acicular precipitates are most favorable for creep resistance.

Although there is no theory at present which permits an explicit quantitative prediction of compositions which have optimum creep strength, the main factors which influence strength characteristics may be delineated. It is implicit in the discussion of dispersed phase strengthening that precipitates which are stable at the temperature of operation are required. Furthermore, it seems apparent that understanding of the factors which control

dispersed phase morphology provides the most fruitful approach to achieving alloys with the desired properties.

Unfortunately the resistance to low temperature fracture is decreased by some of the same factors which enhance elevated temperature strength. Thus it is obvious that trade-offs in creep resistance are necessary to obtain adequate ductility for fabrication purposes.

B. EXPERIMENTAL DESIGN

The solid solution strengthened Ta-W-Hf system has been surveyed by various investigators and portions of the system have been studied in some detail.[8, 9, 10, 11] Ammon and Begley [12] have shown that the temperature at which weldments undergo transition from ductile to brittle behavior is sensitive to the W/Hf ratio. For W/Hf ratios of 1.3 to 6.0 at a tungsten plus hafnium content of 14% a minimum in the weld bend ductile-brittle transition temperature for weldments prepared by the GTA (tungsten-inert gas arc) technique was shown to occur at a W/Hf ratio of 4.

Previous work on columbium alloys [13], and to a lesser extent on tantalum alloys [14] has demonstrated the effectiveness of transition metal carbides and nitrides as dispersed phase strengtheners. The high melting points of hafnium and zirconium carbides and nitrides are indicative of high bonding strengths and consequently of a high modulus. Also, the free energy data tend to indicate that the compounds are thermodynamically stable with respect to the tantalum matrix. (See Table 1). Since carbides and nitrides exhibit a solubility relationship with the tantalum alloy matrix, precipitate morphology will be affected by thermal-mechanical treatment. Observations by Chang [14, 18] and Begley, Ammon, and Stickler [19] have indicated that precipitates are much smaller when they nucleate on dislocations and are usually more effective strengtheners. In many refractory alloy metal systems, classical precipitation strengthening has not been observed, thus a solution anneal followed by an aging treatment does not give rise to pronounced precipitation hardening effects. One exception to this is the Cb-Hf-N system, reported by Begley et al [13], which was shown to exhibit

TABLE 1 - PHYSICAL PROPERTIES OF NITRIDES AND CARBIDES[15,16,17]

Compounds	Melting Point °K	$\Delta H(298^{\circ}K)$ (kcal/mole)
HfC	4170	-47.5
ZrC	3680	-47.6
TaC	4270	-38.5
WC	2990	- 8.4
MoC	2850	- 3.8
HfN	3580	-88.2
ZrN	3255	-87.3
TaN	3360	-60.0
HfO_2	3090	-268.4
ZrO_2	2970	-263.0

classical age hardening behavior.

Alloy compositions for the initial screening investigation were based on the Ta-W-Hf-C system with partial substitution of molybdenum and rhenium for tungsten, zirconium for hafnium, and nitrogen for carbon. Previous investigations[8, 9, 10, 11] have shown that the Ta-W-Hf system affords enhancement of the elevated temperature strength of tantalum without appreciably degrading the fabricating and welding characteristics of tantalum. While it was not expected that molybdenum would be as effective an addition for creep resistance as tungsten, the level of solute addition may effect the carbide-nitride solubility relationships and/or interfacial energy between the precipitate and matrix which in turn may exert pronounced effects on precipitate morphology and hence pronounced effects on resulting creep properties. A survey of portions of the Ta-W-Hf-C system not investigated previously, was conducted using non-consumable electrode melted ingots weighing 3/4 pound. The button ingots were used primarily to delineate effects of gross compositional variations on the fabricating, welding, and strength characteristics. More detailed studies were conducted on material prepared as two-inch diameter ingots weighing seven pounds. All evaluations were conducted on 0.04 inch thick sheet material. The tantalum alloy T-111 (Ta-8W-2Hf) was used as the baseline reference standard throughout this study.

C. EXPERIMENTAL PROCEDURES

1. Starting Material. Tantalum and Ta-10W with a purity equivalent to double electron beam melted material was used as the alloy base. Substitutional alloy additions were of the highest purity commercially available. Interstitial carbon additions for non-consumable electrode melts were made with tantalum-carbide powder and to the consumable electrode melts with graphite cloth. Nitrogen additions were made to non-consumable and consumable melts as a Ta-N master alloy and nitrided tantalum strip respectively. Vendor analysis, shape, and form for all starting materials used are listed in Table 2.

TABLE 2 - VENDOR ANALYSIS OF STARTING MATERIAL

Material	Supplier	Form	Analysis, ppm											
			C	O	N	Cb	Fe	Si	Mo	Zr	Ti	Hf	Re	W
Ta	Wah-Chang	Plate	<30	60	25	130	<15	20	10	--	14	--	--	585
Ta	Wah-Chang	Plate	<30	<50	26	412	<15	<20	<10	70	11	Hf --	--	385
Ta-10W	NRC	Plate	36	15	28	<100	5	<100	20	--	<10	--	--	9.8%
Ta-10W	Fansteel	Plate	10	10	10	<500	40	<10	150	--	<10	--	--	9.95%
Hafnium	Carborundum	Plate	80	100	16	--	40	--	--	2.1%	--	--	--	--
Zirconium	Carborundum	Sheet	100	--	20	--	--	--	--	--	--	68	--	--
Tungsten	Fansteel	Strip	--	--	--	--	--	--	--	--	--	--	--	99.95%
Molybdenum	Rembar	Strip	--	--	--	--	--	--	99.96%*	--	--	--	--	--
Rhenium	Rembar	Strip	--	--	--	--	--	--	--	--	--	--	99.99%	--
Graphite	National Carbon	Cloth	99.9%*	--	--	--	--	--	--	--	--	--	--	--
Tantalum Carbide	Kennametal	-100, -200 mesh powder	6.12%	--	--	--	--	--	--	--	--	--	--	--

*Specification minimum

2. Melting. Non-consumable electrode d-c arc melted compositions were prepared as button ingots in a six station water cooled copper crucible hearth furnace.[8] Prior to melting, the system was evacuated to less than 1×10^{-5} torr and backfilled to a pressure of 1/2 atmosphere with high purity argon containing less than 5 ppm total active impurities. Each button was multiple melted to insure a homogeneous product. The final button size was approximately 3 inches in diameter by 1/2 inch thick, weighing 1-3/4 pounds.

The consumable electrode melted compositions were prepared by double vacuum arc melting using a.c. power. The final ingots were 2 inches in diameter and weighed seven (7) pounds. During consumable electrode melting, pressure in the chamber did not normally rise above 5×10^{-4} torr. The electrodes for consumable melting were prepared using the sandwich construction technique.[9] First melt electrodes were assembled by stacking 1/2 inch wide x 45 inch long strips of each elemental alloy addition of appropriate thickness to give the desired composition. Carbon was added to the electrode in the form of graphite cloth wrapped in tantalum foil and nitrogen by means of nitrided tantalum strip. The assembled composite electrode was then tack welded at 4 inch intervals along its length to hold the alloy additions in place. First melts were made into a 1.4 inch diameter water cooled copper mold. The 1.4 inch diameter ingot was then remelted into a 2 inch diameter mold.

The compositions listed in Appendix I were melted by the above described techniques. Compositions designated with a prefix "NAS" were non-consumable electrode melted and those designated by "NASV" were consumable electrode melted. Chemical analysis results on the as-cast ingots, also tabulated in Appendix I, (Tables 1-3 and 1-4) verified the precise control over the intended level of the substitutional and interstitial additions. Also, the absence of a significant change in the oxygen content from the level present in the starting materials verifies the purity of the melting atmosphere.

3. Primary and Secondary Working. The as-cast ingots were processed to 0.04 inch sheet by the schedule outlined in Figure 1. Primary breakdown was accomplished on a Dynapak Model 1220C, a high energy rate metal working machine. Prior to working the

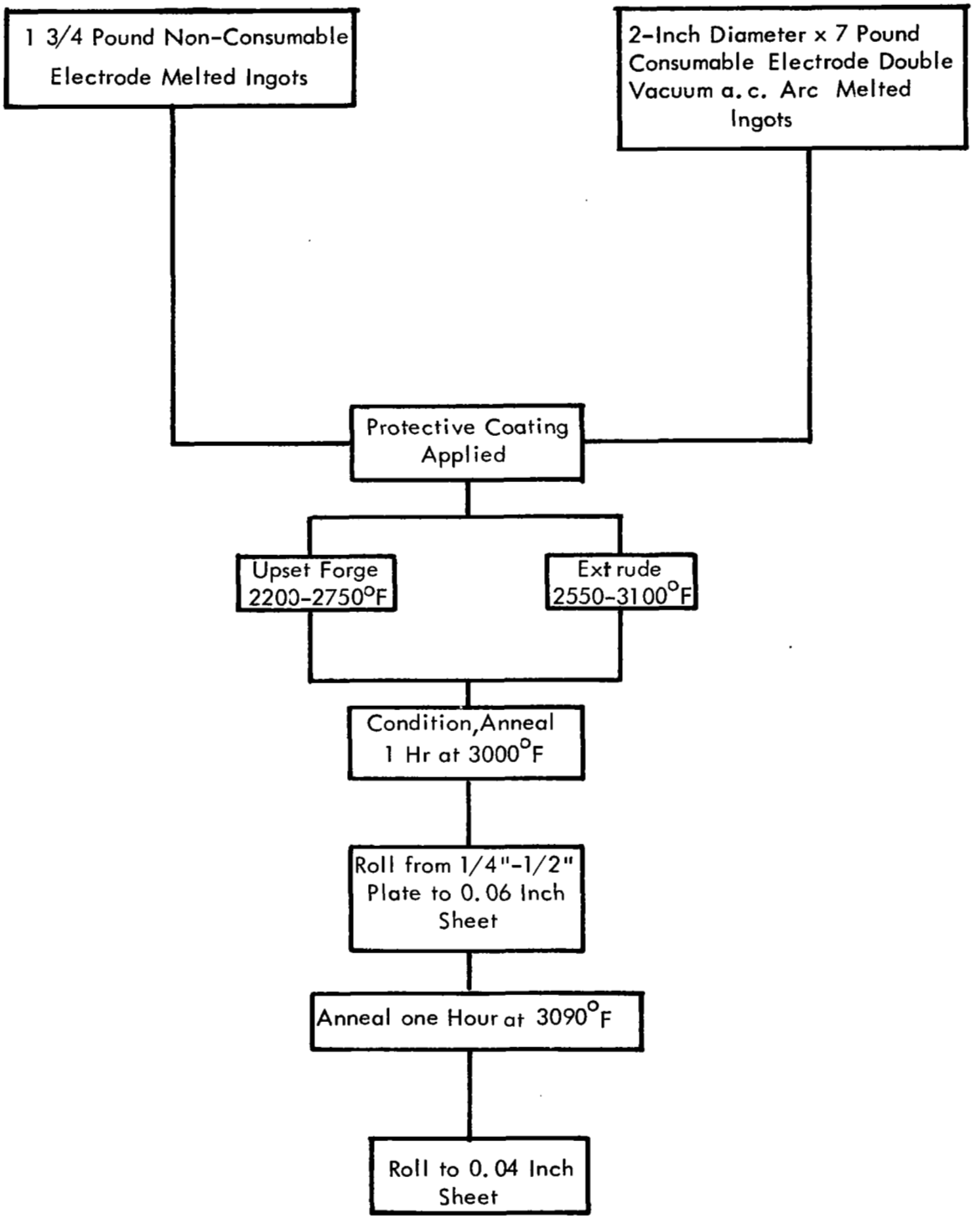

FIGURE 1 - Schedule for Processing of Developmental Tantalum Alloys to Sheet

as-cast ingot structure, the billets were coated to provide protection from environmental contamination during the hot cooling operation. The coatings used were either Al-12Si applied by hot dipping (See Appendix II), or unalloyed molybdenum applied by plasma spraying which also provided lubrication during extrusion. To further minimize the possibility of contamination, heating to the working temperature was under an argon atmosphere. The billets were heated by induction.

Rolling to sheet was done on a laboratory size Stanat 8 inch x 8 inch, two high-four high combination rolling mill. Initial rolling of the sheet bar was done at 800°F. Rolling below 1/8 inch thickness was done at room temperature. If high quality sheet could be processed by this schedule, it was considered highly probable that tubing could be produced using the existing tubing production technology.

4. Heat Treatment. All intermediate and final 1 hour annealing operations were conducted using a split tantalum tube resistance heated cold wall furnace at a pressure of $<1 \times 10^{-5}$ torr. Prior to annealing, the material was chemically cleaned and wrapped with 0.002 inch tantalum foil.

5. Welding. Alloy compositions processed to 0.04 inch sheet were welded by both automatic tungsten arc-inert gas (GTA) welding and electron beam welding techniques. Automatic tungsten arc inert gas welding was performed in a vacuum purged welding chamber equipped with a system which continuously monitors the oxygen and water vapor content in the welding atmosphere.[20]

All GTA welding was accomplished in a high purity helium atmosphere which as backfilled contained typically less than 1 ppm total active impurities. Welding was continued until either of the continuously monitored impurities (O_2 or H_2O) exceeded 5 ppm at which time the weld chamber was re-evacuated and re-backfilled.

The welding specimen, nominally 1/2 inch wide x 5 inches long x 0.04 inch thick, was clamped in a stainless steel fixture using molybdenum bar clamps. All welds were bead-on-plates with 100% penetration to simulate butt welding. Parameters which gave 100% penetration on the 0.04 inch sheet were as follows:

Welding Current	100 amps
Welding Speec	15 in/min
Arc Gap	0.06 inches
Jaw Spacing	3/8 inch
Electrode Diameter	3/32 inch

Electron beam welding was accomplished using a 2 KVA Zeiss electron beam welder. Bead-on plate welds with a 100% penetration were also required. A welding speed of 25 inches per minute with a 0.025 inch transverse deflection of the beam was used for welding the 1/2 inch wide x 5 inch long x 0.04 inch thick specimens. Welding was done after evacuation of the chamber to less than 5×10^{-6} torr.

6. Mechanical Property Evaluation. Mechanical property evaluation of the experimental alloy compsoitions was done according to the schedule shown in Figure 2 for sheet produced from non-consumable electrode melted ingots and Figure 3 for sheet produced from consumable electrode melted ingots. Test procedures when applicable conformed to those recommended by the Materials Advisory Board.[21,22]

a. Bend Test. The ductile-brittle transition behavior in bending was determined on base metal and on GTA and EB welded specimens. Bend test specimens were nominally 1/2 inch wide x 1 inch long x 0.04 inch thick. Specimens were supported on a 0.6 inch wide span and loaded at a one inch per minute deflection rate using a punch with a nose ratio of 0.07/inches. (bend factor 1.8t). The ductile brittle transition temperature was defined as the lowest temperature at which a full 90° bend could be made without evidence of brittle failure. No special pre-test surface preparation was performed on the bend specimens. Base metal specimens were tested in the as-annealed condition and the welded specimens in the as-welded condition with the top of the weld bead the tension side of the bend.

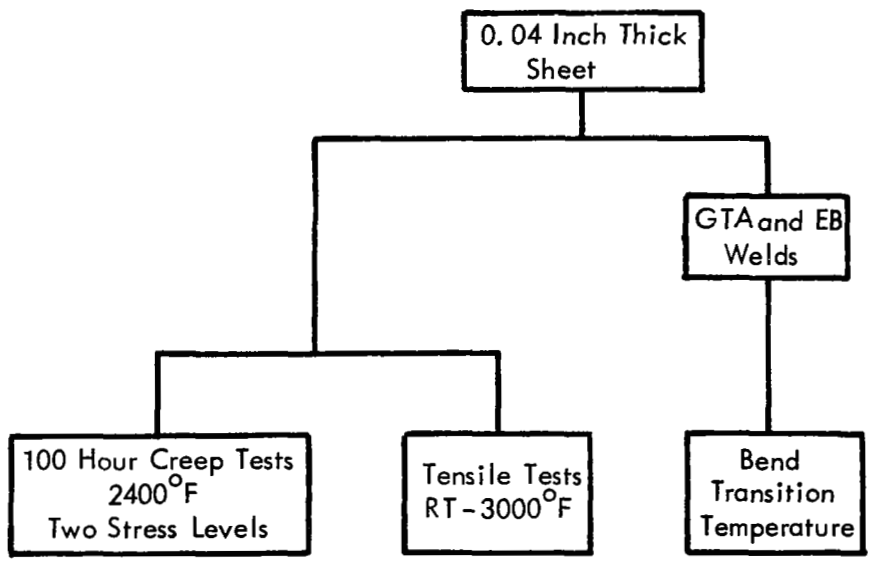

FIGURE 2 - Test Schedule for 0. 04 Inch Sheet Processed From Non-Consumable Electrode Melted Ingot

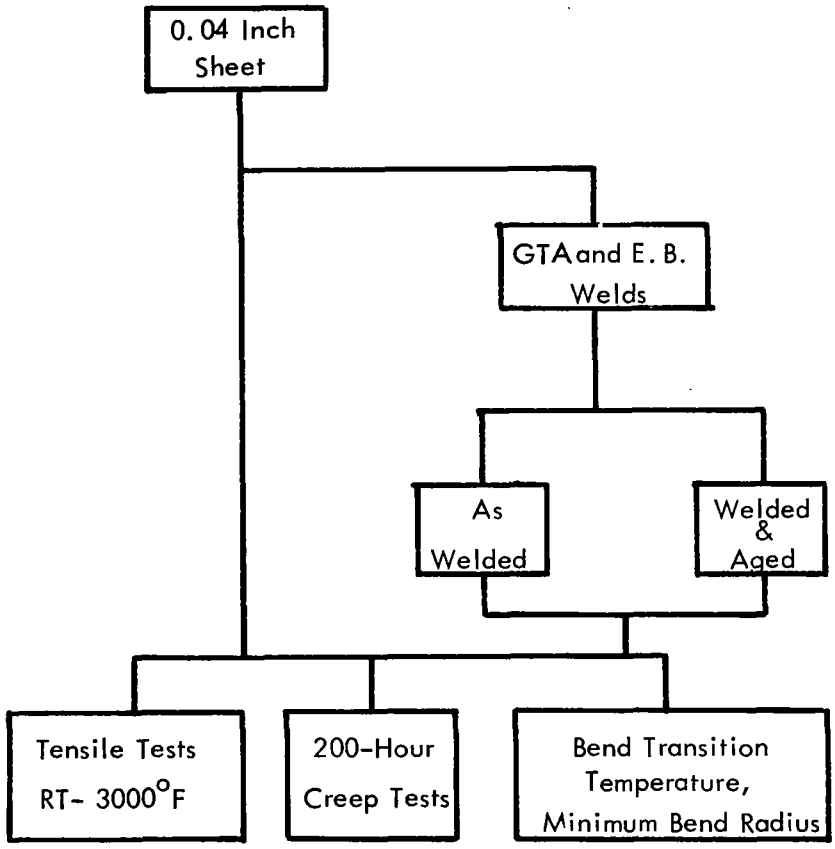

FIGURE 3 - Test Schedule for 0.04 Inch Sheet Processed from Consumable Electrode Double Vacuum Arc Melted Ingots

The weld bead was perpendicular to the bend axis, thus the fusion zone, heat affected zone, and adjacent base metal were strained an equivalent amount during bending. Test temperatures from -320F to room temperature were obtained by a controlled flow of liquid nitrogen into a cryostat. A small resistance heated furnace surrounding the bend test fixture was used for heating specimens for tests above room temperature. A thermocouple located in the nose of the punch was used to monitor and control the test temperature.

(b) Tensile Test. Tensile tests were conducted on 0.04 inch thick sheet metal specimens having a reduced section of 0.250 inches wide x 1 inch long. The strain rate was 0.05 inches per minute based on machine cross head motion. Elevated temperature tests were conducted at a pressure of $\leq 1 \times 10^{-5}$ torr. The gauge length of the test specimen was wrapped with tantalum foil to minimize contamination during test.

(c) Creep Tests. All creep testing was conducted in sputter ion pumped ultra-high vacuum creep systems of the type described by Buckman and Hetherington.[23] These units are similar in operation to those in use at TRW [24] and NASA Lewis Research Center.[25] The ultra low pressures ($< 1 \times 10^{-8}$ torr) obtained in these test systems is required to prevent test environment interactions. For at 10^{-6} torr, there is sufficient interaction of the residual oxygen and carbon with the reactive metal containing tantalum alloys to cause generation of spurrious test results.[26, 27, 28]

D. EXPERIMENTAL RESULTS

Tantalum alloy compositions within the Ta-W-Hf-C system were prepared within the compositional range of 3-15% W, 0.5-4% Hf, and 0.02 - 0.3%C. The effect of substitution of up to 1.5% rhenium and 0.85% molybdenum for tungsten, 0.5% zirconium for hafnium, and 0.08% nitrogen for carbon were studied using the following four base compositions.

Ta-8.6W - 0.53 Hf - 0.02C

Ta-8.6W - 0.53 Hf - 0.035C

Ta-8.2W - 1Hf - 0.035C

Ta-8.2W - 1Hf - 0.07C

Although all percentage values are given normally in terms of weight percent, solute substitutions were made on an equivalent atom percent basis. The atomic weight of Ta, W and Hf, are very similar, thus the value for atomic percent and weight percent are essentially identical. The atom percent values for Zr and Mo in the tantalum alloys are approximately twice the weight percent values while those for carbon and nitrogen are approximately 14 times the weight percent value.

Since sheet and tubing are the primary end products for which the alloys were being developed, evaluation criteria were based on (1) fabricability, (2) weldability, (3) creep resistance, and (4) liquid alkali metal corrosion resistance. Although the reactive metal solid solution additions of hafnium and zirconium would not necessarily make a positive contribution to the creep strength of tantalum based on diffusivity and moduli considerations, the reactive metal additions are nonetheless required for liquid alkali metal corrosion resistance. They would however contribute to the creep strength by providing dispersions of oxides, nitrides and/or carbides. Although liquid alkali metal corrosion resistance was not included in this investigation, sufficient prior work has been done to approximate the limits of reactive metal additions needed to impart corrosion resistance to the tantalum alloy matrix.[29,30]

1. Primary Working. Primary working of the as-cast ingot structure was accomplished by forging and/or extrusion. Forging billets were coated with an Al-12Si alloy applied by hot dipping (See Appendix II). The billets were reduced 50% in thickness by a single blow on the Dynapak. The initial thickness of the non-consumable electrode melted forging billets was 1/2 inch and 1 inch for the consumable electrode melted ingots. Forgeability was judged satisfactory if the billet could withstand the 50% upset without severe edge cracking. Compositions with an as-cast hardness in excess of 300 DPH were heated to 2700°F for forging and those with a hardness less than 300 DPH were heated to 2200-2300°F.

From the wide range of experimental compositions melted, it was evident that tantalum could withstand relatively large additions of both solute and interstitial elements before primary working characteristics were impaired.

(a) Forgeability - Ta-W-Hf-C. The combined effect of carbon and substitutional solutes tungsten and hafnium on the as-cast hardness is illustrated in Figure 4. The dashed line approximates the composition limit beyond which forgeability was impaired, being defined as the onset of edge cracking. The degradation in forgeability could be related to the as-cast microstructures* as shown in Figures 5 and 6. The solubility of carbon in tantalum at 2900°F is very low (less than 100 ppm at 2900°F)[31,32] resulting in the formation of a hard second phase dispersed in a highly ductile matrix. However, as the carbon content is increased the distribution of the carbide phase changes from a random discontinuous to a continuous grain boundary carbide phase. The carbon level at which the continuous carbide phase formed decreased as the W+Hf content was increased. Thus as long as the carbide phase was discontinuous, upset forgeability was satisfactory. At tungsten plus hafnium levels in excess of 12% and carbon levels 0.1%, a sub-boundary network decorated with a continuous carbide phase was observed. As-cast ingots exhibiting this characteristic microstructure had very poor forgeability.

(b) Substitution of N, Re, Mo, and Zr. Substitution of nitrogen for carbon results in degradation of forgeability as the nitrogen level is increased above 400 ppm. Whereas carbon exhibits a very low solubility in the tantalum alloy matrix and dispersed carbide phases are present at carbon contents below 100 ppm, nitrogen has a high solubility and the as-cast microstructure of compositions containing up to 800 ppm nitrogen were single phase. Unalloyed tantalum has a very high solubility for nitrogen,[33,34] 0.58% at 2900°F and 0.44% at 2200°F. However, it will be shown later that the alloy additions have sharply reduced the nitrogen solubility in the tantalum alloy matrix and that the observance of a single phase microstructure in the high nitrogen containing alloys is a result of the sluggishness of the nitride precipitation reaction. Nitrogen in solution is a potent low temperature strengthener of the tantalum alloy matrix as shown in Figure 7. If the nitrogen were in the alloy matrix in interstitial solid solution, there would be little contribution to strength at the forging temperature.[35] Thus,

---

*Additional details and description of all metallographic procedures are listed in Appendix IV.

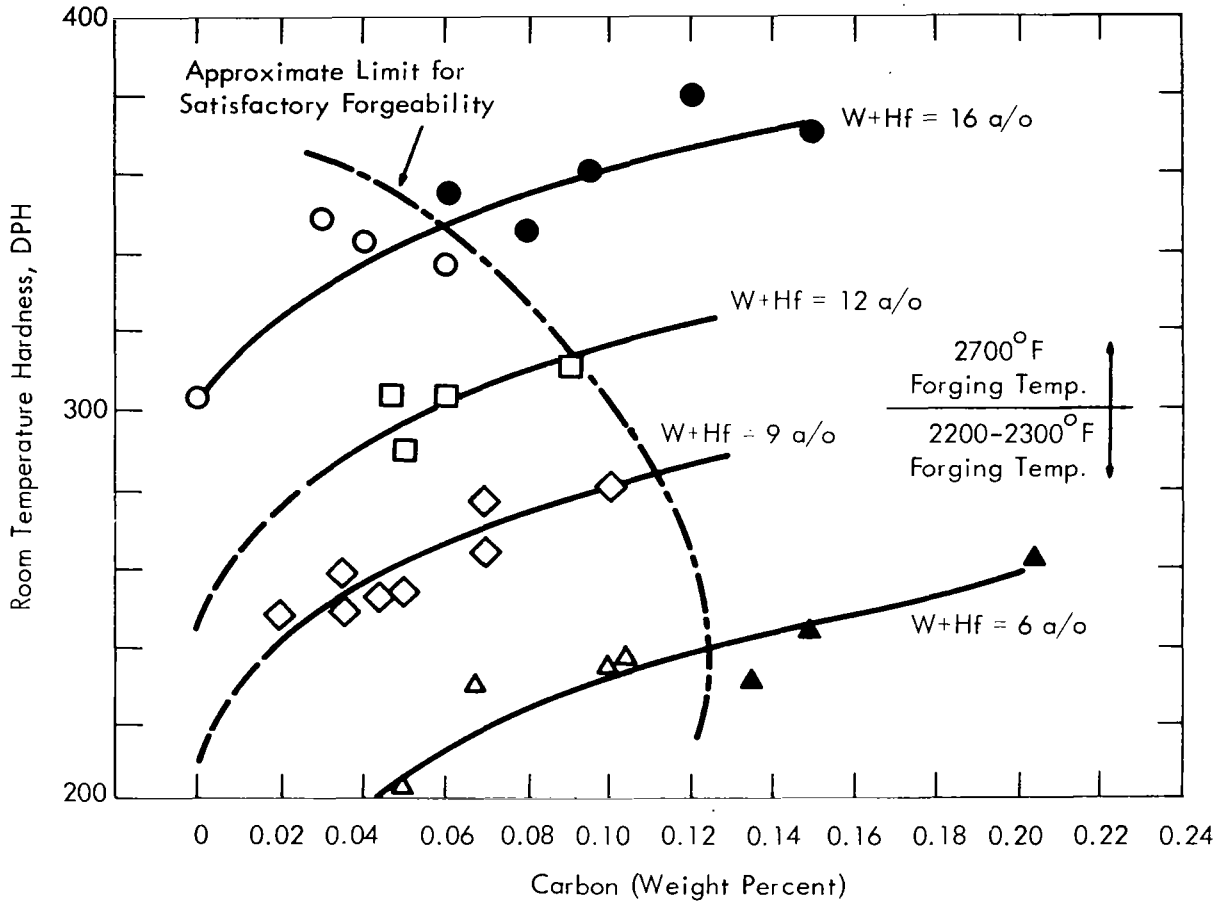

FIGURE 4 - Effect of Carbon on the As-Cast Hardness of Ta-W-Hf Compositions (Open Symbols - Good Forgeability; Closed Symbols - Poor Forgeability)

AS-CAST MICROSTRUCTURE

AS-FORGED INGOT

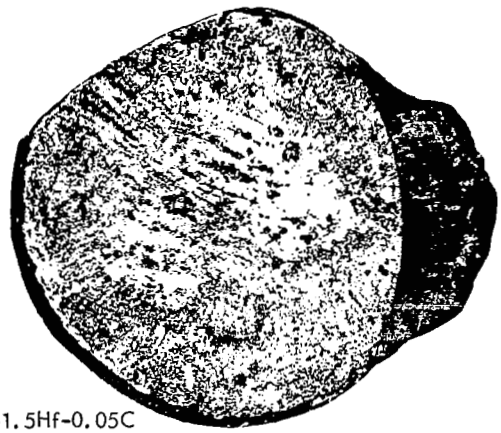

(a) Ta-4.6W-1.5Hf-0.05C

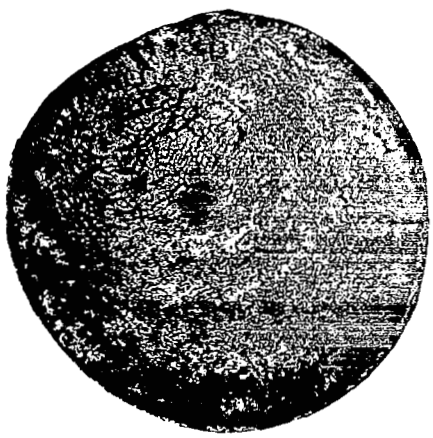

(b) Ta-4.6W-1.5Hf-0.10C

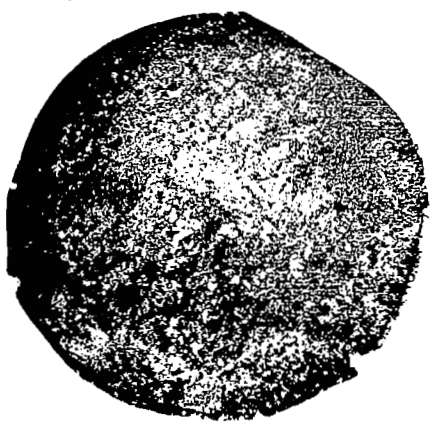

(c) Ta-4.6W-1.5Hf-0.15C

FIGURE 5 - Effect of As-Cast Microstructure on the Forgeability of Ta-W-Hf-C Alloys
Etchant HF-HNO_3 - Glycerine
Mag. = 250X

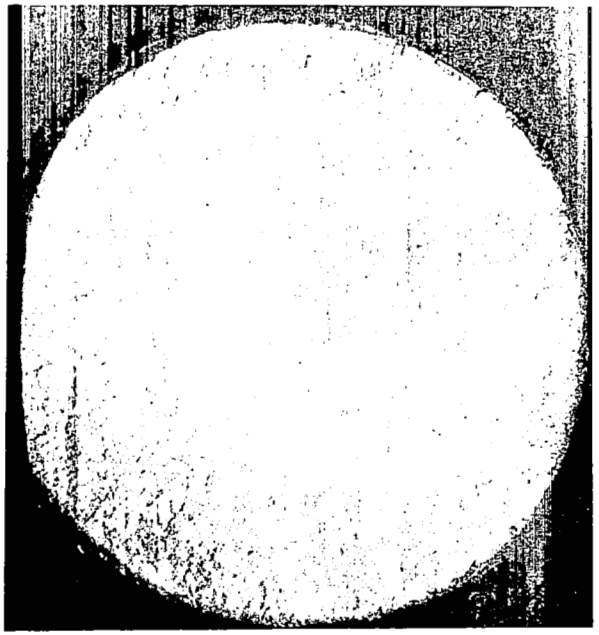

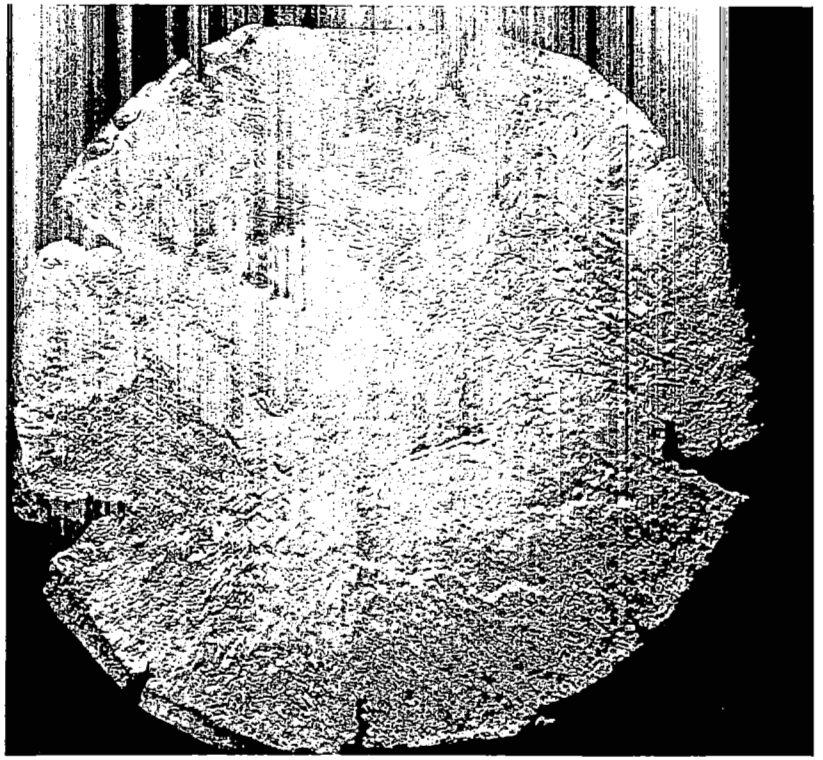

Ta-8. 2W-1Hf-0. 07C

Ta-14. 6W-1. 8Hf-0. 12C

FIGURE 6 - Effect of As-Cast Microstructure on Forgeability, Mag. 250X

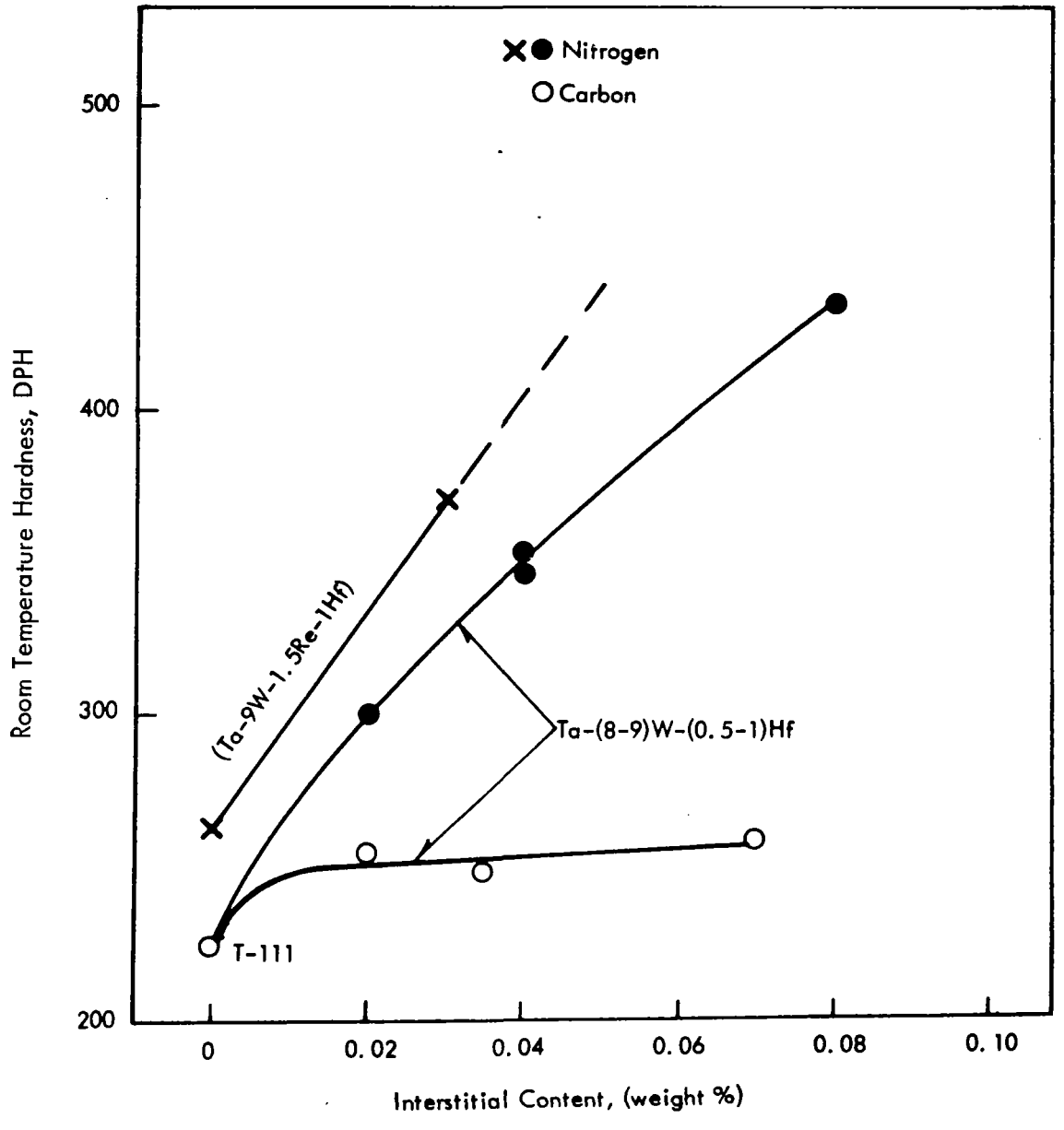

FIGURE 7 - Effect of Carbon and Nitrogen on the Room Temperature Hardness of As-Cast Tantalum Alloys

the marginal forgeability characteristics of the 800 ppm containing alloys were not anticipated. A majority of the forgeability evaluation data were taken on non-consumable electrode melted ingots and due to (1) the poor shape of the as-melted ingot and (2) microstructural and compositional heterogeneity intrinsic to non-consumable melted ingots forgeability characteristics are somewhat poorer than for identical compositions prepared by the consumable electrode melting process.

The level of Zr, Mo, and Re additions investigated had no apparent effect on forgeability. Although rhenium at levels greater than 2 atom percent in tantalum is reported to be about three times more effective in increasing the yield strength as tungsten,[36] compositions containing up to 3% rhenium at a total solute level of 10% exhibited excellent primary working characteristics.

(c) Extrusion. Excellent extrudeability was exhibited by the consumable electrode melted two inch diameter ingots. Extrusion billets, coated with unalloyed molybdenum by plasma spraying, were extruded to sheet bar nominally 1/2 inch thick x 1/2 inch wide. (A reduction of 4:1). Billets were heated by induction to the extrusion temperature of 2550°F under a flowing argon atmosphere. Transfer time from the heating coil to the extrusion container was less than 10 seconds. Typical examples of as-extruded sheet bars are shown in Figure 8.

2. Secondary Working. The as-forged sheet slabs were conditioned, inspected, annealed for 1 hour at 3000°F and then rolled to 0.06 inch thick sheet. From the starting thickness to 0.125 inch, the sheet slab was heated to 800°F for rolling. Rolling from 0.125 inch to 0.06 inch was done at room temperature. This process schedule was selected so that compositions which could be rolled to sheet per this schedule would most likely be readily fabricated to tubing.

Generally, the same trends observed for the primary fabricability were applicable

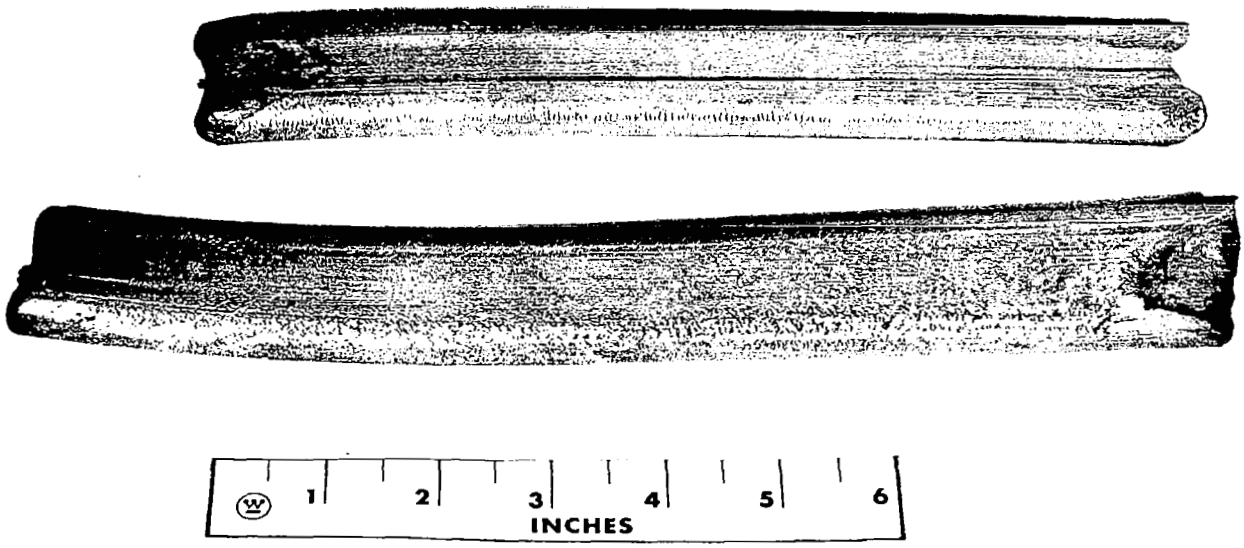

FIGURE 8 - As-Dynapak Extruded Tantalum Alloy Sheet Bar

to secondary working, although as expected, the lower secondary working temperature resulted in a decrease of fabricability at lower total solute levels. Presented in Figure 9 are the approximate compositional limits within the Ta-W-Hf-C system which produced good quality strip. The highly fabricable tantalum base alloy T-111 (Ta-8W-2Hf) was used as the basis for comparison.

The Mo, Re, and Zr substitutions for the W and Hf at the solute level investigated (W+Hf = 9 a/o) did not significantly alter secondary working characteristics. However, nitrogen had a very deleterious effect on sheet rolling characteristics at levels above 400 ppm. At the 200 ppm nitrogen level, tantalum containing 9 a/o (W+Re+Mo+Hf+Zr) exhibited excellent secondary working characteristics at room temperature.

3. Fabricability. Experimental compositions exhibiting marginal fabricating characteristics were readily identified during the primary and secondary working operations. However, the changes in ductile-brittle transition temperature (DBTT) caused by fusion welding was used as a more sensitive fabricability index. Thus those compositions which exhibited the least change in DBTT after fusion welding were rated as having the better fabricability.

As described in the previous section, tantalum alloys can withstand rather large carbon additions before primary and secondary working characterisitcs are severely degraded. Typical examples of Ta-W-Hf-C alloy sheet exhibiting good bend ductility are:

Ta - 8 W - 2Hf (T-111)
Ta- 8 W - 2Hf- 0.05C
Ta - 8 W - 3.15 Hf - 0.1C
Ta - 8 W - 2.7 Hf - 0. 4 Zr - 0.05C
Ta - 9.6W - 3.15 Hf - 0.05C

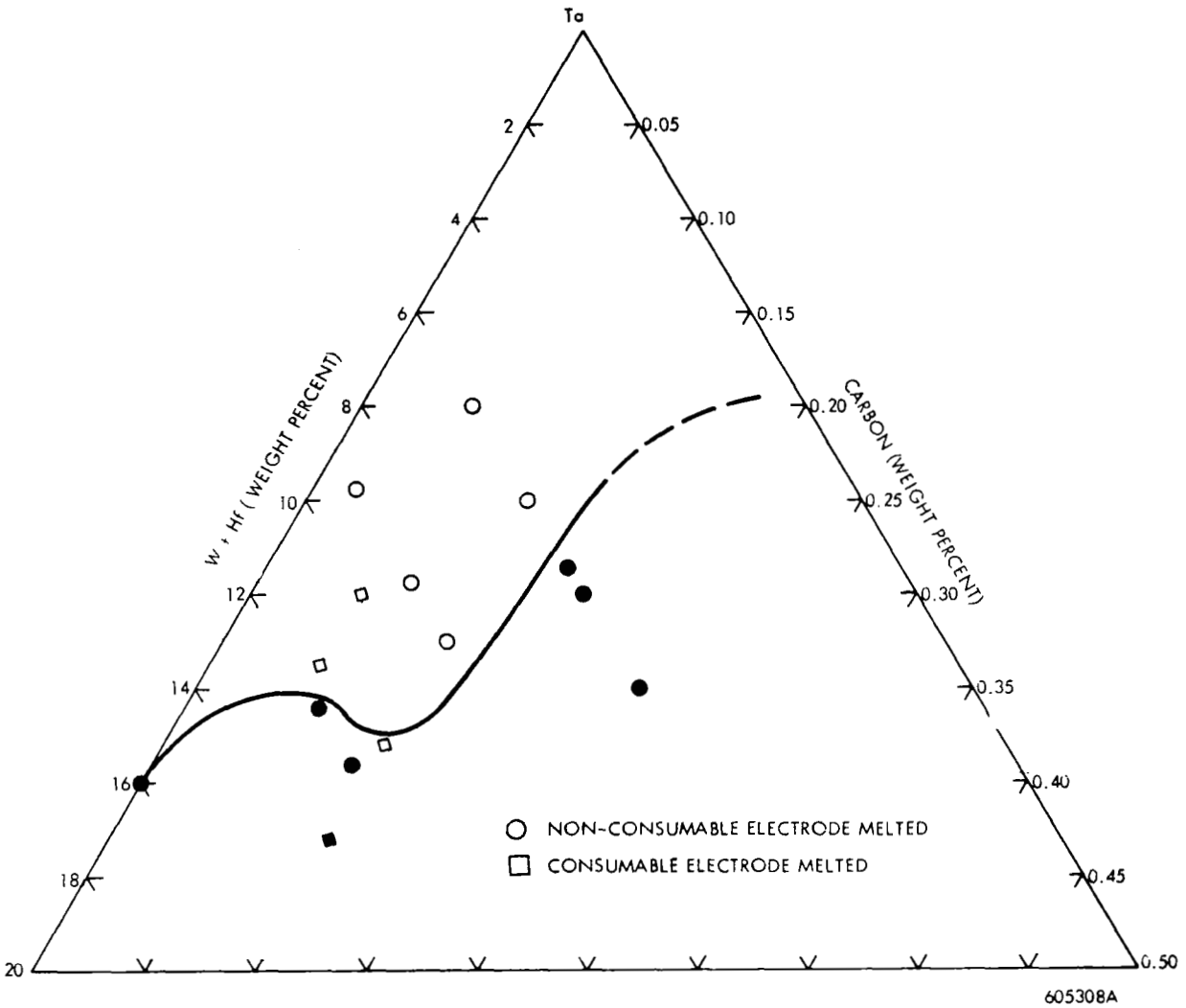

FIGURE 9 - Effect of W, Hf, and C on the Secondary Working Characteristics of Tantalum (Open Symbols Denote Good Quality Strip. Close Symbols Denote Strip Exhibiting Moderate to Severe Edge Cracking.)

The minimum bend radius at room temperature for all these alloys in 0.04 inch sheet, annealed 1 hour at 3000°F prior to test was 0t. i.e., the sample could be bent back on itself without failure. The DBTT temperature for the annealed sheet was less than -320°F. The sheet material 0.04 inch thick could be bent at -320°F over a punch with a radius of 0.071 inch (bend factor 1.8 t) without evidence of failure. Tests were performed on specimens with the bend axis parallel and perpendicular to the rolling direction.

After GTA welding though, there was an increase in the bend ductile-brittle transition temperature as shown in the data plotted in Figures 10 and 11. T-111, the baseline standard exhibited a DBTT <-320°F in both recrystallized base metal and as-GTA welded, thus illustrating its high degree of fabricability. The addition of carbon though results in a significant increase in the ductile-brittle transition temperature. At a W+Hf content of 9-10%, a carbon addition of 400 ppm raises the DBTT to approximately room temperature. The rate of increase of the as-GTA welded bend DBTT is less as the W+Hf content is reduced (See Figure 11).

Metallographic examination of transverse sections of weldments revealed essentially a single phase fusion and adjacent heat affected zone (See Figure 12). Also shown in Figure 12 is the typical microstructure of the base metal after annealing 1 hour at 3000°F. Thus during the welding cycle, the carbides are dissolved and the carbon is retained in solid solution. The hardness traverse data shown in Table 3 confirm that carbon was taken into solution and retained during welding. Thus the rapid increase in DBTT should be expected. However, by an appropriate post weld annealing treatment, the carbon can be precipitated from solid solution resulting in a decrease in the fusion and HAZ hardness and a resultant lowering of the DBTT (See Table 4 and Figure 13). Carbide precipitation from the highly supersaturated solid solution occurred at temperatures as low as 1290°F. Insufficient material did not permit detailed investigation of the lower post weld annealing treatments. Although annealing for 1 hour at 1470°F resulted in approximately the same room temperature hardness as 1 hour at 2730°F, homogenization and re-distribution of the carbide phase was occurring at the higher post weld annealing temperatures (See Figure 13).

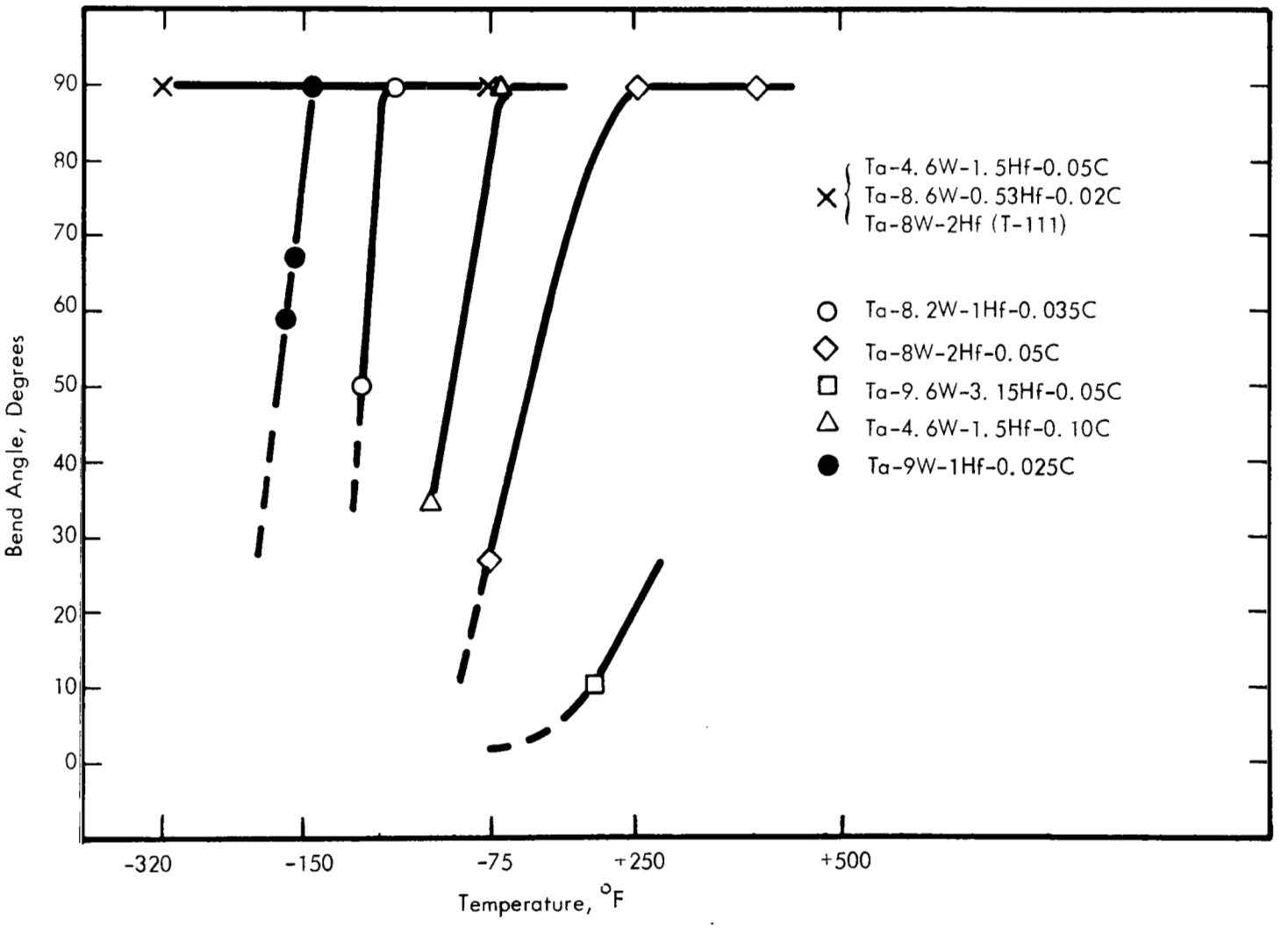

FIGURE 10 - Bend Ductile-Brittle Transition Behavior of Experimental Tantalum Alloys Tested in the As-GTA Welded Condition (Bend Radius 1.8 t)

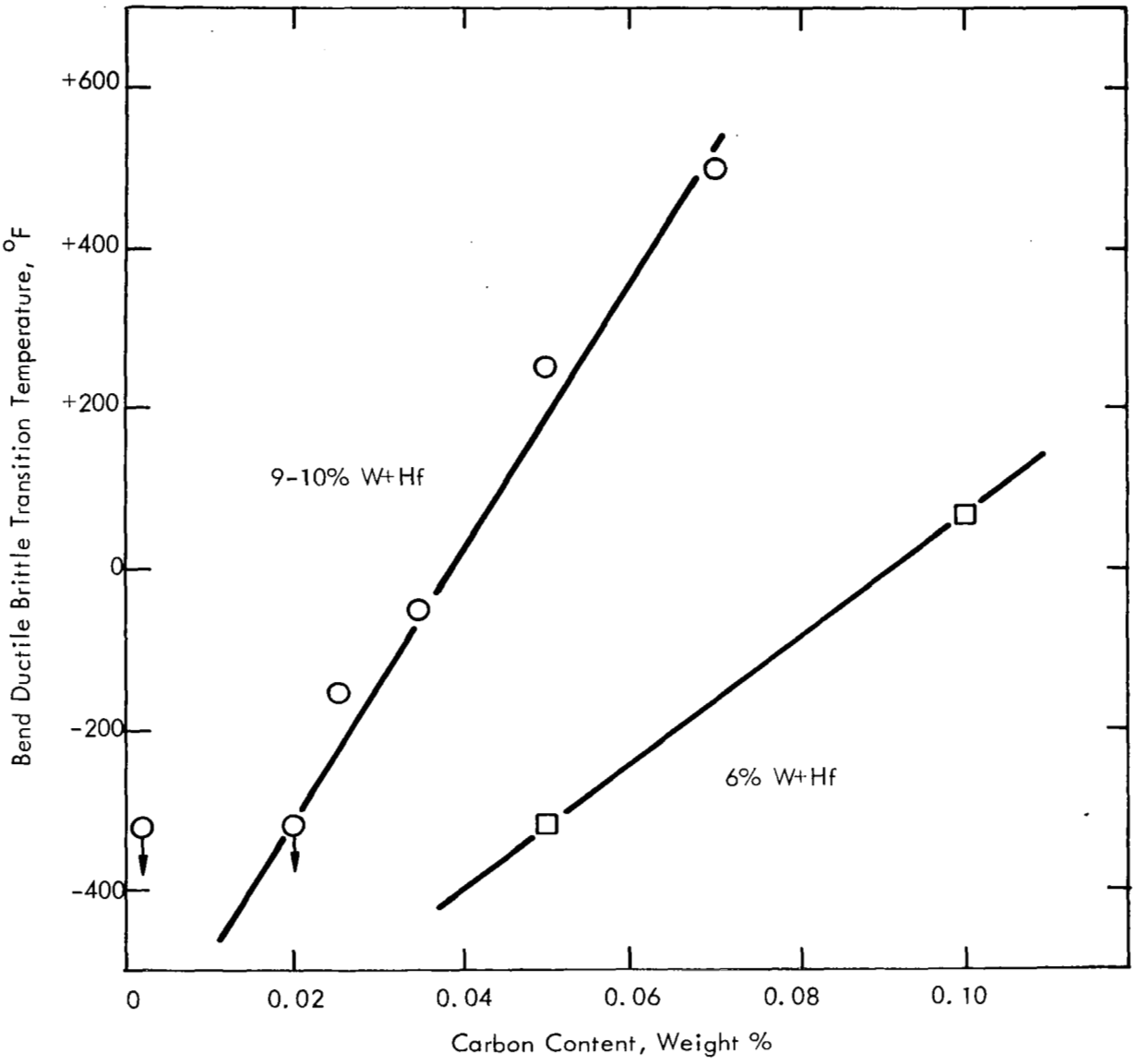

FIGURE 11 - Effect of Carbon on the Ductile-Brittle Transition Temperature of As-GTA Welded Experimental Ta-W-Hf-C Alloy Sheet

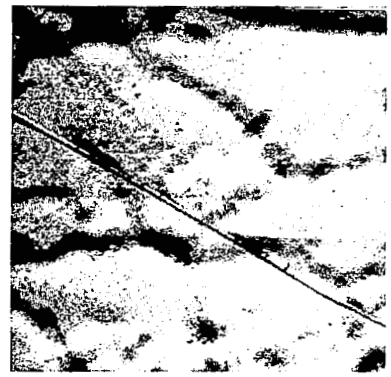

(a) Fusion Zone

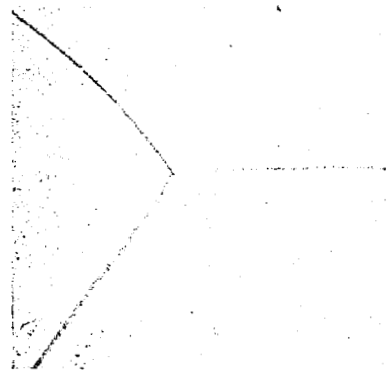

(b) Heat Affected Zone

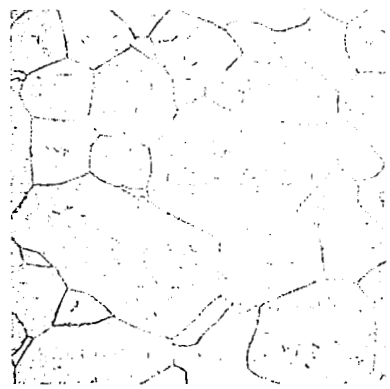

(c) Base Metal (250X)

FIGURE 12 - Photomicrograph Showing Single Phase Fusion and Heat Affected Zone in As-GTA Welded Ta-8.2W-1Hf-0.035C
Etchant - HF-HNO_3 - Glycerine
Mag. - 1500X

TABLE 3 - HARDNESS TRAVERSE RESULTS FOR AS-GTA WELDED TANTALUM BASE ALLOYS

Composition	DPH (Kg/mm^2)		
	Fusion Zone	HAZ	Base Metal[(a)]
Ta-8W-2Hf (T-111)	234	236	210
Ta-8.2W-1Hf-0.035C	332	339	250
Ta-8.5W-0.7Hf-0.045C	380	360	250
Ta-8W-2Hf-0.05C	387	388	270
Ta-9.6W-3.15Hf-0.05C	444	416	320

(a) Annealed 1 hour at $3000^{\circ}F$

TABLE 4 - EFFECT OF 1 HOUR POST WELD ANNEALING ON THE FUSION AND HAZ HARDNESS OF AS-GTA WELDED Ta-8W-2Hf-0.05C

Location	1 Hour Post Weld Annealing Temperature, $^{\circ}F$						
	As-Welded	1290	1470	1830	2010	2550	2730
Fusion Zone	387	305	266	278	277	271	250
HAZ	388	306	262	275	271	268	245

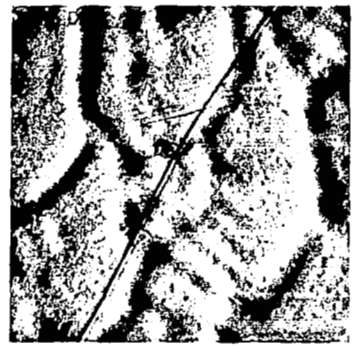

(a) As-GTA Welded
DBTT + 200°F

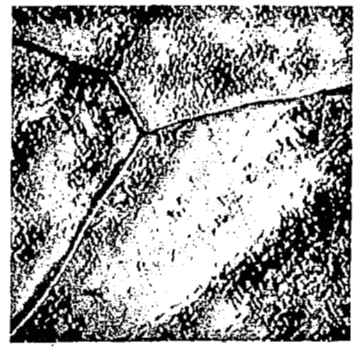

(b) Post Weld Annealed 1 Hr. at 2550°F
DBTT +75°F

(c) Post Weld Annealed 1 Hr. at 2700°F
DBTT 0°F

FIGURE 13 - Effect of Post Weld Annealing on the Fusion Zone Microstructure and bend DBTT (1.8 t Bend Factor) of Ta-8W-2Hf-0.05C (Mag. 1500X)

The DBTT of the compositions containing Mo, Zr, Re and N additions was generally higher than that for the equivalent Ta-W-Hf-C composition. The data plotted in Figure 14 are for as-electron beam welded material. The same behavior pattern was observed for the GTA welded material although the rate of degradation was more rapid, due in part to the greater volume of cast metal in the GTA weld, and the virtual absence of a heat affected zone in the EB weld. Since the substitutions of Re, Mo and Zr are rather dilute, it appears that nitrogen alone is responsible for the upward shift in the ductile brittle transition temperature. As discussed earlier, nitrogen has a higher solubility in the tantalum alloy matrix than does carbon and hence is a much more potent low temperature strengthener. Whereas the DBTT for annealed sheet of Ta-8-10W-0.5-4Hf-0.02-0.04C compositions is below -320°F, the substitution of at least one half or all of the carbon with nitrogen raises the DBTT for annealed sheet to -250 to -150°F.

Rhenium additions are known to severely degrade the low temperature ductility of tantalum when added in excess of 2-3%.[9,37] However, in a Ta-9%W-1Hf-0.025C alloy, substitution of 1% tungsten with rhenium results in essentially no change in the ductile brittle behavior of annealed sheet. (See Table 5). The Ta-8W-1Re-0.7Hf-0.025C composition, designated as ASTAR-811C, is one of the alloy compositions selected for study as a 4 inch diameter ingot and is described in detail later. Also shown in Table 5 are bend ductility data for alloy compositions containing rhenium, molybdenum, zirconium and nitrogen additions. It can be concluded that rhenium additions up to about 3% with the total substitutional solute level about 10% result in weldments having a DBTT of room temperature. Again, it is evident that nitrogen exerts a more significant effect on the low temperature ductility than does carbon. As will be described later under the discussion on mechanical properties, both rhenium and nitrogen have interesting effects on creep behavior. From a weldability consideration, nitrogen has a more deleterious effect on low temperature ductility than does an equivalent amount of carbon. Thus, nitrogen is not considered an optimum addition for a weldable sheet alloy.

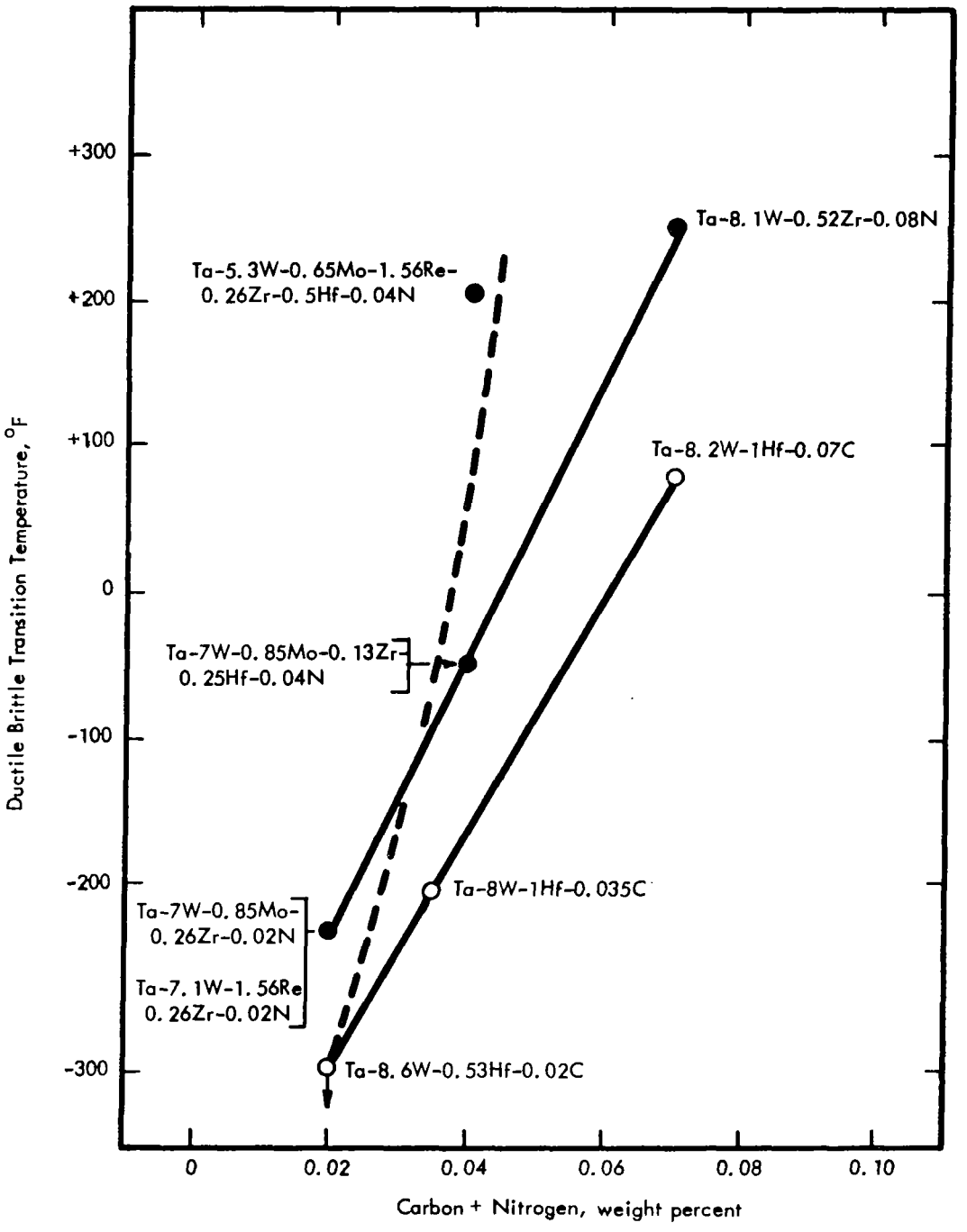

FIGURE 14 - Effect of Carbon and Nitrogen on the Bend Ductile-Brittle Transition Temperature of As-Electron Beam Welded Experimental Tantalum Alloys (Bend Radius 1.8 t)

TABLE 5 - BEND DUCTILITY OF 0.04 INCH THICK EXPERIMENTAL TANTALUM ALLOY COMPOSITIONS*

COMPOSITION, WEIGHT %	BEND DUCTILE BRITTLE TRANSITION TEMPERATURE, °F	
	Annealed Base Metal	As GTA Welded
Ta-9W-1Hf-0.025C	-320	-150
Ta-8W-1Re-0.7Hf-0.025C	-320	-125
Ta-7.5W-1.5Re-0.5Hf-0.015C-0.015N	-175	0
Ta-5.7W-1.56Re-0.7Mo-0.25Hf-0.13Zr-0.015C--0.015N	-200	+ 75
Ta-6.5W-2.5Re-0.3Hf-0.01C-0.01N	-225	-150
Ta-4W-3Re-0.75Hf-0.01C-0.02N	-200	+ 75
Ta-4W-1Mo-2Re-0.3Zr-0.015C-0.015N	-200	+ 25
Ta-9.5W-0.5Re-0.25 Zr-0.02C-0.01N	-200	+ 75

*All sheet material annealed 1 hour at 3000°F prior to testing and/or welding.

4. Recrystallization Behavior and Response to Heat Treatment. The 1 hour recrystallization behavior was determined on 0.06 inch sheet that had been given a prior cold reduction of 68-85%. Isochronal annealing curves which are characteristic of all the Ta-W-Hf-C compositions investigated are illustrated in Figure 15.* The 1 hour recrystallization temperature** for the T-111 sheet was about 2550°F. Adding carbon to the Ta-W-Hf matrix resulted in a hardness minima in the isochronal annealing curve at 2550°F, which did not necessarily coincide with the recrystallization temperature. Thus, although carbon did not appear to alter the rate of recovery, it did exert some effect on grain boundary mobility. Since recovery and recrystallization could be diffusion controlled processes, this behavior would lead one to conclude that carbon additions may not be beneficial in improving resistance to creep deformation. However, this would be an erroneous conclusion as will be discussed later. The increase in room temperature hardness at annealing temperatures above 2550°F is attributed to resolutioning of the carbide phase. Similar behavior has been reported by other investigators.[9,14,37] Substitution of up to 400 ppm nitrogen did not significantly alter the recrystallization behavior. However, at the 800 ppm nitrogen level, recrystallization did not occur until heating for 1 hour at 3600°F (See Figure 15). Although this represents a significant increase in the recrystallization temperature, compositions containing high nitrogen (>400 ppm) are not readily worked to sheet.

(a) Response to Heat Treatment. Both carbon and nitrogen exhibit a solubility relationship with the matrix and exhibit a decreasing solubility with decreasing temperature. Thus the response to high temperature solution annealing treatments followed by low temperature aging anneals was investigated. The following compositions which are representative of both carbide and nitride strengthened matrices were studied.

Ta-5.3W-0.65Mo-1.56Re-0.52Zr-0.08N
Ta-7.1W-1.56Re-0.25Hf-0.13Zr-0.04N
Ta-8.6W-0.53Hf-0.02C

---

* Recrystallization data for all Ta-W-Hf-C compositions is appended in Appendix III.

** Recrystallization temperature is defined here as the temperature at which the microstructure consists of >95% equiaxed grains.

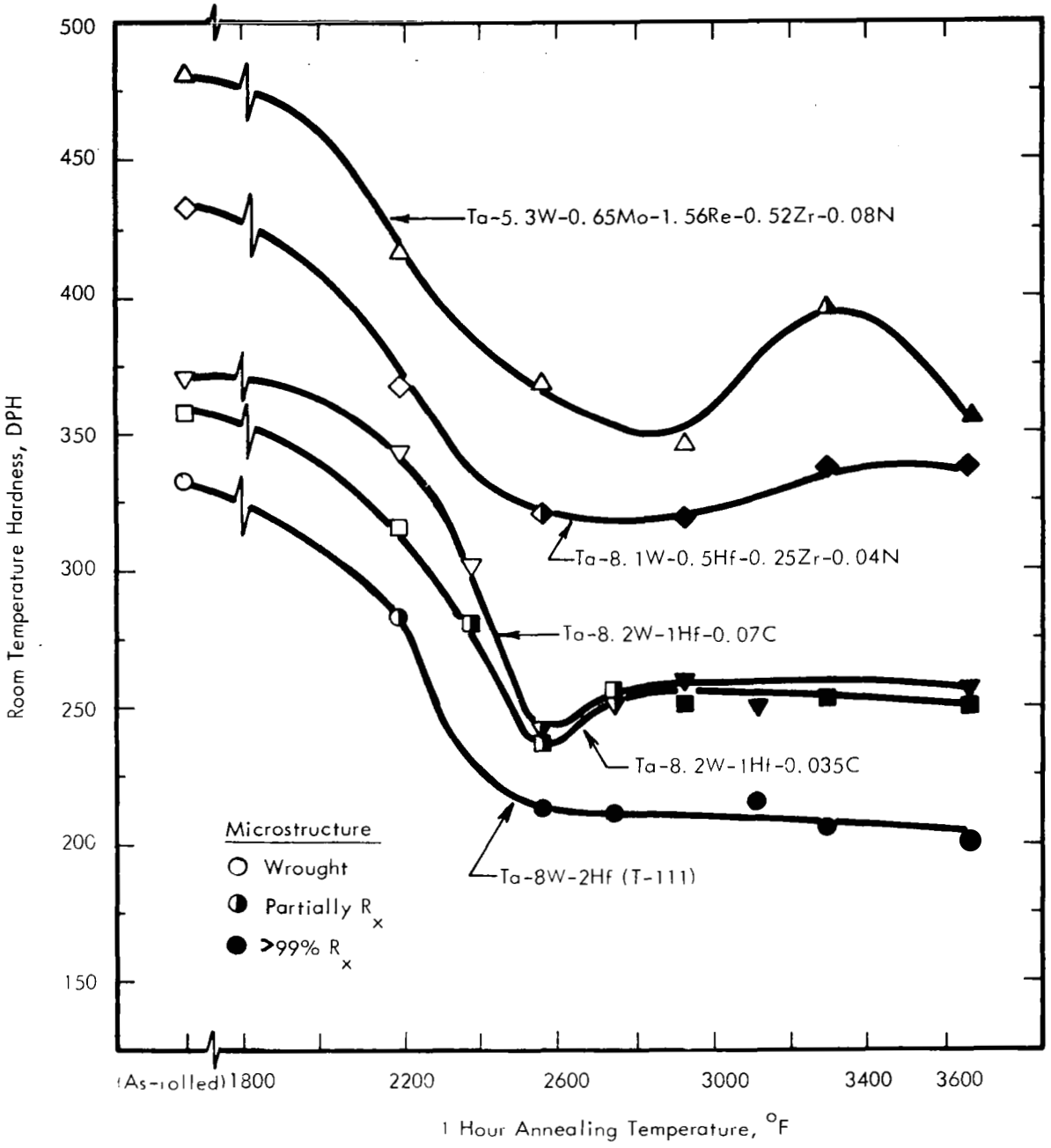

FIGURE 15 - Recrystallization Behavior of Experimental Tantalum Alloy Sheet Given a Prior Cold Reduction of 75%

Sheet samples 0.04 inch thick were annealed at 3630°F for 1 hour and cooled in 90 seconds to less than 1500°F by introducing helium into the furnace chamber as the power was turned off. The as-solution annealed material appeared single phase when examined metallographically at 1500X. Specimens of the solution annealed material were then aged over the temperature range of 1400-2900°F. Changes in microstructure were followed by metallographic examination and room temperature hardness measurements. The 1 hour aging response for all three compositions is illustrated in Figure 16.

Neither the room temperature hardness nor the microstructure of the solution annealed Ta-7.1W-1.56Re-0.25Hf-0.13Zr-0.04N composition underwent any apparent change during the 1 hour aging treatments. The room temperature hardness of the high nitrogen bearing composition Ta-5.3W-0.65Mo-1.56Re-0.52Zr-0.08N increased after annealing for 1 hour up to about 2400°F and then decreased abruptly after heating 1 hour at 2550°F. Concurrent with this drop in hardness was the appearance of general precipitation throughout the matrix (See Figure 17). No precipitates were observed optically in samples annealed at less than 2370°F. This sequence of precipitation and change in hardness is similar to coherent precipitation hardening behavior. Similar phenomena have been observed in the Cb-Hf-N system by Begley et al where overaging occurred at approximately 1800°F.[38] The strong evidence for a coherent precipitate is surprising since there is about a 39% misfit between ZrN and the matrix lattice. Most systems which give rise to coherent precipitation hardening have misfits between the precipitate and the matrix of only approximately 11%.[39]

The solution annealed carbon containing composition(Ta-8.6W-0.53Hf-0.02C) softened on subsequent aging at 1400-2400°F indicative of the precipitation of a non-coherent precipitate. This sequence of precipitation in carbide containing tantalum alloys has been reported by other investigators.[12,40,41] The dispersed second phases were chemically extracted and identified as Ta_2C. Similar behavior was observed in the Ta-9.6W-3.15Hf-0.05C composition where the precipitating phase was identified as the monocarbide phase, $(Hf,Ta)C_{1-x}$. The phase relationships in the Ta-W-Hf-C system will be discussed in detail later.

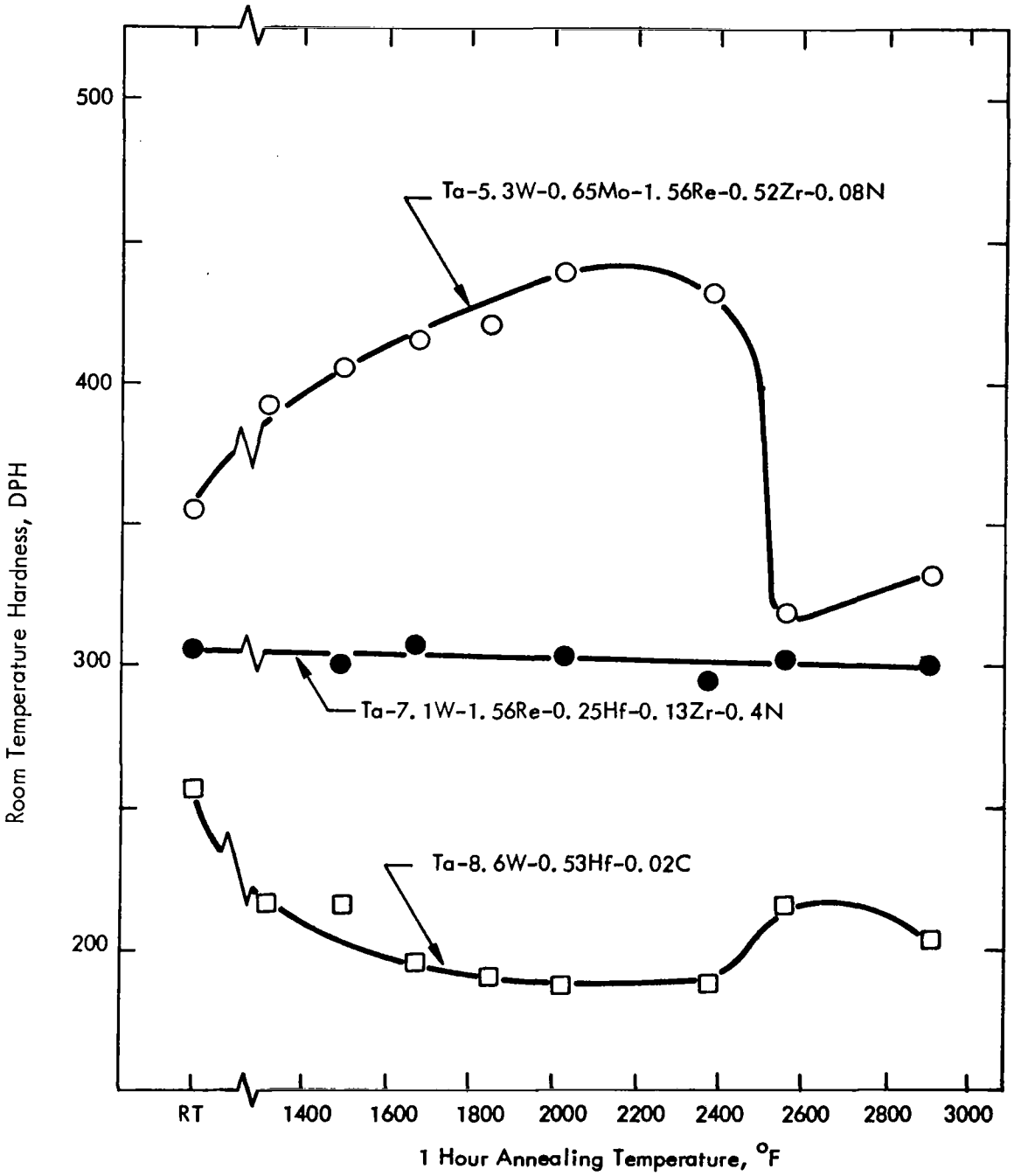

FIGURE 16 - Aging Response of Nitrogen and Carbon Bearing Tantalum Alloys Solution Annealed for 1 Hour at 3630°F and Rapidly Cooled

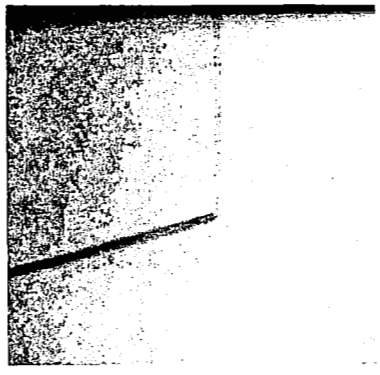

(a) Aged 1 Hour at 2000°F
360 DPH

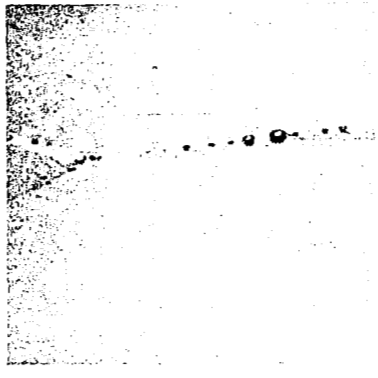

(b) Aged 1 Hour at 2370°F
430 DPH

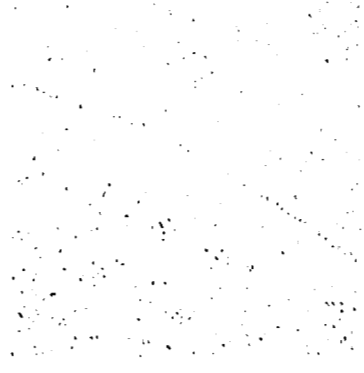

(c) Aged 1 Hour at 2550°F
320 DPH

FIGURE 17 - Microstructure of Solution Annealed and Aged Ta-5.3W-1.56Re-0.65Mo-0.52Zr-0.08N Etchant - NH_4HF-HF-HNO_3-H_2O
Mag. 1500X

5. Mechanical Properties

(a) Tensile Properties. Carbon additions of up to 0.1% to the Ta-W-Hf alloy matrix results in an increase in the room temperature yield and ultimate tensile strength with little change occurring in the tensile elongation (Table 6 and Figure 18). The excellent room temperature ductility retained even at a carbon content of 0.1% is of course due to the low solubility of carbon in the alloy matrix. Thus the very hard carbide particles are randomly dispersed in a highly ductile matrix. Substitution of nitrogen for carbon results in a further increase in the tensile strength. As discussed earlier, nitrogen exhibits a much higher solubility in the tantalum alloy matrix and thus appears to be a more effective low temperature strengthener than does carbon. However, if carbon could be retained in solid solution, the strengthening effectiveness of both would be similar. Neither molybdenum nor zirconium substitutions appeared to be any more effective than the equivalent amount of tungsten and hafnium. The effect of rhenium on the room temperature tensile strength was strongly dependent on the level of rhenium added. For example, substitutions for 1% tungsten with an equivalent amount of rhenium in a Ta-9W-1Hf-0.025C alloy did not result in any change in room temperature, tensile strength (See Table 6). However, as the rhenium level was increased above 1.5% with the total substitutional solute level at 9-10%, rhenium increased the room temperature tensile strength at a much faster rate than an equivalent amount of tungsten. For example, the Ta-9.5W-0.5Re-0.25Zr-0.02C-0.01N alloy had a room temperature yield strength of 102,000 psi while the Ta-6.5W-2.5Re-0.3Hf-0.01C-0.01N alloy had a room temperature yield strength of 142,000 psi. This behavior most likely reflects the greater effect rhenium has on the temperature dependent portion of the yield strength.

Carbon significantly increases the 2400°F yield strength of Ta-W-Hf and appears to be an effective strengthener at 3000°F, although to a much lesser extent. (See Figure 19 and Table 7). The short time tensile strength improvement caused by carbon is most likely related to a dispersed phase strengthening mechanism as it would be unlikely that interstitial carbon would be an effective strengthener at 2400°F which is about 0.5 Tm of tantalum. The

TABLE 6 - ROOM TEMPERATURE TENSILE PROPERTIES OF TANTALUM BASE ALLOYS ANNEALED 1 HOUR AT 3000°F PRIOR TO TEST

Composition (w/o)	0.2%Y.S. (psi)	UTS (psi)	% Elongation	
			Uniform	Total
Ta-8W-2Hf (T-111)	69,000	85,900	20.2	36.3
Ta-8W-2Hf-0.05C	74,600	105,000	15.6	21.8
Ta-8W-3.15Hf-0.1C	98,100	126,300	16.2	28.0
Ta-9.6W-3.15Hf-0.05C	107,900	129,500	18.6	28.7
Ta-8.2W-1Hf-0.035C	71,400	102,000	18.3	29.7
Ta-11.3W-0.92Hf-0.06C	101,800	126,200	14.7	22.3
Ta-9W-1Hf-0.025C	78,600	106,800	14.8	23.5
Ta-8W-1Re-0.7Hf-0.025C	78,000	105,000	16.7	28.0
Ta-7W-0.85Mo-0.025Hf-0.13Zr-0.04N	121,200	130,800	14.2	20.3
Ta-7W-0.85Mo-0.26Zr-0.02N	101,000	111,700	15.6	25.6
Ta-5.7W-0.7Mo-1.56Re-0.25Hf-0.13Zr -0.017C-0.02N	127,100	134,000	13.0	23.8
Ta-7.1W-1.56Re-0.26Zr-0.02N	106,600	118,500	15.6	25.9
Ta-8.7W-0.26Zr-0.008C-0.01N	99,800	113,200	14.2	22.0
Ta-7.5W-1.5Re-0.54Hf-0.015N-0.015C	132,200	138,800	8.6	15.3
Ta-6.5W-2.5Re-0.3Hf-0.01C-0.01N	142,000	146,300	6.5	12.7
Ta-4W-1Mo-2Re-0.3Zr-0.015C-0.015N	138,200	142,700	10.4	17.3
Ta-9.5W-0.5Re-0.25Zr-0.02C-0.01N	102,000	116,400	15.9	28.9
Ta-4W-3Re-0.75Hf-0.01C-0.02N	132,000	133,200	12.2	22.7
Ta-5W-1Re-0.3Zr-0.025N	110,300	112,300	11.6	18.5

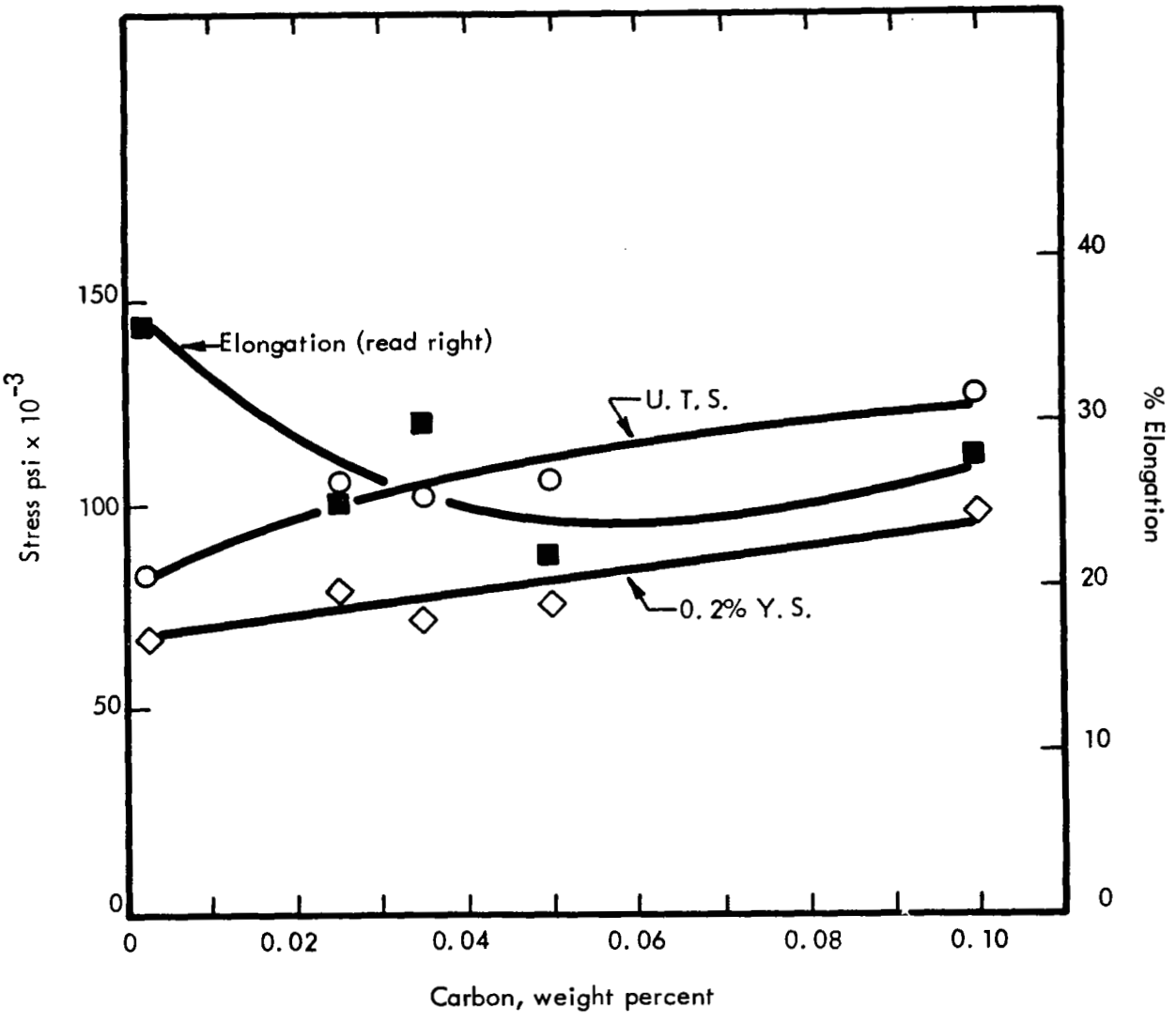

FIGURE 18 - Effect of Carbon on the Room Temperature Tensile Properties of Ta(8-9)W-(1-3)Hf Alloys (Annealed 1 Hr. at 3000°F Prior to Test)

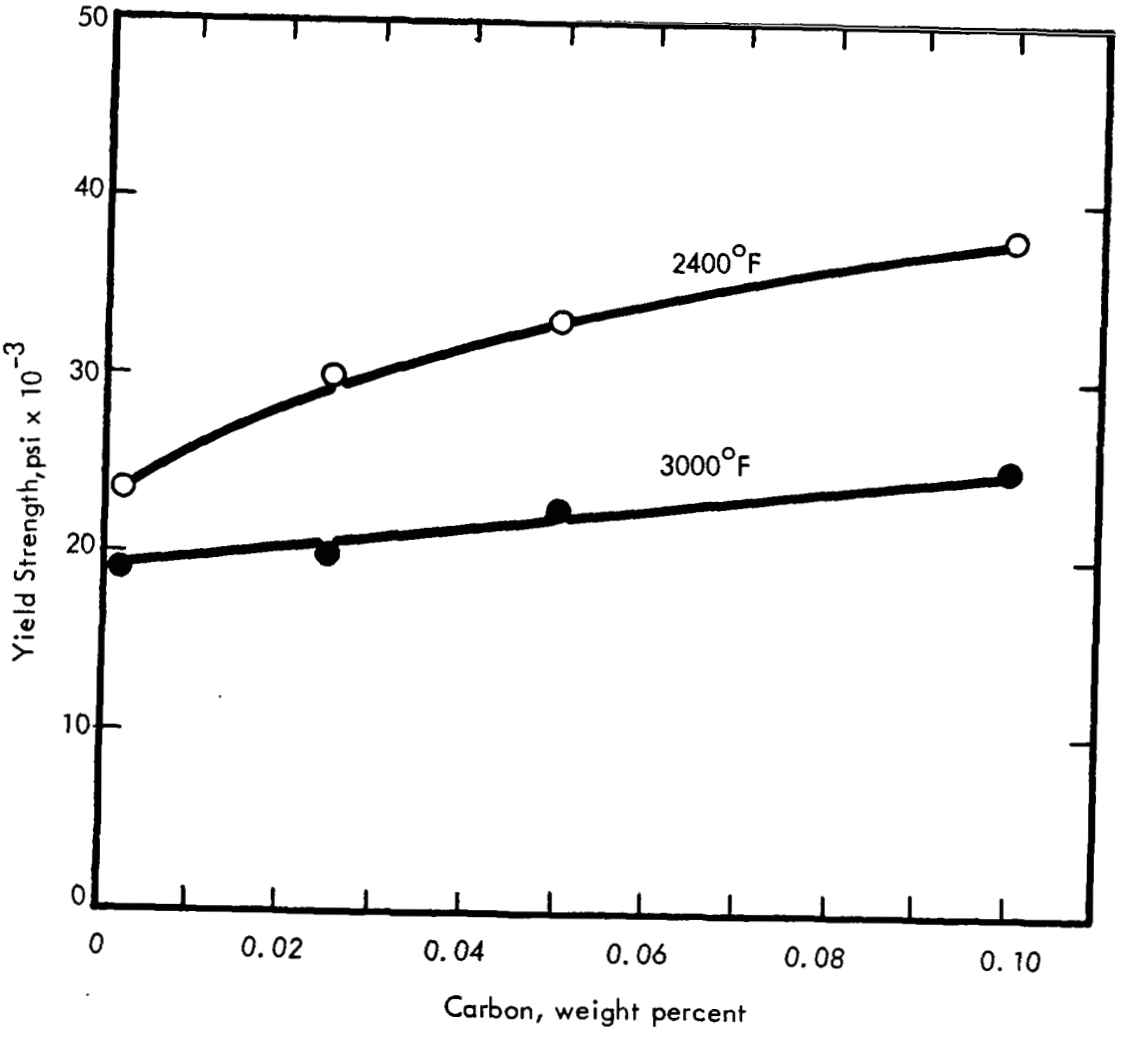

FIGURE 19 - *Effect of Carbon on the Elevated Temperature* Tensile Strength of Ta-(8-9)W-(1-3)Hf Alloys (Annealed 1 Hr. at 3000°F Prior to Test)

TABLE 7 - ELEVATED TEMPERATURE TENSILE PROPERTIES OF EXPERIMENTAL TANTALUM ALLOY SHEET (ANNEALED 1 HOUR AT 3000°F PRIOR TO TEST)

Composition (w/o)	Test Temperature (°F)	0.2% Offset Y.S. (psi)	UTS (psi)	Elongation (%)
Ta-8W-2Hf (T-111)	2000	28,000	52,900	24
	2400	23,400	36,400	40
	3000	18,000	19,500	36
Ta-8W-2Hf-0.05C	2400	33,700	47,400	36
	3000	22,500	24,400	95
Ta-8W-3.15Hf-0.01C	2400	37,800	51,500	38
	3000	24,700	25,700	135
Ta-9W-1Hf-0.025C	2000	33,400	72,800	21
	2400	29,400	43,200	36
	3000	19,400	20,600	71
Ta-7.5W-1.5Re-0.5Hf -0.015C-0.015N	2400	32,200	44,900	29
	2800	25,400	28,900	50
Ta-6.5W-2.5Re-0.3Hf -0.01C-0.01N	2400	32,300	42,800	38
	2800	22,900	26,000	42
Ta-4W-1Mo-2Re-0.3Zr -0.015C-0.015N	2400	37,000	51,500	28
	2800	23,000	25,400	31
Ta-9.5W-0.5Re-0.25Zr -0.02C-0.01N	2400	34,100	47,700	24
	2800	29,800	33,100	24
Ta-4W-3Re-0.75Hf-0.01C -0.02N	2400	34,800	45,600	29
	2800	25,400	27,600	50
Ta-5W-1Re-0.3Zr-0.025N	2400	25,700	39,700	26
	2800	20,800	22,700	46
Ta-5.7W-1.56Re-0.7Mo -0.25Hf-0.13Zr-0.015C -0.015N	2000	41,200	69,800	22
	2400	36,300	48,900	29
	3000	21,800	22,700	64
Ta-8.5W-1.5Re-1Hf	2400	24,900	35,900	19
	2600	24,500	32,000	21
	3000	22,000	23,500	11
Ta-10W-1Re-0.5Hf	2400	23,400	34,300	27
	2600	23,000	30,000	27
	3000	20,500	22,100	18

strengthening advantage of rhenium over tungsten at room temperature is not evident at 2400°F and above as illustrated by the tensile data in Table 7.

The potent short time strengthening of nitrogen is illustrated by data shown below in Table 8.

TABLE 8 - EFFECT OF NITROGEN ON THE 2400°F TENSILE STRENGTH OF TANTALUM ALLOYS TESTED IN THE AS-WORKED CONDITION (PRIOR 33% REDUCTION)

Composition	Yield Strength (psi)	Tensile Strength (psi)
Ta-7.1W-1.56Re-0.26Zr-0.02N	61,300	67,900
Ta-5.3W-0.65Mo-1.56Re-0.52Zr -0.08N	80,800	105,100

The 105,000 psi ultimate tensile strength at 2400°F is truly remarkable considering that the composition contains only 9% substitutional solute. This same composition tested at room temperature after annealing for 1 hour at 3000°F exhibited a 141,000 psi yield strength with 13.7% uniform elongation and a total elongation of 17.6%. The 1 hour at 3000°F did not recrystallize the wrought microstructure but resulted in a stress relief anneal. The 1 hour recrystallization temperature for this composition was 3630°F. As discussed earlier, high nitrogen bearing compositions have extremely interesting strength properties but they also exhibit poor as-welded bend ductility and thus could not be considered as a fabricable sheet alloy.

(b) Creep Behavior. Short time tensile properties were evaluated to better characterize the strength level and to assess the effects of the solute additions on the tantalum alloy matrix. The short time tensile behavior is also useful for evaluating the potential secondary

working characteristics. However, resistance to creep deformation was the mechanical property of prime interest in this investigation. Screening creep tests were conducted at 2400°F and at stress levels ranging from 10,000 to 20,000 psi. Since creep is a very structure sensitive property and a wide compositional range was investigated, it was not feasible to standardize on the final metallurgical condition. To illustrate the effect of metallurgical condition on creep, examine the creep curves shown in Figure 20 for a Ta-8.2W-1Hf-0.07C alloy tested at 2400°F and 15,000 psi. The specimen tested in the as-worked condition (33% prior cold work) exhibited a large primary creep strain (Curve A) and had elongated about 10% in 50 hours. The second specimen, annealed for 1 hour at 3000°F exhibited no loading or primary creep strain. After 100 hours, the total creep elongation was 1.57%. The accelerated creep for the as-worked specimen can be attributed to recovery and recrystallization occurring during test which could result in a much greater number of mobile dislocations than are present in the annealed test specimen. Similar behavior has been observed by other investigators and has been described by Perryman.[42] To avoid the accelerated creep exhibited by the as-cold worked condition, creep specimens were tested in the recrystallized condition. All specimens were annealed for 1 hour at 3000°F prior to test. Since metallurgical condition could not be readily maintained constant, the effects of the various solute additions on creep behavior are qualitative. However, trends were clearly indicated which aided in establishing compositional ranges for the various alloy additions.

Another factor which complicated somewhat the interpretation of the creep data was the shape of the creep curve normally obtained under the conditions of test. Creep curves at 2400°F were characteristically identified by essentially no elongation on loading, an incubation period during which little or no extension occurs and then extension at a constantly increasing rate. (See Figure 21). Therefore the time to elongate 1% was the creep evaluation criterion used, since the nominally used value of secondary creep rate ($\dot{\epsilon}_s$) had little significance in assessing creep resistance. This characteristically shaped creep curve has been observed by other investigators who have tested tantalum and columbium base alloys in dead-weight loaded systems under ultra-high vacuum conditions.[24,43,44]

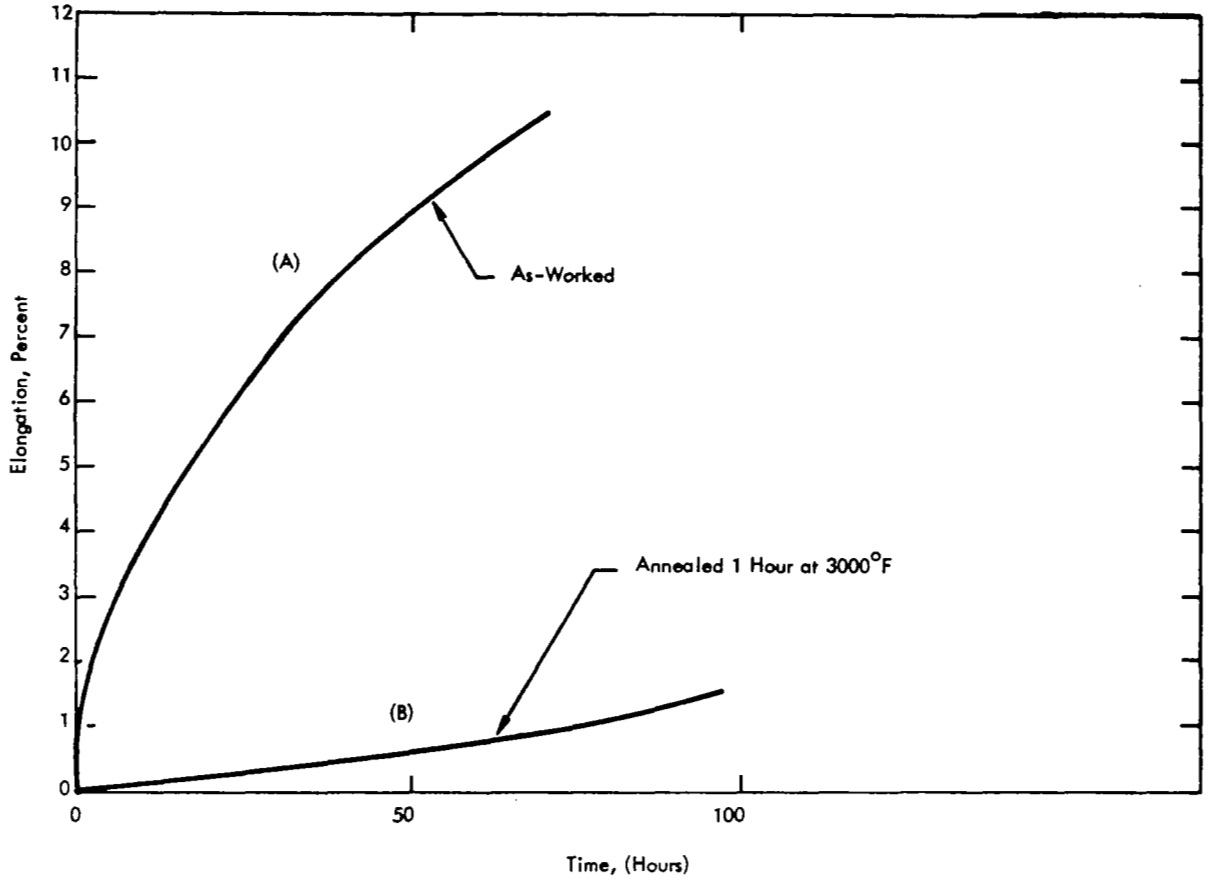

FIGURE 20 - Effect of Metallurgical Condition on Creep Behavior of Ta-8.2W-1Hf-0.07C at 2400°F and 15,000 psi

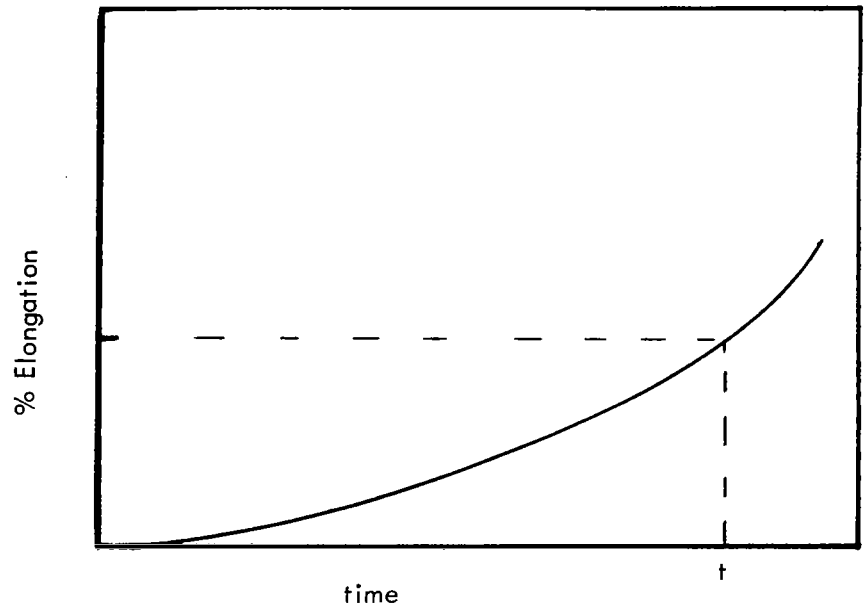

FIGURE 21 - Typical Creep Curve Shape Obtained in Deadweight Loaded Ultra-High Vacuum Creep System at 2400°F and 10,000 to 20,000 psi Applied Stress

The creep data obtained during the screening investigations are summarized in Table 9. As discussed previously, the large number of experimental compositions investigated did not permit detailed evaluation of the stress and temperature dependence of creep. Thus the conclusions that will be discussed are from observations made at 2400°F which is approximately 0.5 T_m of tantalum and would be in a temperature region where creep would normally be a diffusion controlled process. The stress levels were from 30 to 65% of the 2400°F, 0.2% offset yield strength.

Carbon additions to the Ta-W-Hf matrix result in an improvement in creep resistance, indicating that the dispersed carbide phase is making a significant contribution to creep resistance (See Figure 22). However, it is also apparent from Figure 22 that for the conditions of test, there is a maximum carbon content (~300 ppm) above which the creep resistance is degraded. Thus it would appear that there is an optimum carbon content for creep resistance. Although not confirmed metallographically, it is postulated that since all specimens were given the same final annealing treatment, the resulting carbide phase was much coarser in the higher carbon containing alloys. The carbon solubility in the Ta-W-Hf matrix at 3000°F is approximately 100 ppm, thus only a small fraction of the carbon of the high carbon containing alloys was dissolved at the final annealing temperature of 3000°F. It would be expected that if the solvus was exceeded and the cooling sufficiently fast to precipitate a fine carbide phase that the creep resistance would naturally be higher for the higher carbon containing compositions. However, as discussed earlier, a Ta-W-Hf matrix containing 9-10% W+Hf could withstand only about 300 ppm carbon before as GTA welded bend ductility was seriously degraded. Thus there was little practical interest in further investigation of the higher carbon containing compositions.

The carbide precipates extracted from the creep specimens were identified as either or mixtures of the dimetal and monometal carbide phases which is discussed in more detail under the phase relationship section. The 2400°F creep behavior of the experimental

TABLE 9 - CREEP TEST RESULTS FOR EXPERIMENTAL TANTALUM ALLOY COMPOSITIONS TESTED AT $\leq 1 \times 10^{-8}$ TORR

(0.0 4 inch thick sheet, annealed one hour at 3000°F prior to test)

Composition (weight %)	Test Temperature °F	Stress psi	Total Test Time (hours)	Total Plastic Strain (%)	Time to Strain 1% (hours)
Ta-8W-2Hf(T-111)	2400	14,100	73	2.56	42
	2400	10,000	150	0.5	(300)[a]
	2400	15,180	43	3.3	18
	2500	12,700	51	3.4	26
Ta-8W-2Hf-0.05C	2400	14,095	96	2.08	50
	2400	10,000	172	0.9	192
Ta-8W-2.7Hf-0.4Zr-0.05C	2400	14,000	70	4.86	21
	2400	12,780	51	1.88	32
Ta-9.6W-3.15Hf-0.05C	2400	15,000	79	4.91	23
	2400	12,670	95	2.31	50
Ta-9.6W-3.9Hf-0.1C	2400	15,000	41	4.35	12
Ta-8.2W-1Hf-0.035C	2400	14,770	172	1.35	128
	2400	20,000	102	4.06	34
Ta-8-2W-1Hf-0.07C	2400	14,974[b]	65	11.50	2
	2400	14,530	96	1.57	65
Ta-8.2W-1Hf-0.1C	2400	16,510	67	11.1	10
Ta-8.6W-0.53Hf-0.02C	2400	15,070	96	1.33	72
	2400	20,000	44	6.37	10

(a) - Values in parentheses are extrapolated
(b) - Tested in as worked condition, 33% C.W.

TABLE 9 - (continued)

Composition (weight %)	Test Temperature °F	Stress psi	Total Test Time (hours)	Total Plastic Strain (%)	Time to Strain 1% (hours)
Ta-8.6W-0.53Hf-0.035C	2400	13,770	41	2.02	25
Ta-4.6W-1.5Hf-0.05C	2400	10,000	76	1.10	72
	2400	20,000	4	5.49	1
Ta-4.6W-1.5Hf-0.1C	2400	10,000	70	3.86	26
	2400	20,000	2	4.9	0.4
Ta-9W-1Hf-0.025C	2500	12,830	138	3.97	60
	2400	15,000	209	2.17	115
	2400	12,750	507	2.27	280
	2400(c)	15,160	501	4.70	180
Ta-8W-1Re-0.7Hf-0.025C	2400	12,690	190	0.21	(510)(a)
Ta-6.8W-0.85Mo-0.26Zr	2400	15,000	91	1.03	91
	2400	20,000	91	2.97	50
Ta-5.7W-0.7Mo-1.56Re-0.25Hf -0.13Zr-0.0.017C-0.02N	2400	15,000	193	0.25	(770)(a)
Ta-7.1W-1.56Re-0.26Zr-0.02N	2400	15,390	94	0.20	(475)(a)
	2400	20,000	146	3.19	77
Ta-7.1W-1.56Re-0.25Hf-0.13Zr -0.04N	2400	20,000	197	0.21	(655)(a)

(a) - Values in parentheses are extrapolated

(c) - Annealed one hour at 3270 °F prior to test

TABLE 9 - (continued)

Composition (weight %)	Test Temperature °F	Stress psi	Total test Time (hours)	Total Plastic Strain (%)	Time to Strain 1% (hours)
Ta-8.7W-0.26Zr-0.008C -0.01N	2400	15,000	162	1.62	125
		20,000	54	5.53	25
Ta-8.7W-0.25Hf-0.13Zr -0.017C-0.02N	2400	14,500	187	2.22	120
		20,000	71	2.07	47
Ta-5.3W-0.65Mo-1.56Re -0.52Zr-0.08N	2400	20,000	142	1.25	124
Ta-6.5W-0.8Mo-0.5Hf -0.26Zr-0.017C-0.02N	2400	15,000	102	1.32	90
		20,000	45	2.89	40
Ta-5.7W-1.56Re-0.7Mo-0.25Hf -0.13Zr-0.015N-0.015C	2400	15,000	190	0.57	(325)[a]
	2400	12,670	305	0.16	(1,430)[a]
	2400	20,730	213	17.74	70
	2500	12,860	99	0.92	(107)[a]
	2400[c]	15,000	816	4.88	400
Ta-5.7W-1.56Re-0.7Mo-0.7Hf -0.13Zr-0.015N-0.015C	2400	13,340	400	0.34	(1,170)[a]
Ta-8.5W-1.5Re-1Hf	2400	15,400	211	1.24	180
	2400	12,500	239	0.48	(416)[a]
	2600	10,000	381	5.60	160
	2600	8,000	232	1.49	180
Ta-10W-1Re-0.5Hf	2400	15,600	210	1.83	127
	2600	10,000	258	2.36	170
	2600	8,000	402	1.85	284

(a) - Values in parentheses are extrapolated

(c) - Annealed one hour at 3270°F prior to test

TABLE 9 - (continued)

Composition (weight %)	Test Temperature °F	Stress psi	Total Test Time (hours)	Total Plastic Strain (%)	Time to Strain 1% (hours)
Ta-7.5W-1.5Re-0.5Hf-0.015C -0.015N	2400	15,000	445	0.39	(1,140)[a]
	2400	12,680	258	0.0	--
	2400	20,180	171	7.93	54
	2600	8,000	513	0.89	(575)[a]
	2600	10,000	260	6.47	78
Ta-6.5W-2.5Re-0.3Hf-0.01C -0.01N	2400	15,000	212	0.31	(685)[a]
	2400	12,620	284	0.21	(1,350)[a]
	2600	7,950	187	0.79	(237)[a]
	2600	10,000	260	2.20	171
Ta-4W-1Mo-2Re-0.3Zr-0.015C -0.015N	2400	15,000	230	0.41	562
	2400	12,810	211	0.12	(1,750)[a]
	2600	8,000	194	0.62	(312)[a]
	2600	10,000	330	2.54	153
Ta-9.5W-0.5Re-0.25Zr-0.02C -0.01N	2400	15,000	196	0.40	(490)[a]
	2400	12,500	235	0.16	(1,470)[a]
	2600	8,000	209	0.56	(370)[a]
	2600	10,000	286	2.60	150
Ta-4W-3Rd-0.75Hf-0.01C -0.02N	2400	15,000	200	0.29	(690)[a]
	2400	12,500	284	0.27	(1,050)[a]
	2600	10,000	210	1.46	175
	2600	8,000	331	0.96	(346)[a]
Ta-5W-1Re-0.3Zr-0.025N	2400	15,000	93	2.10	67
	2600	10,000	117	6.58	42

(a) - Values in parentheses are extrapolated

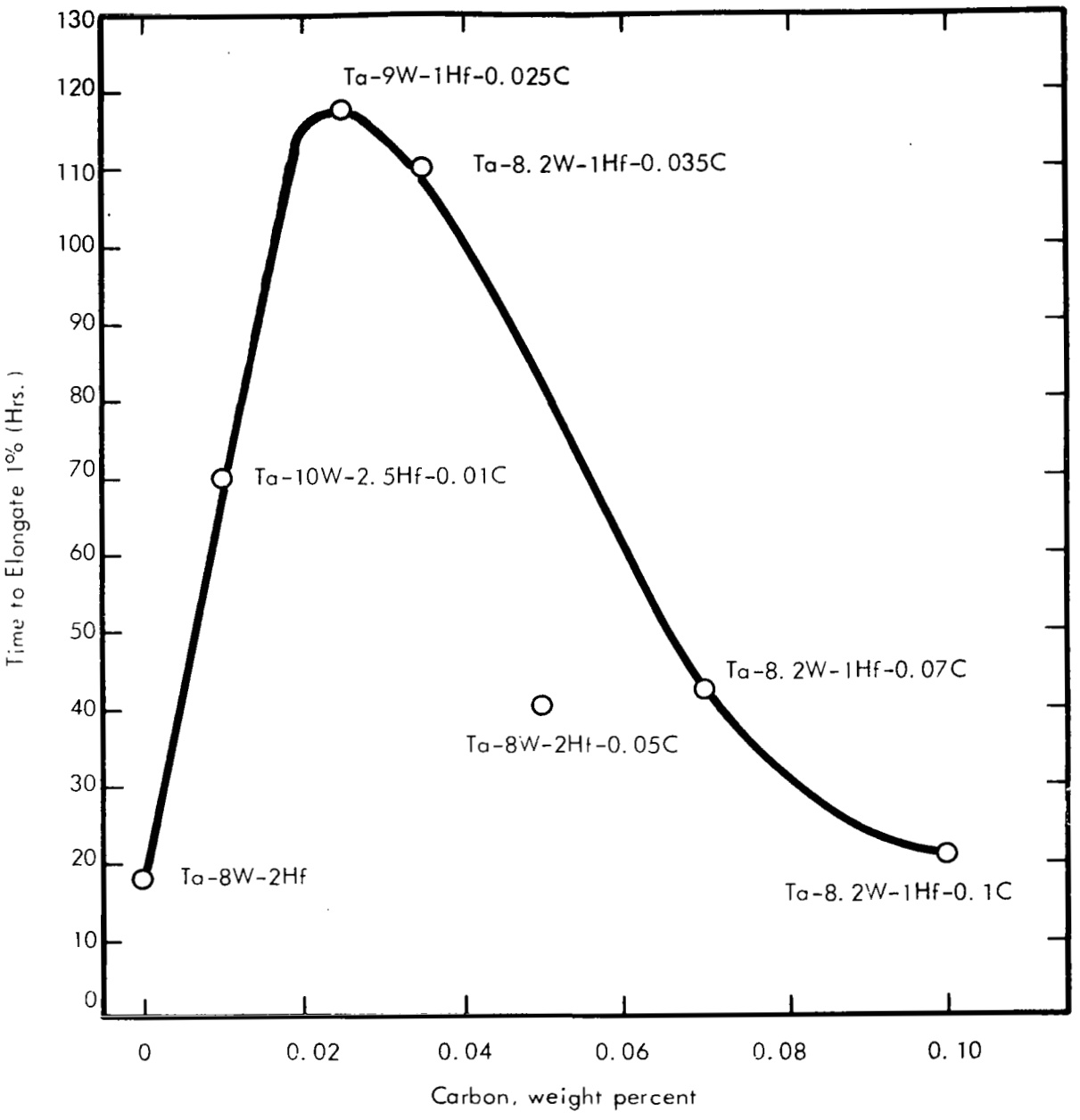

FIGURE 22 - Effect of Carbon on the Creep Behavior of Ta-W-Hf Alloys at 2400°F and 15,000 psi (Annealed 1 Hour at 3000°K Prior to Test)

Ta-W-Hf-C alloy composition is summarized in Figure 23. Illustrated here is the time-elongation history curves which could be separated, based on the precipitating phase. It is apparent from this data that the compositions exhibiting the best creep resistance contained only the dimetal carbide (Ta_2C) as the precipitating phase while the compositions containing only the monometal carbide $(TaHf)C_{1-x}$ exhibited the poorest creep resistance. During the investigations on Cb-W-Zr-C alloys, it was reported that optimum creep resistance was achieved when the reactive metal/carbon ratio approached unity and here the precipitating phase was identified as the monometal carbide.[45] The work on the columbium alloys preceded development of similar tantalum alloys and it was assumed that the same phase relationships would exist at similar composition levels.[46] However, as shown here and as will be discussed later, the phase relationships in the Ta-W-Hf-C system are slightly different than in the Cb-W-Hf-C system. Thus the composition of the carbide phase per se may not be critical but the morphology and distribution of the precipitate may have the greatest effect on the creep behavior. At the 500 ppm carbon level for example, reactive metal additions of approximately 3% were required to stabilize the monometal carbide phase. Thus there is always an excess of reactive metal which is present as a substitutional solute. From the theoretical considerations discussed earlier, one would assume that hafnium or zirconium additions would result in degradation of creep resistance of the tantalum alloy matrix. (See Figure 24). Thus it is probably futile to attempt to stabilize the monocarbide phase since the reactive metal addition causes a precipitious decrease in creep resistance. Although there was a decrease in creep resistance as the reactive metal content was increased, the elevated temperature tensile strength increased which illustrates the fallacy of extrapolating long time behavior from short time property data.

The minor compositional variations investigated by substituting different atom species, i.e., nitrogen for carbon and rhenium and molybdenum for tungsten provided a dramatic change in the 2400°F creep resistance. As shown in Figure 25, the tantalum

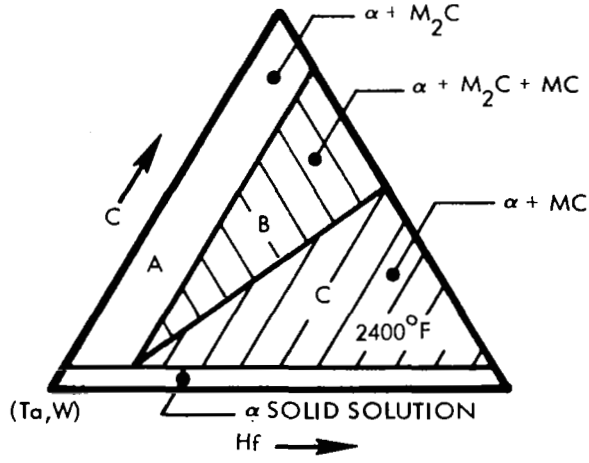

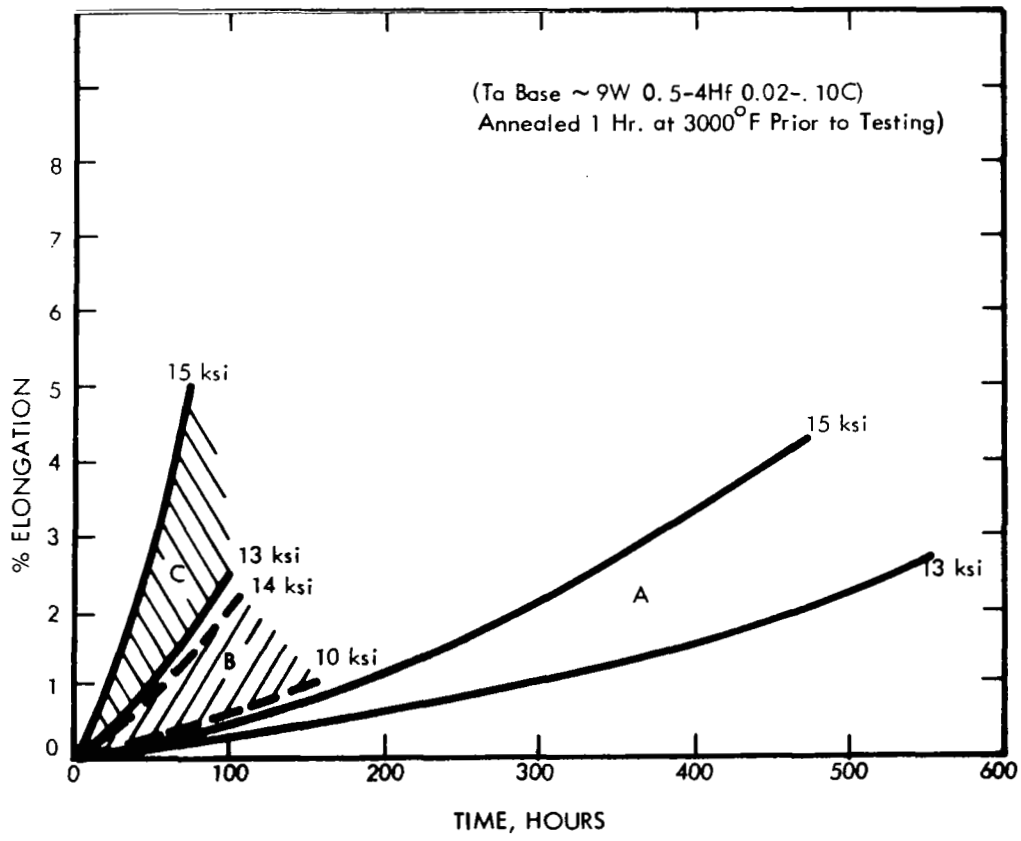

FIGURE 23 - 2400°F Creep Behavior of Ta-W-Hf-C Alloys (Composition of Carbide Precipitate for Each Group of Time Elongation Curves Shown in 2400°F Isotherm of the (Ta,W)-Hf-C Psuedo-Ternary)

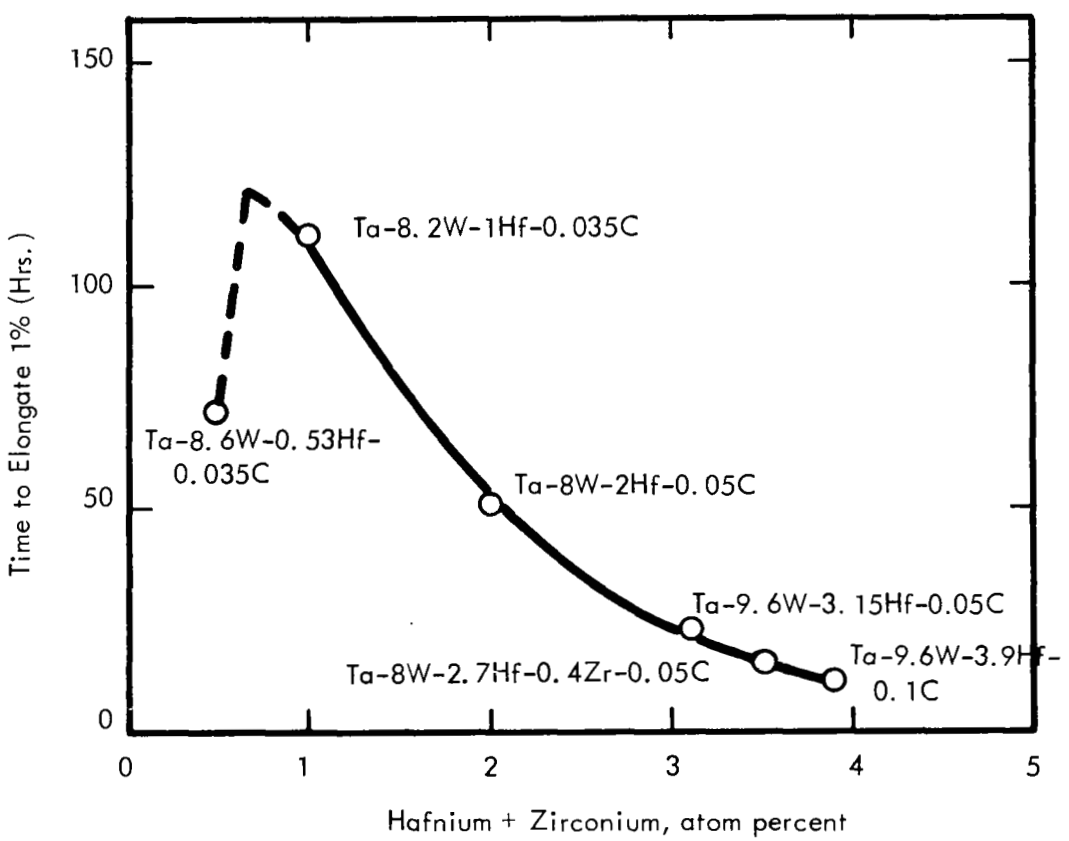

FIGURE 24 - Effect of Reactive Metal (Hf+Zr) Addition on the Creep Behavior of Tantalum Alloys Tested at 2400°F and 15,000 psi

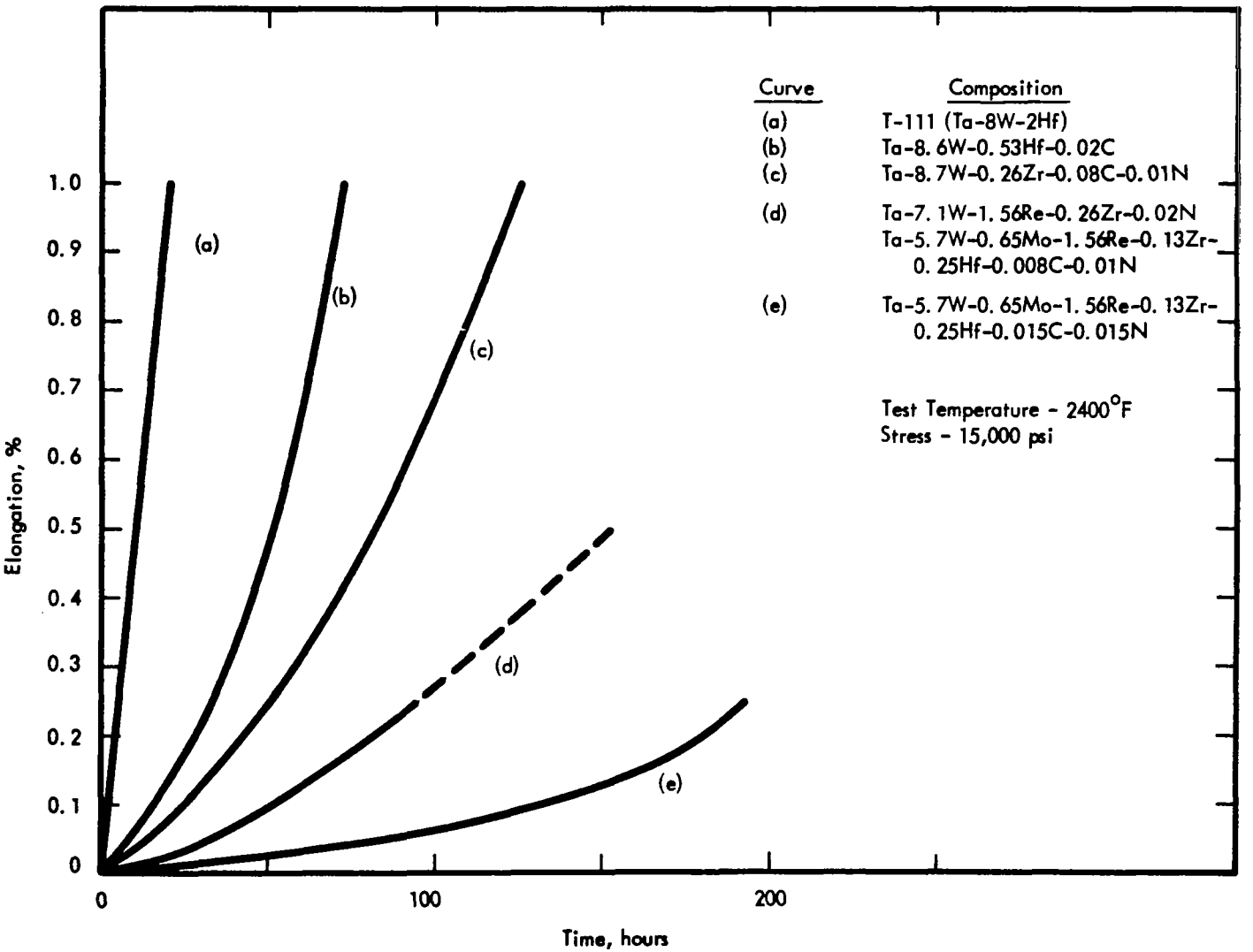

FIGURE 25a - Effect of Composition on the 2400°F Creep Behavior of Experimental Tantalum Alloys

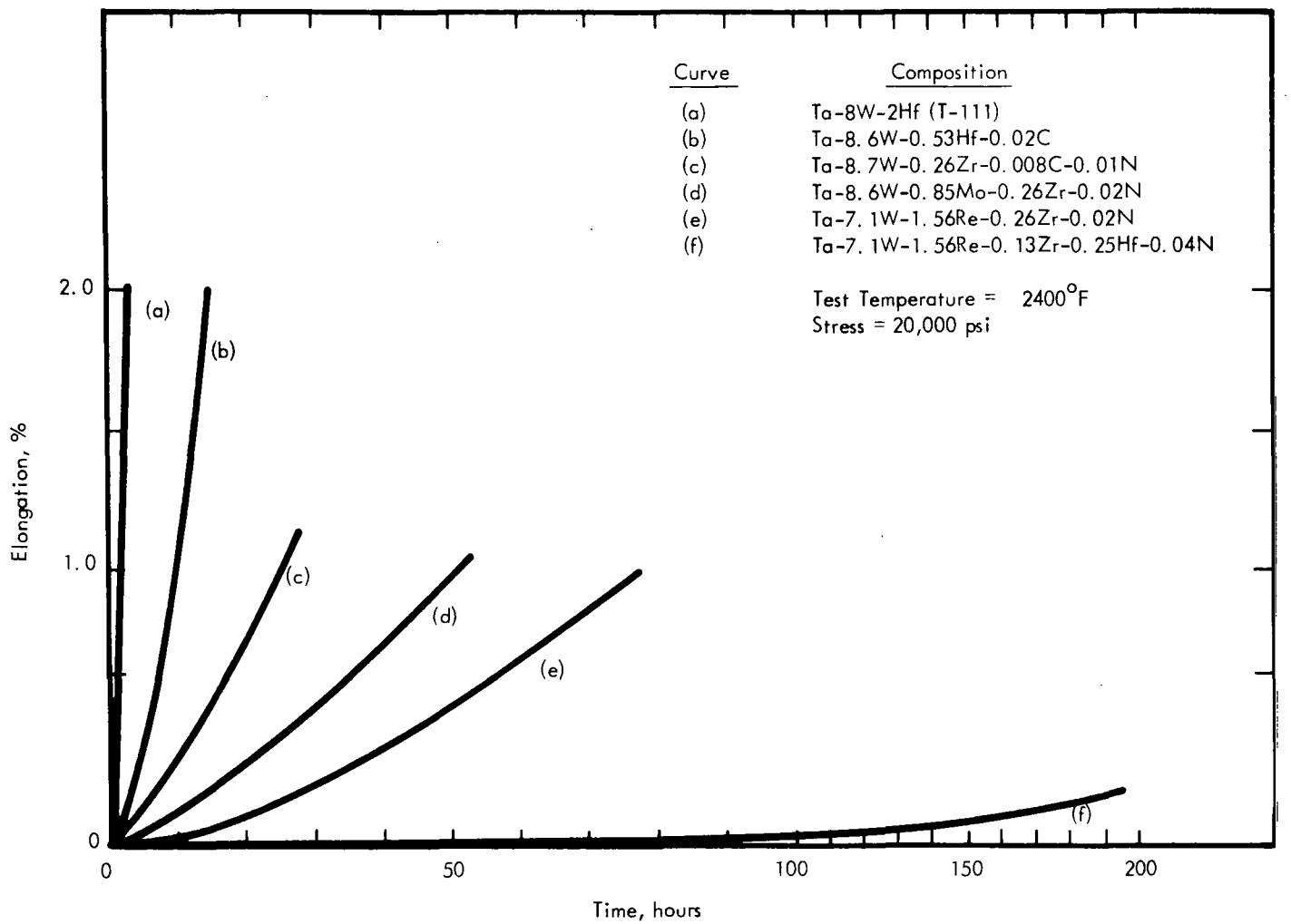

FIGURE 25b - Effect of Composition of the 2400°F Creep Behavior of Experimental Tantalum Alloys

compositions with a nitride dispersion exhibit better 2400°F creep resistance than those containing the carbide dispersion. The creep curves b, c, d and e in Figures 25a and 25b are for tantalum alloys having 9 atom percent substitutional solute additions (W+Mo+Re+Hf+Zr=9 a/o) and a carbon+nitrogen/hafnium+zirconium atom ratio of 0.5. As discussed earlier, the carbon precipitates as Ta_2C which contained little or none of the reactive metal additions. However, the nitrogen precipitates as the reactive metal mononitride, thus effectively removing the Hf and/or Zr from solid solution. As discussed earlier, increasing the reactive metal content generally resulted in a lowering of the creep resistance. As the volume fraction of nitride was increased, a further improvement in creep resistance was observed (see Figure 25b, curves e and f). The remarkable strength properties of the nitride bearing compositions is evidenced by the composition Ta-5.3W-0.65Mo-1.56Re-0.52Zr-0.08N. In the as-worked 33% prior reduction, the ultimate tensile strength at 2400°F was 105,000 psi and the 0.2% offset yield strength was 80,000 psi. When given a prior anneal of 1 hour at 3000°F which results in overaging, and then tested in creep at 2400°F and 20,000 psi, the specimen elongated 1 percent in 124 hours. Although this composition demonstrated remarkable strength properties, the fabricability and weldability characteristics were such that it could not be considered a sheet alloy; however, it does possess considerable potential as a bar and forging alloy.

Of the substitutional solute additions, the effect of rhenium additions on creep strength was most interesting. Rhenium substitution did not significantly improve the short time elevated temperature tensile properties (See Table 7) at levels up to 3%, although at this level, a significant degradation of the GTA weld bend ductility did occur. However, minor amounts of rhenium did exert a pronounced influence on creep behavior as illustrated in Figure 26. The interesting feature of Figure 26 is that the greatest improvement in creep resistance occurs after only about 1% rhenium is added and further additions result in essentially no further benefit. This is rather fortuitous since at the 9-10% solute level (W+Hf),substitution of 1% tungsten with rhenium has no adverse effect on low temperature bend ductility of GTA welded material. However at the 3% Re level the ductile brittle transition temperature has been raised to room temperature.

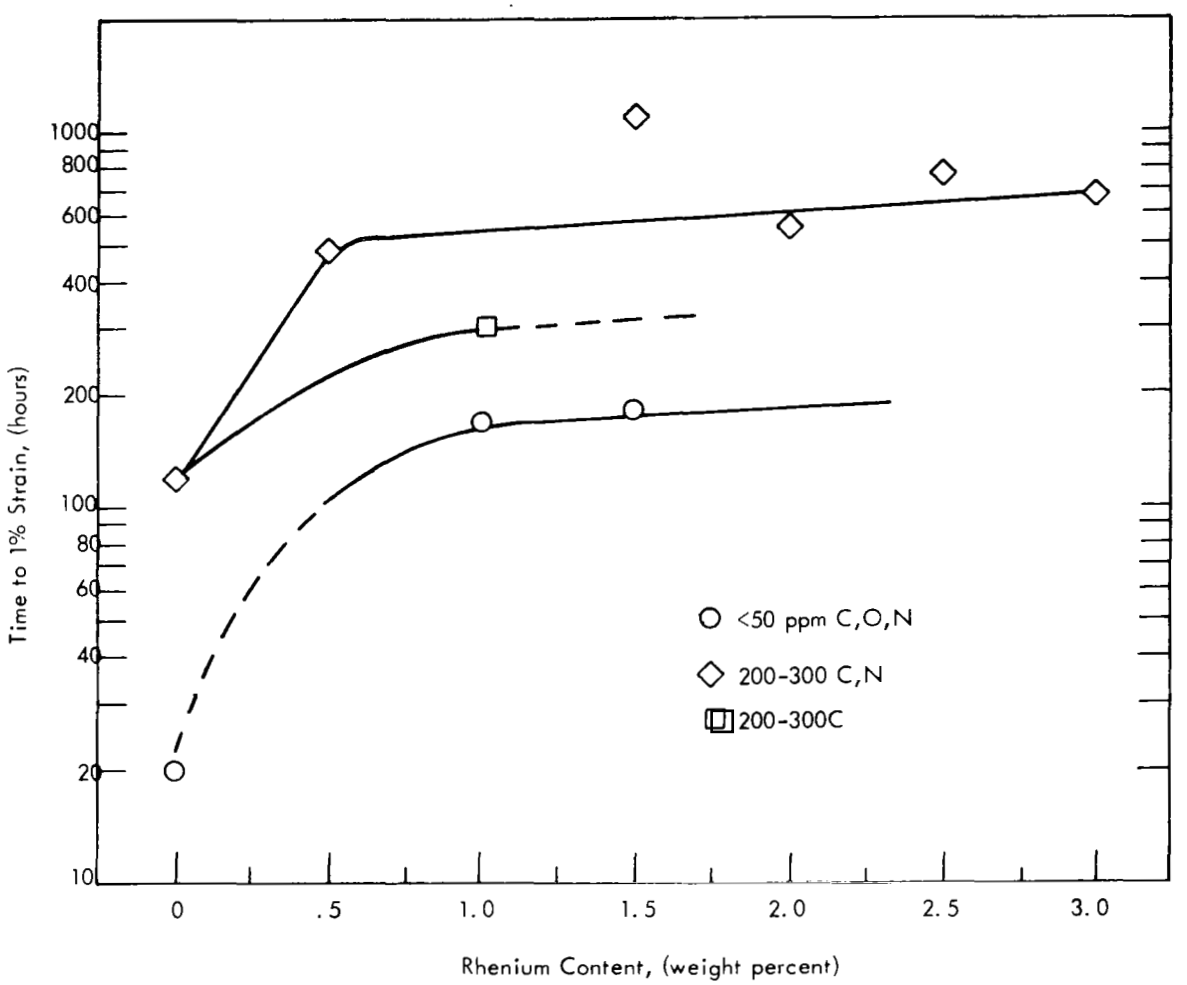

FIGURE 26 - Effect of Rhenium on Creep Properties of Ta-W-Hf Alloys Tested at 2400°F and 15,000 psi (Specimens Annealed 1 Hr. at 3000°F Prior to Test)

A fairly wide range of creep behavior was exhibited by the experimental tantalum alloy compositions investigated. The range of properties obtained which represent a significant improvement over the properties exhibited by T-111 are compared in Figure 27 on a parametric plot. The stress for time to 1% elongation is normalized using the Larson-Miller relation $P = To_R$ (constant + t) where t is the time in hours to elongate 1%. The value of 11.1 was used for the constant in the L-M expression since Sawyers and Steigerwald[24] found that it provided the best curve fit for their data. The data for T-111 generated by these investigators is included in Figure 27 and compares very well with the T-111 creep data generated during this program.

As has been discussed earlier, creep is a structure sensitive property and the influences of structure cannot be quantitatively defined at this time. However, a number of observations were made which illustrate the influence of structure on creep.

Grain Size. Increasing the final annealing temperature from 3000°F to 3270°F for Ta-9W-1Hf-0.025C resulted in an increase for the time to elongate 1% at 2400°F and 15,000 psi from 108 to 180 hours. Metallographic examination revealed no apparent difference in the dimetal carbide precipitate morphology or distribution although the final grain diameter had increased from 0.014 mm to 0.028 mm. (See Figure 28). Grain size has been shown to exert an effect on the creep and creep rupture behavior of pure metals and alloys with the bulk of the work reported on face centered cubic (FCC) materials.[47-52] For example, Feltham and Meakin[51] have shown for copper at 930°F ($0.6T_m$) that the creep rate is proportional to the square of the grain diameter, with the creep rate increasing with increasing grain diameter. A most significant observation however, is that there is an optimum grain size for optimum creep resistance[47-50]. This observation was made by Hanson[47] as early as 1939. Crussard[48] showed a minima in the secondary creep rate as a function of grain size for zinc tested at 200°F ($0.55T_m$) and aluminum tested at 390°F ($0.5T_m$). His explanation was based on transition of the major deformation process from the boundary to the grain as the volume-to-boundary ratio increased with each process of equal importance at the

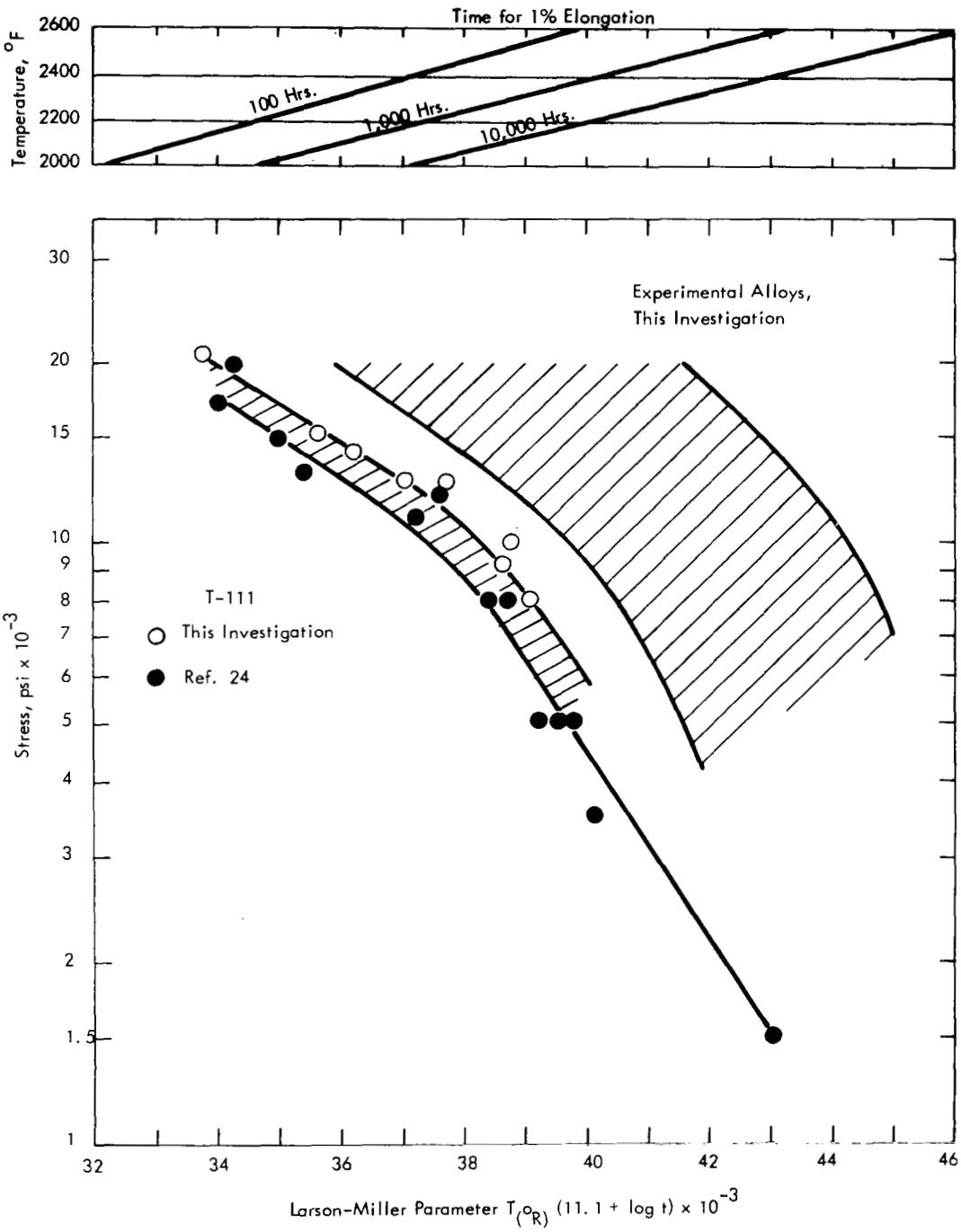

FIGURE 27 - Creep Behavior of Experimental Tantalum Base Alloys

1μ

(a) Annealed 1 Hr./3000°F then tested for 210 hours at 2400°F and 15,000 psi (G. S. - 0.014 mm) Mag. 1500X

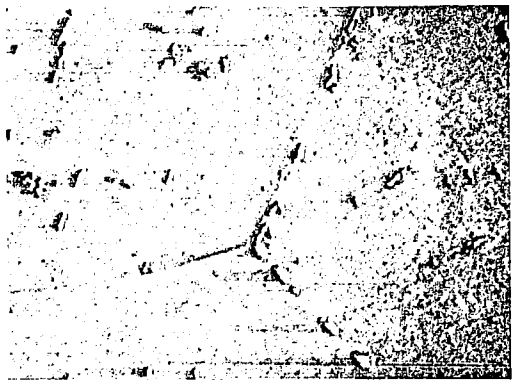

1μ

(b) Annealed 1 Hr./3270°F then tested for 500 hours at 2400°F and 15,000 psi (G. S. - 0.028 mm) Mag. 1500X

1μ

(c) Annealed 1 Hr./3270°F then tested for 500 hours at 2400°F and 15,000 psi (G. S. - 0.028 mm) Mag. 20,000X

FIGURE 28 - Effect of Final Annealing Temperature on Grain Size and Carbide Morphology and Distribution in Ta-9W-1Hf-0.025C

optimum grain size. Shahinian and Lane[49] in their study of monel described this behavior in terms of the equi-cohesive temperature (T_E)*. At low temperature ($< T_E$) increasing grain size caused reduced rupture life and increased the creep rate while at high temperature ($> T_E$) there was an optimum size for maximum rupture time which varied with test temperature and applied stress. Garafalo[50] also demonstrated similar high temperature behavior for an austenitic stainless steel. However, data reported has generally been for FCC solid solution strengthened metals and a paucity of data are available for BCC refractory metals. Begley and Cornie[53] have shown completely opposite behavior for a solid solution columbium base alloy and a carbide strengthened columbium base alloy where increasing grain size resulted in increased creep rate for the solid solution alloy while the creep rate of the carbide strengthened alloy decreased.

Although there was not an apparent change in the optically observable carbide precipitates, examination of the chemically extracted precipitates did reveal an influence of final annealing temperature on carbide morphology. The investigation of effect of final annealing temperature on creep behavior is covered in more detail under the scale-up section of this report. The control over the creep properties which can be exercised by varying thermal mechanical treatment is, however, a very important aspect, since fabricating considerations limit the total solute level which can be tolerated.

(d) Temperature Change Test. Since creep is thermally activated, creep behavior can be expressed in terms of the following equation:

$$\dot{\epsilon} = Ae^{-Q/RT}$$

Where $\dot{\epsilon}$ is the secondary creep rate, A is a constant, Q is the activation energy, R is the gas

---

*The temperature at which the failure mode changes from intragranular to intergranular.

constant and T is absolute temperature. Both A and Q are dependent on the applied stress, test temperature, and merallurgical structure. To evaluate the activation energy, a series of temperature changes were made during the creep testing of Ta-5W-1Re-0.3Zr-0.03N. The initial test conditions were 2400°F and 15,000 psi. The temperature was decreased in three stages to approximately 2000°F. The creep behavior is shown in Figure 29. Using the creep rate just preceding and following the temperature change values for the activation energy were obtained and are listed below in Table 10.

TABLE 10 - ACTIVATION ENERGY VALUES FOR Ta-5W-1Re-0.3Zr-0.03N ALLOY TESTED IN CREEP AT AN APPLIED STRESS OF 15,000 PSI

T_1 (°F)	T_2 (°F)	$\dot{\epsilon}_1$ (%/hour)	$\dot{\epsilon}_2$ (%/hour)	Q kcal/mole
2400	2350	0.0374	0.0268	58.3
2350	2257	0.014	0.014	95.2
2257	1987	0.027	0	∞

The activation energy for self diffusion of tantalum has been reported to be 110,000 cal/mole[54] and it has been generally observed that the activation energy for creep at temperatures above $0.5\ T_m$ corresponds to the activation energy for self diffusion[50]. It has been postulated that the rate controlling mechanism is one of dislocation climb [55]. The range of test temperatures used for this test was 0.42 to 0.48 Tm. The value of the apparent activation energy increased with decreasing test temperature. The rapid increase in Q over the rather narrow temperature range is similar to the effect that was observed by Dorn[56] when testing an Al-Mg alloy. There is apparently a change in structure which resulted in the drastic change in creep behavior. Identification of the rate controlling mechanisms of creep in the bcc tantalum alloys is an area where much work yet remains to be done.

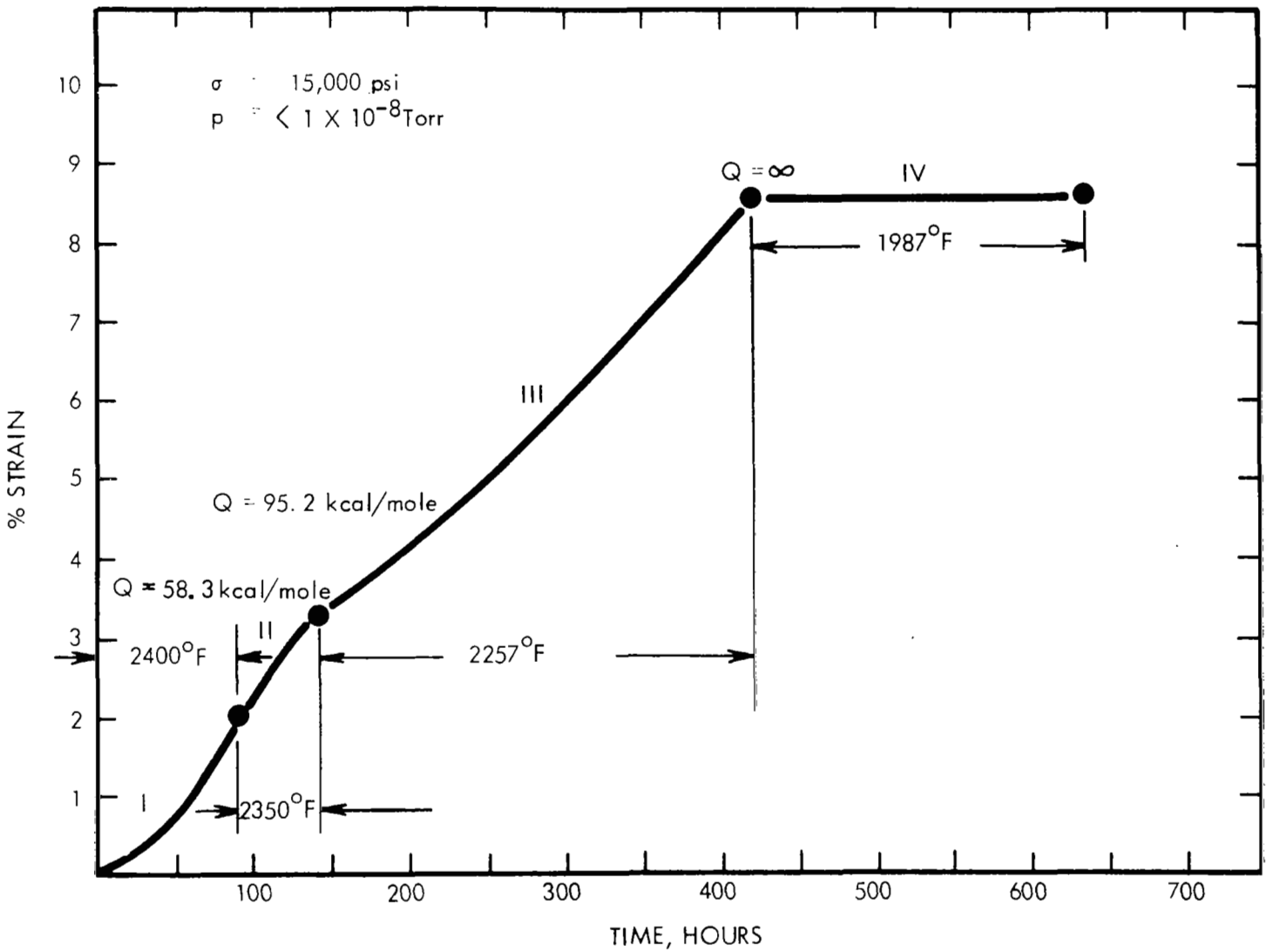

FIGURE 29 - Temperature Dependence of Creep Behavior of Ta-5W-1Re-0.3Zr-0.03N

6. Phase Relationships. The intersection of the phase field boundaries in the tantalum rich corner of the (Ta+W)-Hf-C phase diagram, 2400°F isotherm, is shown in Figure 30. The boundaries were established by identifying bulk extracted residues (See Appendix IV for detailed procedure) from specimens that had been solution annealed and aged for times up to 1000 hours. All aging exposures greater than 10 hours were done at $\leq 1 \times 10^{-8}$ torr to limit oxygen contamination. The lattice parameters of the dimetal carbide phase varied from $a_o = 3.10$ to 3.11 Å and $c_o = 4.92$ to 4.96 Å. These values compare closely with the reported values for Ta_2C[57,58] of $a_o = 3.106$ Å and $c_o = 4.945$ Å. Only minor substitution of W and/or Hf for Ta occurs in Ta_2C[57,58]. To stabilize the monocarbide $(Ta\ Hf)C_{1-x}$ at the 500 ppm carbon level requires approximately 3% reactive metal (Hf+Zr) addition. However, as illustrated previously, an excessive amount of reactive metal severely degrades the time dependent properties.

The substitution of 1% rhenium for an equivalent amount of tungsten in a Ta-9W-1 Hf-0.025C alloy did not result in any alteration of the composition of the precipitating phases. When all of the carbon was replaced with nitrogen, only the reactive metal mononitride (HfN_{1-x}, ZrN_{1-x}, or $(Hf\ Zr)N_{1-x}$) was formed. Substitution of a portion of the carbon with nitrogen in compositions containing 0.5 atom percent Zr+Hf and up to 300 ppm carbon and nitrogen with the C/N atom ratio equal to unity resulted in the following two reactions at 2400°F.

1. $\left[Ta\text{-}9(W+Re+Mo)+0.5(Zr+Hf)\right]_{SS} + C_{SS} + N_{SS} \rightleftharpoons Ta_2C + \left[Matrix\right]_{SS}$
2. $\left[Ta\text{-}9(W+Re+Mo)+0.5(Zr+Hf)\right]_{SS} + C_{SS} + N_{SS} \rightleftharpoons Ta_2C + (Zr,Hf)N_{1-x} + \left[Matrix\right]_{SS}$

Reaction (1) occurred in solution annealed material subsequently aged for 1-16 hours at 2400°F and reaction (2) occurred when the aging time was much greater than 16 hours. Transmission electron micrographs of bulk extracted residues from a Ta-5.7W-1.56Re-0.7Mo-0.25Hf-0.13Zr-0.015C-0.015N specimen solution annealed for 1 hour at 3270°F and aged for 820 hours at 2400°F are shown in Figure 31. The structure of individual particles was determined

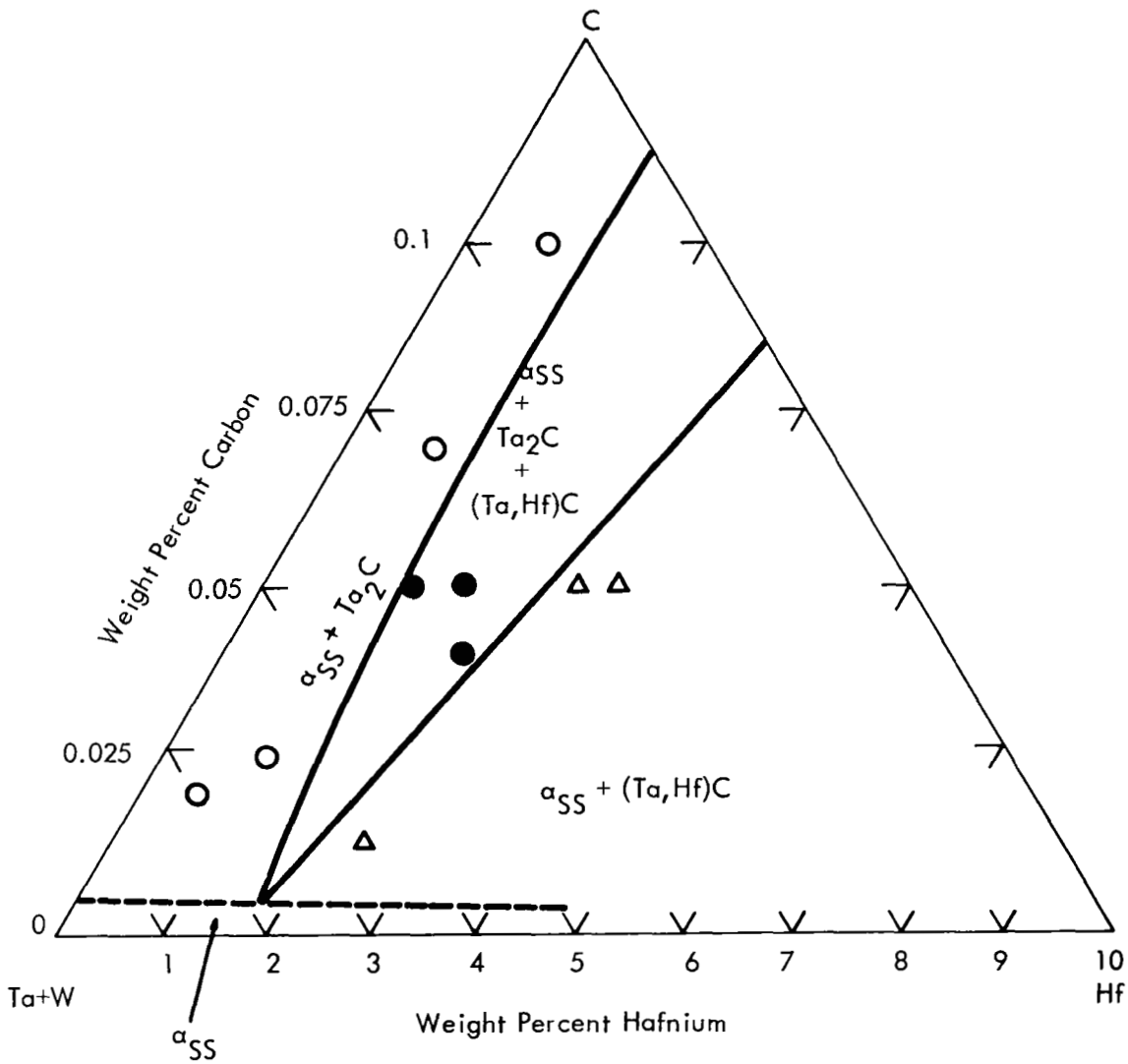

FIGURE 30 - Tantalum Rich Corner of the (Ta+W)-Hf-C Psuedo Ternary Phase Diagram 2400°F Isotherm

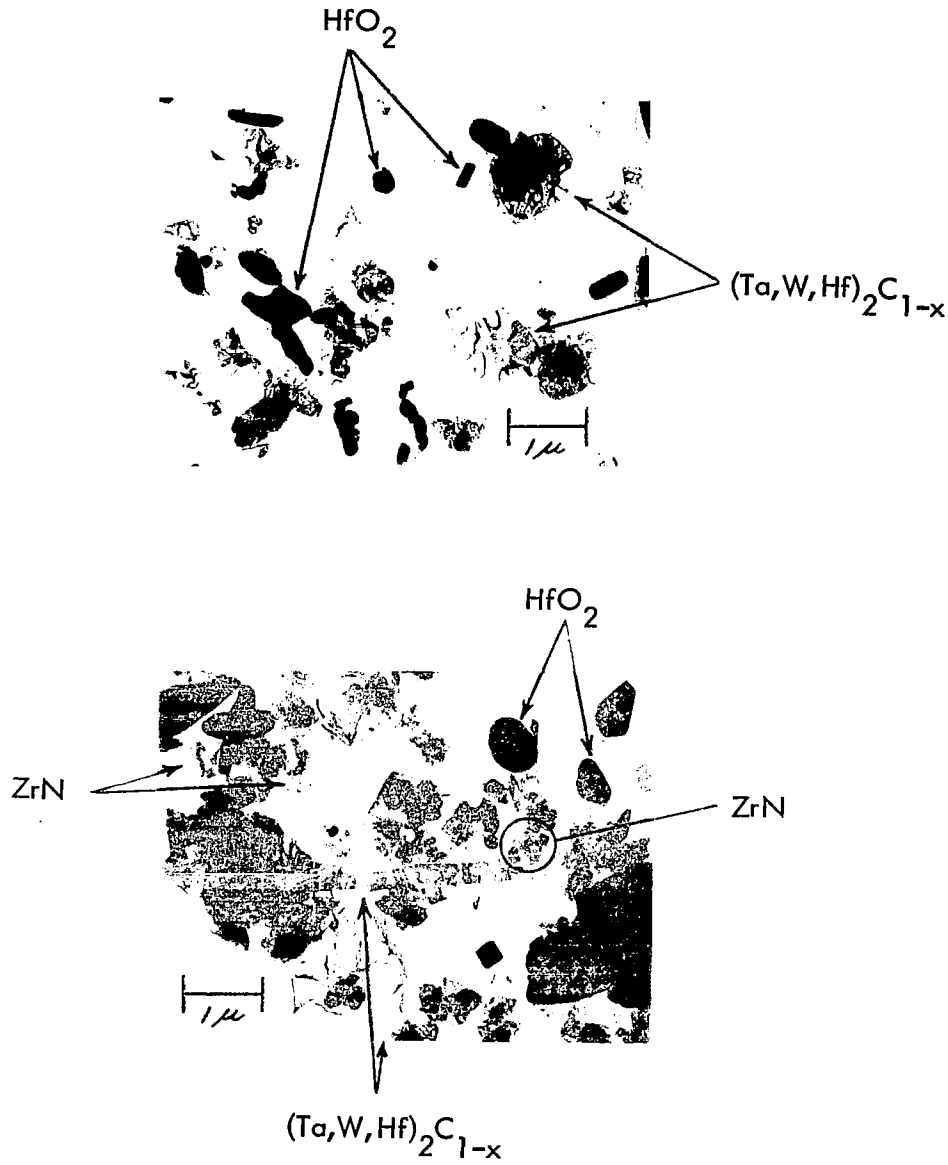

FIGURE 31 - Transmission Electron Micrograph of Precipitates Extracted from Ta-5.7W-1.56Re-0.7Mo-0.25Hf-0.13Zr-0.015C-0.015N Alloy, Solution Annealed 1 Hr. at 3270°F and Aged for 820 Hrs. at 2400°F

by selected area electron diffraction. A minor amount of ZrO_2 and/or HfO_2 precipitates were generally found in all the extracted residues even though the total oxygen content of the sample was generally much less than 50 ppm. Thus the oxygen solubility in the alloy matrix is extremely low. The dimetal carbide phase was generally more massive than was the mononitride.

When the reactive metal (Zr+Hf) content was increased above 3/4 atom percent, the precipitation reaction (1) was again observed for short time (<16 hours) aging exposures at 2400°F. However as the exposure time was increased to longer times (i.e., >16 hours), the Ta_2C phase completely disappeared and was replaced by a FCC phase identified as the reactive monometal carbonitride $(Ta,Hf,Zr)(C,N)_{1-x}$.

The rather interesting feature of the nitride precipitation reaction in the tantalum alloy matrix is its apparent sluggishness. This precipitation reaction is occurring over a long time period and thus could explain the higher creep resistance of the nitride bearing compositions. However, the nitride reaction involves removal of the reactive metal from solid solution also and this in itself could make a positive contribution to the creep resistance.

E. CONCLUSION - PHASE I SCREENING INVESTIGATION

It was demonstrated during the Phase I screening investigation that significant improvements in the creep resistance of tantalum alloys could be achieved without compromising low temperature fabricability and as-welded ductility. A number of conclusions can be drawn from the results obtained during this phase of the investigation and are enumerated as follows:

1. Tantalum containing 8-10%W+0.5-1.5%Re+1%Hf can withstand carbon additions up to 300 ppm without seriously degrading as-welded bend ductility.

2. The amount of rhenium and hafnium were both shown to be critical and that for optimum creep resistance without compromising low temperature ductility, rhenium should be present in an amount of 0.5 to 1.5% and hafnium 0.5 to 1%.

3. The carbide phase Ta_2C makes a significant contribution to the creep properties.

4. Nitrides are much more effective as a dispersed phase strengthener than the carbides, but because of the deleterious effect of nitrogen on the low temperature ductility of the tantalum alloy matrix, nitrogen is not as desirable an addition as carbon.

5. The final annealing temperature has a pronounced effect on the creep behavior of tantalum alloys containing carbides.

III. PHASE II - SCALE-UP INVESTIGATION

During this phase of the experimental investigation, three compositions were selected based on the results of the Phase I screening investigation. These compositions which are,

1. Ta-8W-1Re-0.7Hf-0.025C (ASTAR-811C)
2. Ta-8W-1Re-1Hf
3. Ta-7W-1Re-1Hf-0.012C-0.012N

were melted as four inch diameter ingots weighing approximately 85 pounds. The ingots were processed to 0.04 inch sheet which was subjected to detailed evaluation to characterize the low temperature base metal and weld metal ductility and elevated temperature mechanical properties. Experimental procedures used during this phase of the investigation were similar to those described previously under Phase I - Screening Investigation.

A. EXPERIMENTAL RESULTS AND DISCUSSIONS

1. Melting. Each of the three compositions were prepared by the double consumable electrode vacuum arc melting technique. Two first melt electrodes, each weighing approximately 40 pounds, were required for each heat. Sandwich type electrodes were fabricated from alloy and elemental metal strip. A typical cross-section of a first melt electrode is shown in Figure 32. The average cross-section composition of each electrode was the nominal value for each element except the nitrogen addition. A 30% excess nitrogen was added to the first melt electrode to compensate for anticipated loss during the double melting operation.

The first melt electrodes were cast into a water cooled 2-1/2 inch diameter copper mold using AC power. A total of four first melt ingots were produced for each heat. The ends of the first melt ingots were faced, butted together, and then welded to form the second melt electrode which was then cast into a 4 inch diameter mold using DC power since there was insufficient A.C. power to make the second melt.

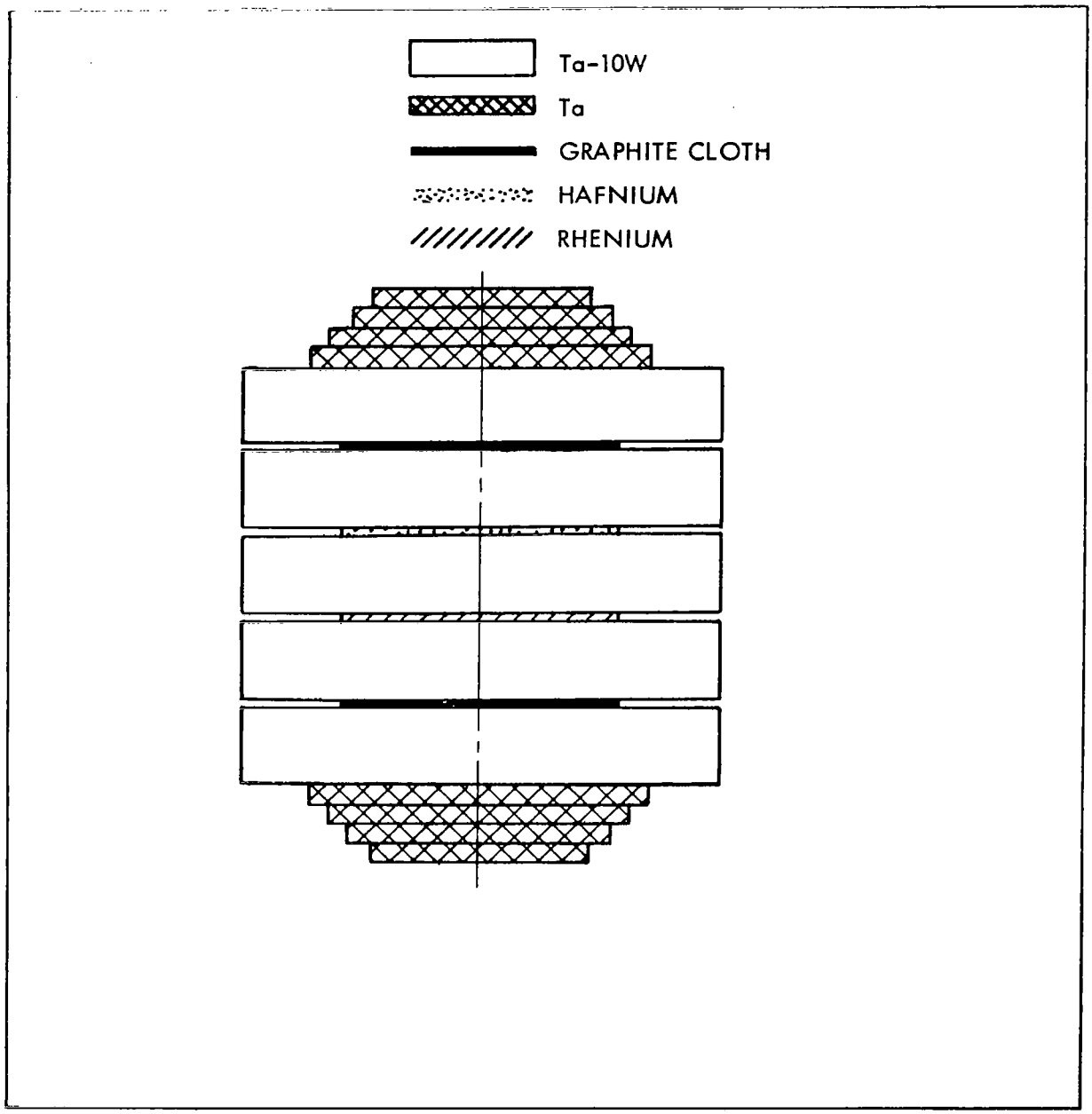

FIGURE 32 - First Melt Electrode Configuration for Ta-8W-1Re-0.7Hf-0.025C (ASTAR-811C)

First and second melt data for all three compositions are listed in Table 11 and a first and final melted ASTAR-811C ingot are shown in Figures 33 and 34 respectively. The total time required for casting the final ingot was about 22 minutes with the last five minutes of melting used to hot top the ingot. Prior to arc initiation the furnace chamber was evacuated to $< 1 \times 10^{-5}$ torr and during melting the pressure in the chamber was generally less than 5×10^{-4} torr.

(a) Ingot Chemistry. Samples were removed from the top and bottom of each ingot and analyzed for the metallic and interstitial additions. The chemical analysis results summarized in Table 12 illustrate the excellent compositional control achieved by the melting techniques used.

(b) Ingot Microstructure. The as-cast microstructure of the Ta-8W-1Hf alloy was essentially single phase (See Figure 35a) while the other two compositions to which an intentional carbon and/or nitrogen addition had been made contained a dispersed second phase (See Figure 35b and 35c). The metallographic samples are from the bottom portion of the ingot. The dispersed phase shown in Figure 35b and 35c was chemically extracted and identified as Ta_2C.

2. Primary and Secondary Working. Sections of the as-cast ingot 4 inch diameter x 1 inch thick were either upset forged at 2550°F by a single blow on the Dynapak or 4 inch diameter x 5 inch long sections of ingot were side forged using multiple blows on the Dynapak. The forged billets were conditioned and annealed and rolled to 0.04 inch sheet by a combination of warm rolling (500-800°F) and cold rolling. The processing sequence used to process all three scale-up compositions is described in Figure 36. All three compositions exhibited excellent primary and secondary working characteristics. Typical examples of the excellent quality upset and side forged billets, as rolled plate and final sheet are illustrated in Figures 37 and 38. Results of the primary working operations are summarized in Table 13. The excellent working characteristics exhibited by these compositions at the 4 inch diameter ingot

TABLE 11 - FIRST AND SECOND MELT DATA FOR SCALE-UP ALLOYS

Composition (Heat No.)	Melt	Melt Parameters (c)		
		Volts	Power (K.W.)	Melt Rate(lbs/min)
Ta-8W-1Re-0.7Hf-0.025C (NASV-20) ASTAR-811C	1st(a)	29 ac	95	6.2
	2nd	30 dc	175	3.5(b)
Ta-8W-1Re-1Hf (NASV-22)	1st(a)	29 ac	92	6.5
	2nd	29 dc	170	3.1(b)
Ta-7W-1Re-1Hf-0.012C-0.012N (NASV-23)	1st (a)	29 ac	92	6.2
	2nd	30 dc	170	3.1(b)

(a) Values are average of four first melts per composition

(b) Based on total melt duration which includes time for hot topping

(c) Chamber pressure during all melting was less than 5×10^{-4} Torr

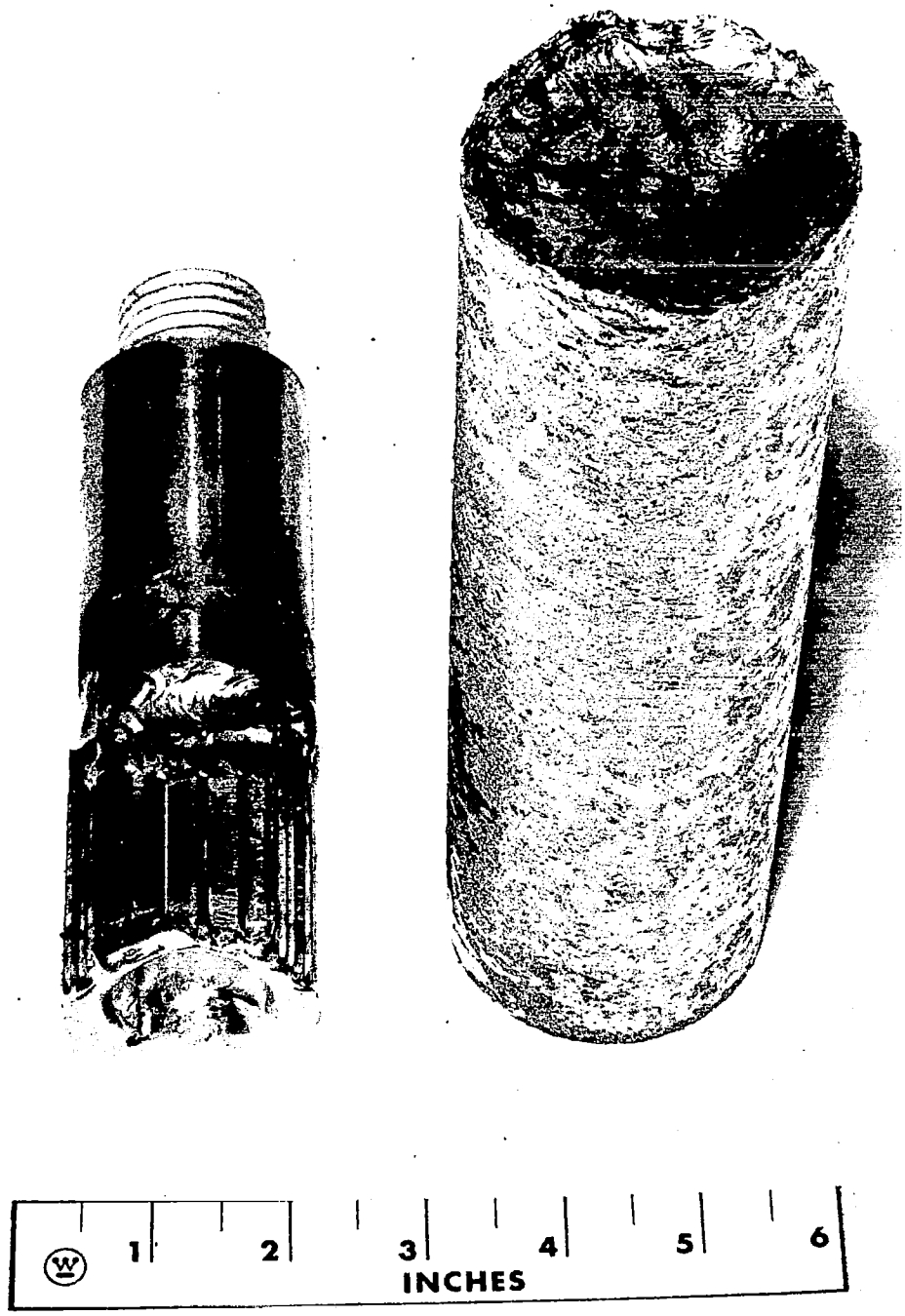

FIGURE 33 - ASTAR-811C First Melt Ingot

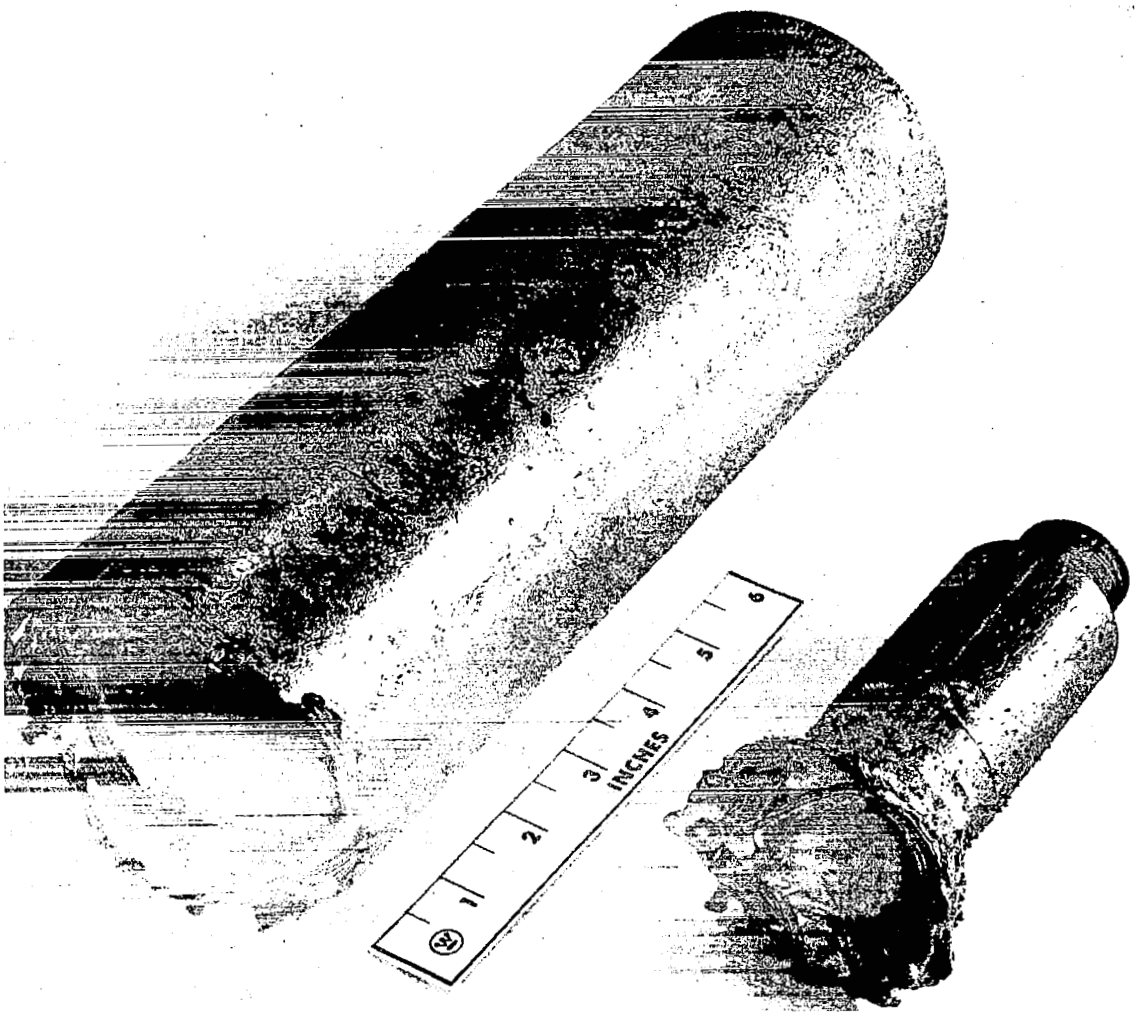

FIGURE 34 – ASTAR-811C Four Inch Diameter Ingot

TABLE 12 - CHEMICAL ANALYSIS RESULTS FOR FOUR INCH DIAMETER INGOTS

Nominal Composition w/o	Ingot Location	Chemical Analysis, weight percent					
		W	Hf	Re	C	N	O
Ta-8W-1Re-0.7Hf-0.025C (ASTAR-811C)	Top Bottom	7.4 7.2	0.71 1.01	1.04 0.92	0.024 0.023	0.0013 0.0027	0.0006 0.0021
Ta-8W-1Re-1Hf	Top Bottom	7.8 7.5	0.95 1.06	1.04 0.99	0.0009 0.0016	0.0010 0.0013	0.0012 0 0020
Ta-7W-1Re-1Hf-0.012C-0.012N	Top Bottom	6.5 6.4	0.98 1.01	1/05 1.01	0.013 0.011	0.013 0.011	0.0018 0.0018

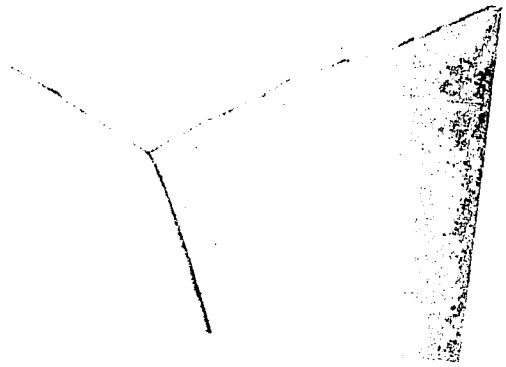

(a) Ta-8W-1Re-1Hf
As-Cast Hardness - 231 DPH

(b) Ta-8W-1Re-0.7Hf-0.025C
ASTAR-811C
As-Cast Hardness - 237 DPH

(c) Ta-7W-1Re-1Hf-0.012C-0.012N
As-Cast Hardness - 300 DPH

FIGURE 35 - As-Cast Microstructure and Hardness of Scale Up Ingot Compositions
Mag = 500X

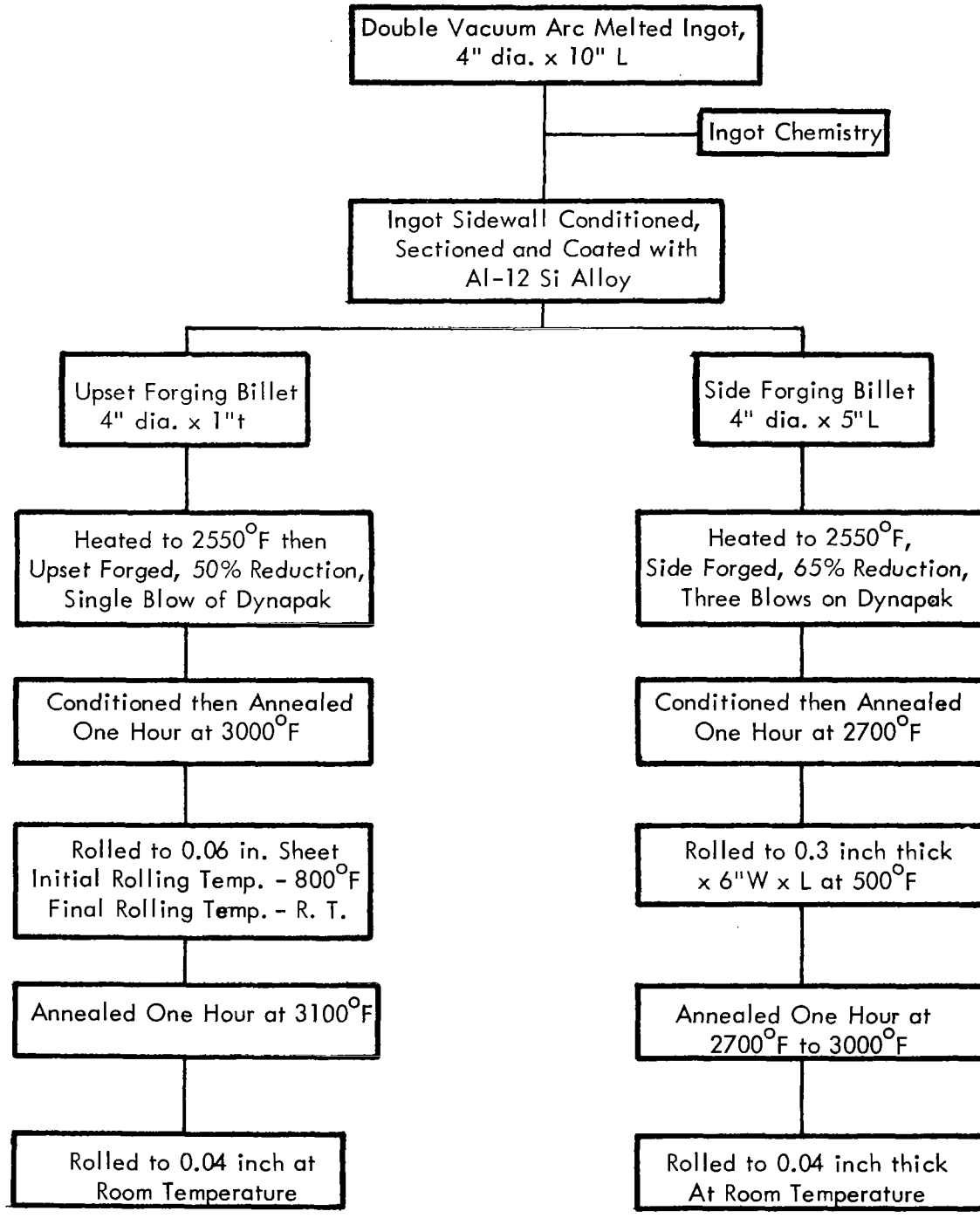

FIGURE 36 - Processing Schedule for Scale-Up Alloy Compositions

(a)

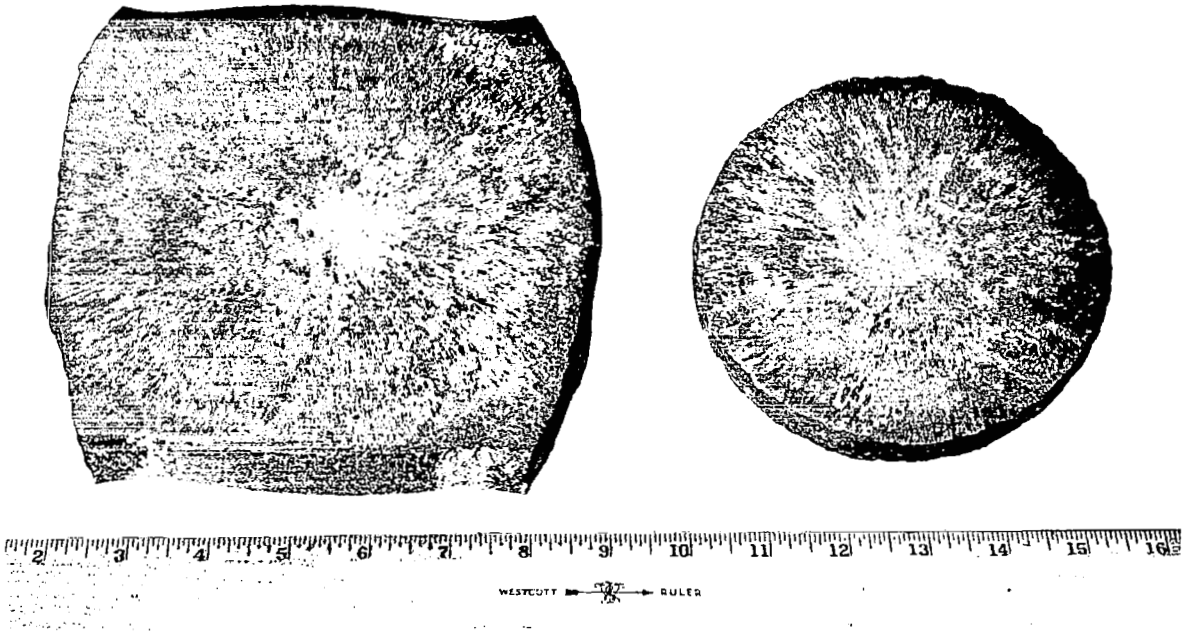

(b)

FIGURE 37 - (a) Al-12Si Coated ASTAR-811C Forging Billet and (b) Side Forging and Upset Forging

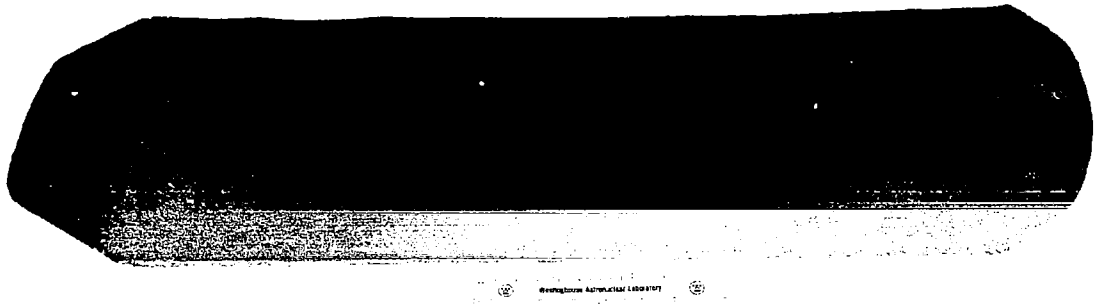

(a)

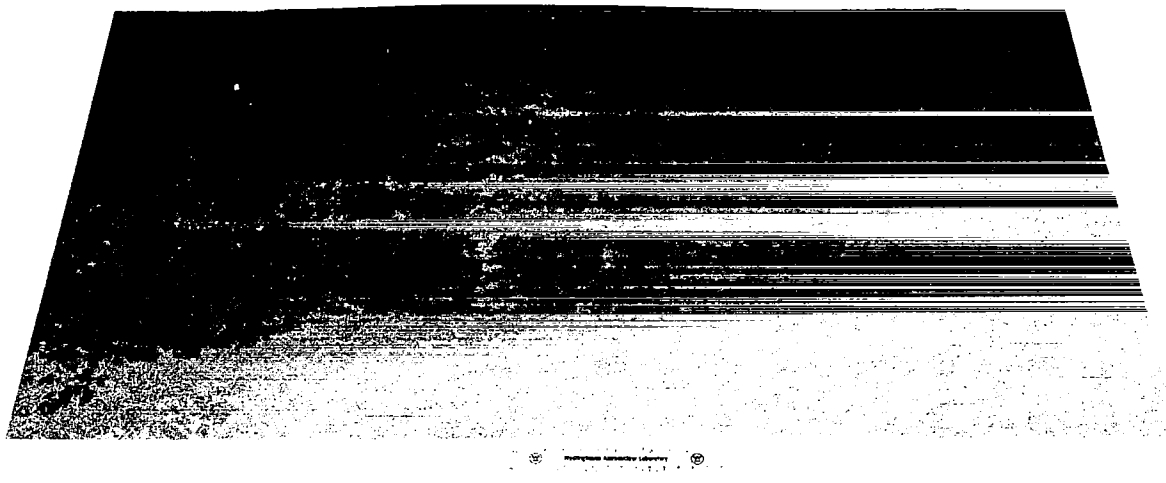

(b)

FIGURE 38 - (a) As-Rolled 1/4 Inch Thick ASTAR-811C Plate and (b) As-Rolled 0.04 Inch Thick ASTAR-811C Sheet

TABLE 13 - FORGING RESULTS FOR SCALE-UP COMPOSITIONS

Composition/Heat No.	Type of Forging	Forging Temperature (°F)	Billet Dimensions, Inches				Thickness Reduction (%)	K Forging Constant[d] (psi)	DPH	
			Initial		Final				Initial	Final
			Dia.	Height	Dia.	Thickness				
Ta-8W-1Re-0.7Hf-0.025C	Upset	2550	3.9	1	5.9	0.38	62	115,000	237	338
(NASV-20) ASTAR-811C	Upset	2550	3.9	1.4	4.9	0.82	40	146,000	---	---
	Upset	2550	3.9	1.4	5.8	0.57	59	130,000	---	---
	Side	2550	3.9	5	7.2 x 7.5 x	1.13	67	111,000	237	318
Ta-8W-1Re-1Hf (NASV-22)	Upset	2550	3.9	1	5-1/4	0.44	56	---	230	292
	Upset	2550	3.9	1.1	6.4	0.38	66	108,000	---	---
	Upset	2550	3.9	1.1	6.2	0.42	63	116,000	---	---
	Side	2550	3.9	5	7.5 x 7-3/4 x	1.17	66	99,000	---	---
Ta-7W-1Re-1Hf-0.012C	Upset	2550	3.9	1	5-1/4	0.44	56	---	300	355
-0.012N (NASV-33)	Upset	2550	3.9	1.4	5.5	0.67	51	147,000	---	---
	Side	2550	3.9	5	7 x 7-1/4 x	1.28	63	146,000	---	---

a) $K = \frac{E}{V Z}$ where E = energy used, V = volume of material deformed, Z = emperical factor

b) Forged with 3 successive blows of Dynapak. No reheat between blows.

c) Corrected for geometry

size is indicative that scale-up to larger ingot sizes is readily feasible. The primary working characteristics of all three compositions is very similar to that exhibited by T-111, which is successfully being produced on a commercial basis.

The final as-rolled sheet was of excellent quality and the secondary working characteristics are essentially identical to those of T-111. Chemical analyses for interstitials on the final sheet confirm the absence of contamination pickup during processing. (See Table 14).

3. Recrystallization Behavior and Grain Growth Characteristics. The recrystallization behavior of all three compositions was very similar as might be expected since only minor compositional variations exist between them. The 1 hour recrystallization behavior for as-worked sheet is summarized in Table 15. Plotted on Figure 39 is the 1 hour recrystallization behavior of all three scale-up compositions which were cold worked nominally 80 percent prior to annealing. Also included is the isochronal curve for T-111. The three scale-up compositions exhibit almost identical annealing response as T-111. However, the compositions containing intentional interstitial additions exhibit an increase in hardness on annealing at temperatures above 2550°F. This increase is attributed to resolutioning of the carbides. The higher hardness levels at room temperature of the nitrogen containing composition is due to the absence of any nitride precipitates after the 1 hour annealing treatments. Thus the nitrogen is retained in solid solution and as has been shown earlier exerts a pronounced effect on the low temperature strength of tantalum.

The recrystallized grain size after the 1 hour annealing treatment was similar for all three compositions after equivalent prior reductions. The similarity in recrystallized grain size would indicate that the dispersed second phase is ineffective as a grain refiner. Or, it may be that the very small amount of second phase observed in the solid solution alloy (Ta-8W-1Re-1Hf) is sufficient to cause grain refinement. As shown by the plot in Figure 40, the

TABLE 14 - CHEMICAL ANALYSIS RESULTS FOR FINAL 0.04 INCH SHEET

Composition	Condition	Chemical Analysis, weight percent			
		Carbon	Oxygen	Nitrogen	Hydrogen
Ta-8W-1Re-1Hf (NASV-22)	As Rolled	--	0.0009	--	--
	1 hr at 3000°F	--	0.0009	--	--
	1 hr at 3000°F[(a)]	0.0020	0.0014	0.0011	0.0001
Ta-8W-1Re-0.7Hf-0.025C (NASV-20), ASTAR-811C	1 hr at 3000°F	0.020	0.0013	0.002	--
Ta-7W-1Re-1Hf-0.012C-0.012N (NASV-23)	As Rolled	0.0148	--	--	--
	1 hr at 3000°F	0.0151	--	--	--
	1 hr at 3000°F[(a)]	0.0126	0.0016	--	0.0004

(a) Chemical Analysis Performed at G. E., Evendale, Ohio

TABLE 15 - RECRYSTALLIZATION BEHAVIOR OF SCALE-UP TANTALUM BASE ALLOYS

Composition	Sheet Thickness (Inches)	Prior Cold Reduction (%)	DPH[a], Microstructure[b], and Grain Size[c] after annealing for one hour at Indicated Temperature, °F								
			As Rolled	2190	2370	2550	2730	2910	3090	3270	3450	3630
Ta-8W-1Re-0.7HI-0.025C ASTAR-811C	0.04	33	321	282	283	263	258	254	245	240	248	246
			W	W	W	R_5	R_X	R_X	R_X	R_X	R_X	R_X
			---	---	---	---	0.020	0.023	0.043	0.063	0.091	0.182
	0.04	83	350	313	249	232	258	251	257	242	242	248
			W	R_5	R_{50}	R_X	R_X	R_X	R_X	R_X	R_X	R_X
			---	---	---	---	0.0009	0.013	0.025	0.048	0.120	0.200
	0.06	73	387	319	252	245	263	260	253	253	250	248
			W	R_{50}	R_{90}	R_X	R_X	R_X	R_X	R_X	R_X	R_X
			---	---	---	0.011	0.013	0.017	0.033	0.057	0.091	0.167
Ta-8W-1Re-1Hf	0.04	33	280	225	232	228	216	206	200	201	200	198
			W	W	W	R_5	R_{90}	R_X	R_X	R_X	R_X	R_X
			---	---	---	---	---	0.047	0.048	0.091	0.108	0.148
	0.06	83	331	308	260	218	217	217	219	215	216	213
			W	W	R_5	R_{90}	R_X	R_X	R_X	R_X	R_X	R_X
			---	---	---	---	0.016	0.02	0.039	0.052	0.08	0.129
Ta-7W-1Re-1Hf-0.012C-0.012N	0.04	33	333	319	301	288	281	293	298	296	282	276
			W	W	W	W	R_{35}	R_X	R_X	R_X	R_X	R_X
			---	---	---	---	---	0.033	0.047	0.058	0.115	0.175
	0.06	85	389	355	336	302	304	312	311	318	294	282
			W	W	W	R_5	R_{95}	R_X	R_X	R_X	R_X	R_X
			---	---	---	---	---	0.016	0.035	0.048	0.095	0.170

(a) 30 Kg Load

(b) Microstructure - W = Wrought

R_n = n equal % recrystallized grains

R_X = 100% recrystallized grains

(c) Grain Size in mm determined by line intercept method

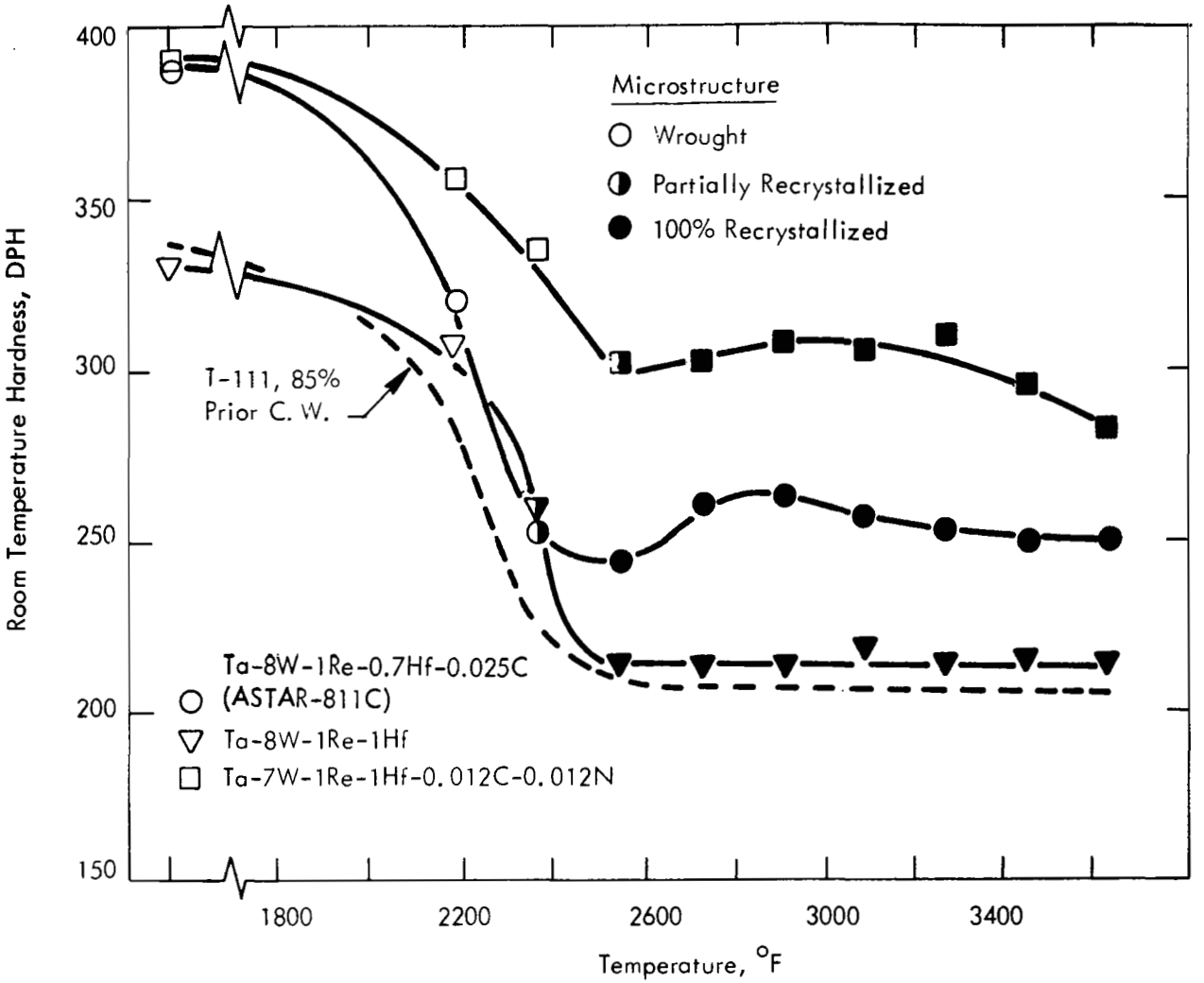

FIGURE 39 - One Hour Recrystallization Behavior of Scale-Up Compositions

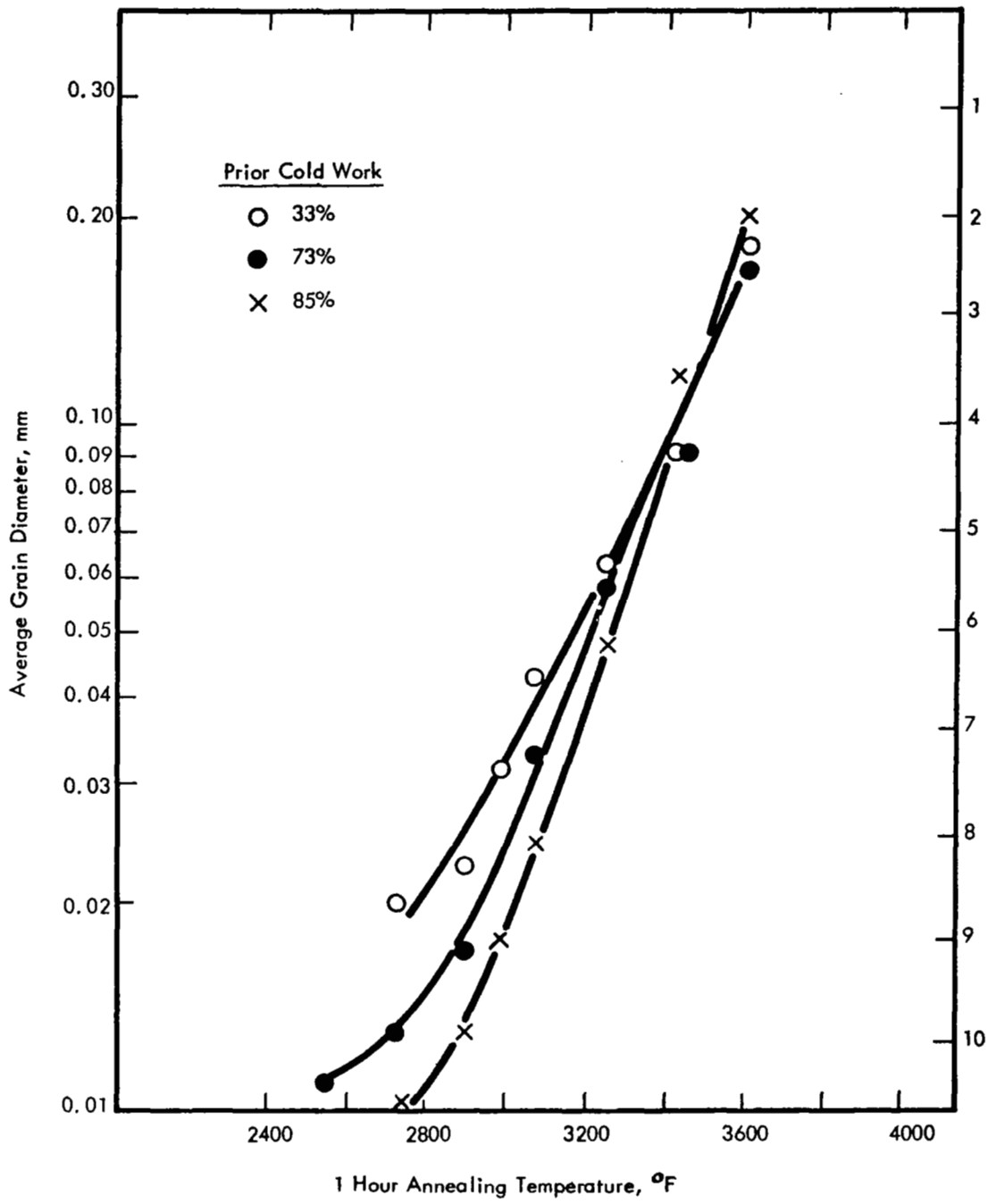

FIGURE 40 - Effect of Prior Cold Work on the Recrystallized Grain Size of ASTAR-811C(Ta-8W-1Re-0.7Hf-0.025C)

greater the amount of prior reduction the finer the as recrystallized grain size. At annealing temperature above about 3300°F though, grain growth is so rapid that the amount of prior cold work had essentially no effect on the final grain size after the 1 hour annealing treatment.

The grain growth characteristics of sheet cold worked 80% was determined at temperatures of 3270, 3450, 3630 and 3810°F at annealing times of 1/2, 5 and 15 minutes. The annealing sequence consisted of slowly heating the specimen to about 2200°F to remove the adsorbed gas from the specimen and furnace components and to maintain the pressure at $\leq 1 \times 10^{-5}$ torr. The specimen was then heated to the test temperature within 5-10 seconds. After the prescribed time, the furnace power was shut off and the furnace chamber immediately back filled with helium gas to accelerate cooling. The grain sizes after the various annealing treatments, determined by the line intercept method, are listed in Table 16. Under isothermal conditions, grain size (D) varies with time (t) according to the following expression:

$$D^2 = K \gamma V t$$

Where the surface energy of the boundary (γ) is the driving force for boundary migration. K is the rate constant and V is the grain atomic volume. The good linear fit when the grain diameter is plotted as a function $\sqrt{t}$ is illustrated in Figure 41. The slope of this curve $\frac{\partial D}{\partial t^{1/2}}$ is proportional to $\sqrt{K}$ the parabolic rate constant which varies with temperature according to the familiar Arrhenius rate equation:

$$K = K_o \exp^{-Q/RT}$$

where Q is the activation energy for boundary migration, R is the gas constant, T is absolute temperature and K_o is a proportionality constant. The value of the activation energy calculated from the slope of the log D^2/t vs 1/T plot shown in Figure 42 yielded a value of Q = 92 kcal/mole.

TABLE 16 - EFFECT OF ANNEALING TIME AND TEMPERATURE ON GRAIN SIZE

Composition	Annealing Time (Minutes)	Grain Size (in mm) after annealing at indicated Temperature, °F			
		3270	3450	3630	3810
Ta-8W-1Re-1Hf	1/2	0.016	0.024	0.029	0.042
	5	0.024	0.038	0.077	0.098
	15	0.045	0.079	0.118	0.186
Ta-8W-1Re-0.7Hf -0.025C (ASTAR-811C)	1/2	0.016	0.021	0.033	0.038
	5	0.026	0.030	0.067	0.093
	15	0.045	0.065	0.100	0.178
Ta-7W-1Re-1Hf -0.012C-0.012N	1/2	0.013	--	0.031	--
	5	0.026	--	0.067	--
	15	0.039	--	0.107	--

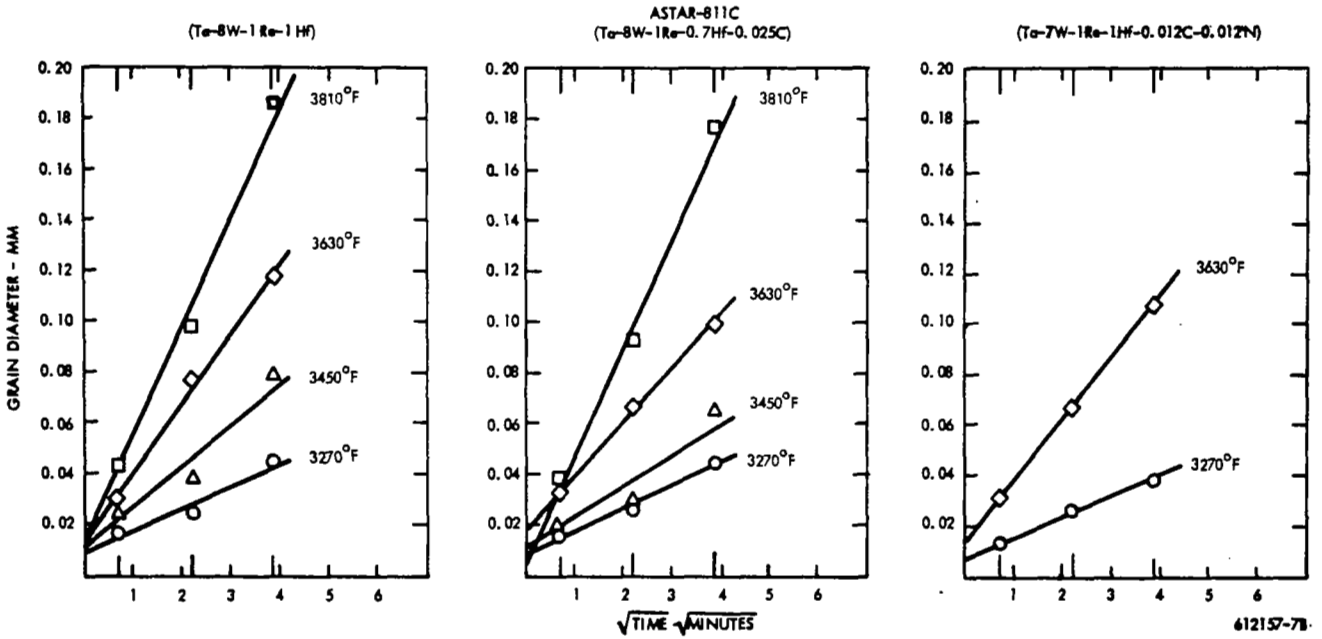

FIGURE 41 - Grain Growth Behavior of Scale-Up Alloy Sheet (Prior Cold Reduction, 80%)

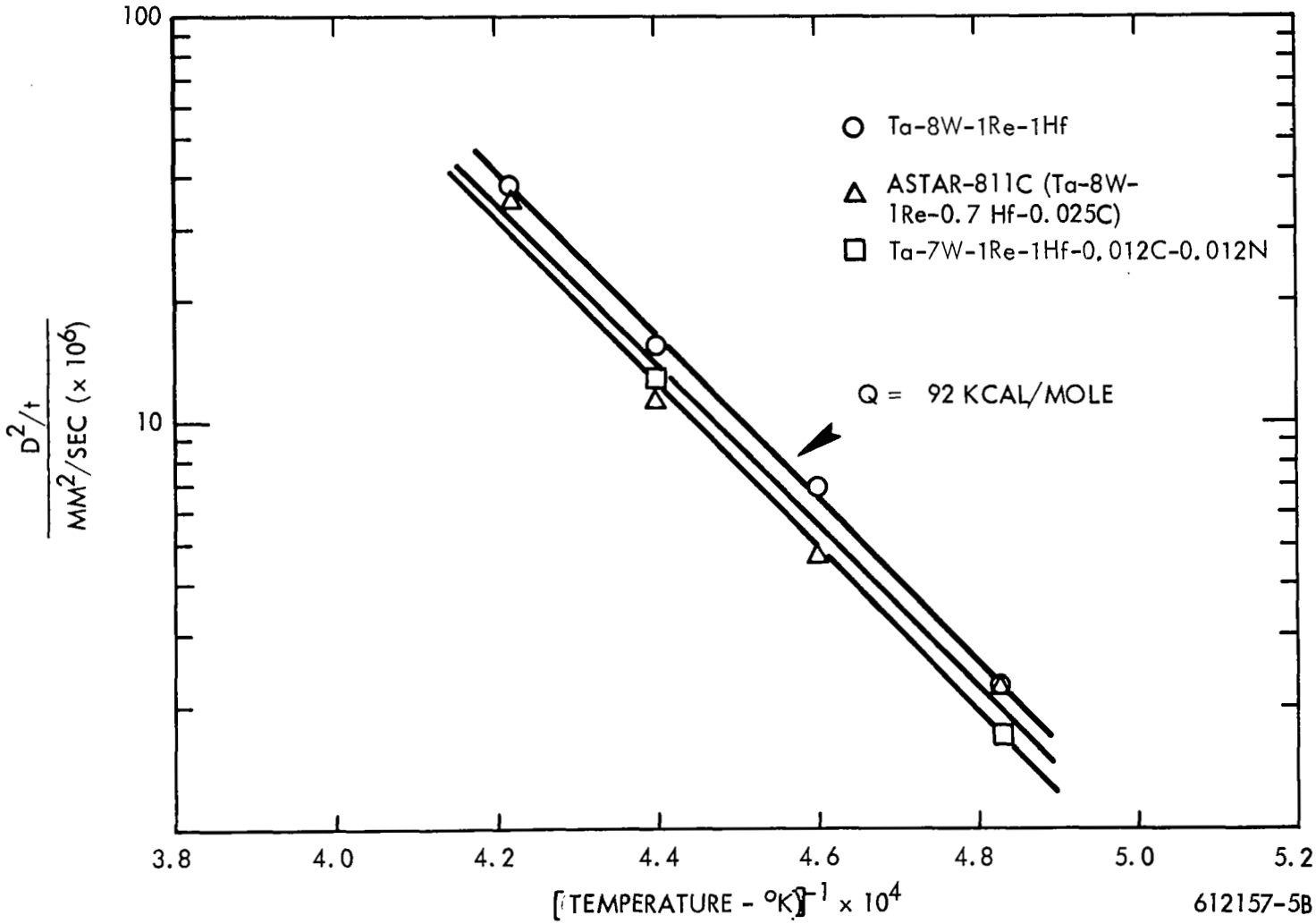

FIGURE 42 - Arrhenius Plot for Parabolic Rate Constant of Grain Growth for Scale-Up Alloys

Generally, the activation energy for grain boundary migration in a pure metal is considerably less than for self diffusion, the values being about 1/2 that for bulk diffusion[58]. The value of the activation energy for grain boundary migration of 92 kcal/mole measured for the tantalum alloys is similar to the activation energy of 110 kcal/mole [54] for the self diffusion of tantalum. The reason for this high value may be that adsorption of one or all of the alloy additions at the grain boundary may decrease the surface energy at the boundary, thus necessitating the adsorbed components to migrate through the metal by bulk diffusion when the boundary migrates[59].

4. Weldability. All three scale-up compositions exhibited as GTA welded bend ductility at temperatures below -200°F. A summary of the bend ductility of the base metal and after welding is in Table 17. As expected, the base metal exhibited good bend ductility at the lowest test temperature of -320°F in the as-recrystallized condition (1 hour at 3000°F). Fusion welding by the GTA process resulted in a slight increase in the DBTT; however, it was still well below room temperature. The weldments were made using the parameters which were described under the Part I - Screening Investigation.

The response of ASTAR-811C to widely varying welding conditions was evaluated by making a series of six GTA welds to determine the effect of welding speed and fusion zone size on the ductile brittle transition temperature. Welding speeds of from 7.5 to 30 ipm with a welding current of 75 to 160 amperes resulted in fusion zones of two sizes. Their dimensions are shown in Table 18 along with the DBTT results. ASTAR-811C exhibited little sensitivity to the widely varying weld parameters used. This behavior is similar to that of T-111. During welding, carbon was retained in solution in the fusion and heat affected zone with a corresponding higher hardness in these areas as illustrated in Figure 43. However, the hardness of the Ta-8W-1Re-1Hf did not vary across the fusion and heat affected zone or base metal and was 200-215 DPH. Similar behavior was also observed on the Ta-7W-1Re-1Hf-0.012C-0.012N alloy although the hardness was 280-300 DPH. As discussed previously all of the nitrogen and most of the carbon is in solid solution after annealing 1 hour at 3000°F and thus the higher hardness level is expected.

To evaluate the response of the weldments to post weld annealing treatments, as GTA welded specimens were annealed for various times and temperatures. As welded sheet specimens of the Ta-8W-1Re-1Hf alloy were post weld annealed for 1 hour at 1800, 2200 and 2600°F. The ductile-brittle transition temperature of the solid solution alloy (Ta-8W-1Re-1Hf) was -320°F as GTA welded and did not change as the result of post weld annealing.

TABLE 17 - BEND DUCTILITY OF BASE METAL AND WELDED SHEET MATERIAL

FOR SCALE-UP COMPOSITIONS (BEND FACTOR 1t)

Composition	Condition[a]	Test Temperatures °F	No. Load Bend Angle (Degrees)	Remarks	DBTT °F
Ta-8W-1Re-1Hf	Base Metal	-320	92	Bend	<-320
	As E. B. Welded	-320	90	Bend	<-320
	As GTA Welded	-320	91	Bend	<-320
Ta-8W-1Re-1Hf-0.012N	Base Metal	-320	89	Bend	<-320
-0.012C	As E. B. Welded	-320	89	Bend	<-320
	As GTA Welded	-250	90	Failed	--
		-225	91	Bend	-225
Ta-8W-1Re-0.7Hf-0.025C	Base Metal	-320	96	Bend	<-320
ASTAR-811C	As E. E. Welded	-320	96	Bend	<-320
	As GTA Welded	-250	95	Bend	-250
		-320	60	Break	--

(a) All material annealed one hour at 3000°F prior to test and/or welding

TABLE 18 - EFFECT OF WELDING PARAMETERS ON DUCTILE BRITTLE TRANSITION TEMPERATURE OF Ta-8W-1Re-0.7Hf-0.025C (ASTAR-811C)

DBTT [b], °F, for narrow [c] GTA welds for welding parameters of			DBTT [b], °F, for wide [d] GTA welds for welding parameters of		
7.5 ipm 76 amps	15 ipm 80 amps	30 ipm 124 amps	7.5 ipm 103 amps	15 ipm 118 amps	30 ipm 158 amps
-200	< -250	< -250	-250	-175	-200

(a) 0.035 inch sheet, annealed one hour at 3000°F prior to welding

(b) bend radius 1t, ram speed inches per minute, DBTT defined as lowest temperature for full 90° bend without evidence of failure

(c)

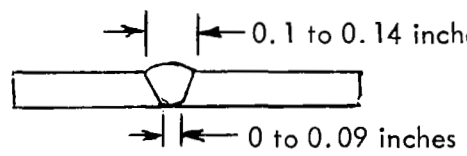

(d)

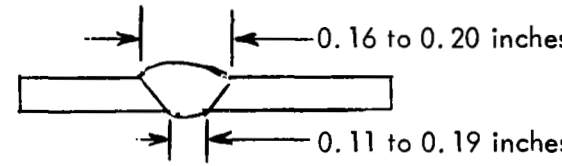

Fusion Zone
290 DPH 1500X

HAZ
270 DPH 1500X

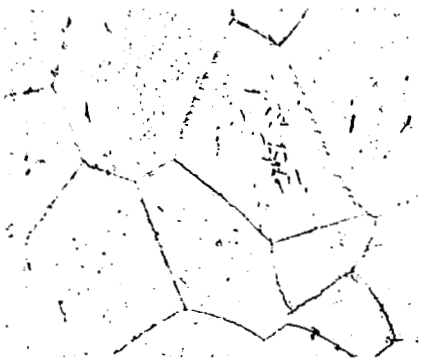

Base Metal
232 DPH 500X

FIGURE 43 - Microstructure and Hardness of GTA Weld in 0.035 Inch ASTAR-811C Sheet (As-Welded Condition. Base Metal Annealed 1 Hour at 3000°F Prior to Welding)

More extensive post weld annealing evaluation was conducted on ASTAR-811C (Ta-8W-1Re-0.7Hf-0.025C) and the Ta-7W-1Re-1Hf-0.012C-0.012N composition. Post weld annealing times out to 1000 hours were investigated. Again the shift in DBTT was used to evaluate the changes occurring during post weld annealing and the data are summarized in Table 19.

The DBTT of ASTAR-811C was relatively insensitive to post weld annealing under the conditions investigated. This composition by virtue of its combination of creep strength, fabricability and weldability is the most promising of the tantalum alloy compositions and more detailed studies beyond the limited investigations conducted here will have to be made to fully characterize the behavior of this alloy. During the 1000 hour post weld thermal exposure, the hardness level of the base metal, heat affected and fusion zone decreased to a uniform value of 190 DPH. The decrease in hardness is attributed to the precipitation of Ta_2C which is illustrated in Figure 44. The single phase fusion and heat affected zone of the as-welded ASTAR-811C has been previously shown in Figure 43. The carbide (Ta_2C) precipitate is blocky and massive, particularly in the grain boundary area in the heat affected and fusion zone of the aged specimen. Post weld annealing of ASTAR-811C for 2 hours at temperatures up to 2400°F had little effect on the weld DBTT. Thus, post weld annealing treatments which are required from liquid alkali metal corrosion considerations will not adversely effect ductility.

The nitrogen bearing Ta-7W-1Re-1Hf-0.012C-0.012N alloy exhibited the greatest change in DBTT as a result of the post weld thermal annealing treatments. The response of this composition to post weld annealing is illustrated in Figure 45. From the behavior illustrated by the data plotted in Figure 45, it would appear that the shift in DBTT may be associated with an aging-overaging reaction. As discussed earlier under the Part I - Screening Investigation, the reactive metal nitride precipitation reaction was shown to follow classical precipitation hardening behavior. Optical metallographic examination of the post weld annealed samples did not give a clue as to the cause of the shift in ductile brittle behavior (See Figure 46). The room temperature hardness values were less than the as welded level of 275 DPH indicating a removal of a strengthener from solid solution. Up to 16 hours exposure

TABLE 19 - EFFECT OF POST WELD ANNEALING ON THE DBTT[(a)] OF ASTAR-811C

(Ta-8W-7Re-0.7Hf-0.025C) and Ta-7W-1Re-1Hf-0.012C-0.012N

Composition	Post Weld Annealing Conditions		DBTT °F
	Time (hours)	Temperature	
ASTAR-811C	none	--	-250
	2	2200	-175
	2	2400	-200
	10	2400	-200
	1000	1800	-100
Ta-7W-1Re-1Hf 0.012C-0.012N	none	--	-225
	1	1800	-200
	1	2200	-100
	1	2600	0
	1	3000	-100
	16	1800	-200
	16	2200	+125
	16	2600	-175
	500	2200	-225

(a) Bend factor 1t, punch speed of 1 inch per minute

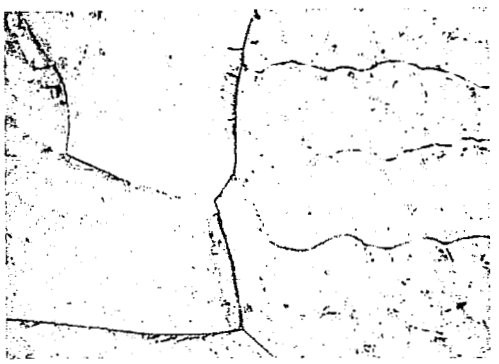

(a) Weld Zone 195 DPH

(b) HAZ 190 DPH

(c) HAZ 190 DPH

(d) Base Metal 188 DPH

FIGURE 44 - Microstructure of As-GTA Welded ASTAR-811C Sheet After a Post Weld Thermal Exposure of 1000 Hours at 1800°F 500X

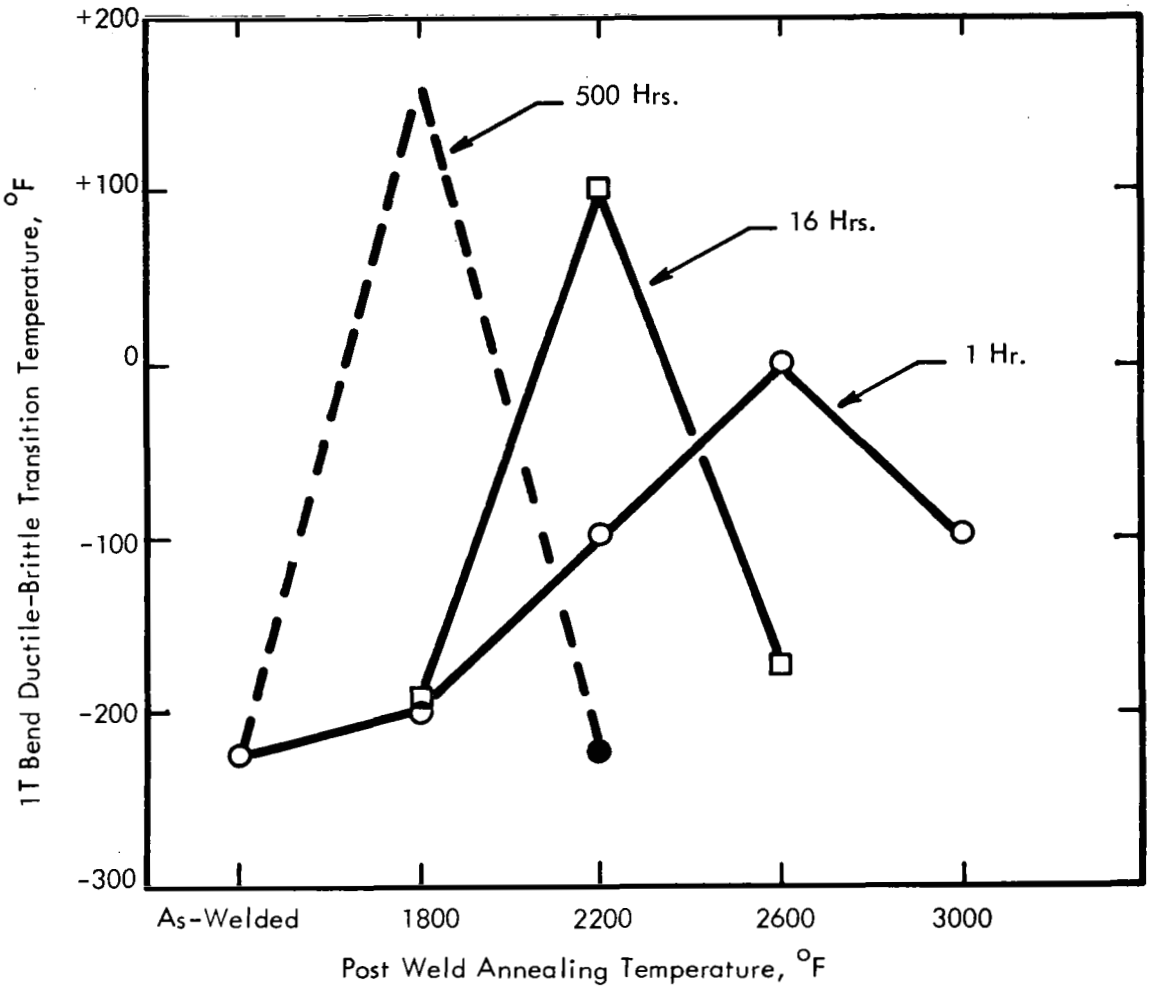

FIGURE 45 - Effect of Post Weld Annealing on the Ductile-Brittle Transition Temperature of GTA Welded Ta-7W-1Re-1Hf-0.012C-0.012N

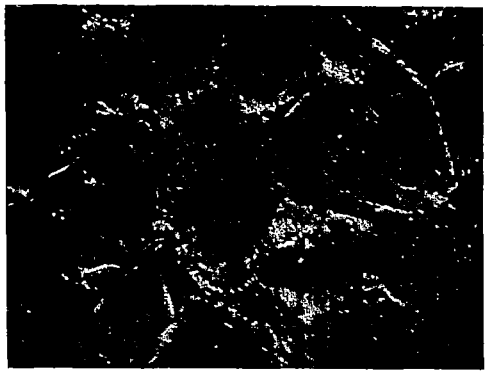

Weld Zone 1500X

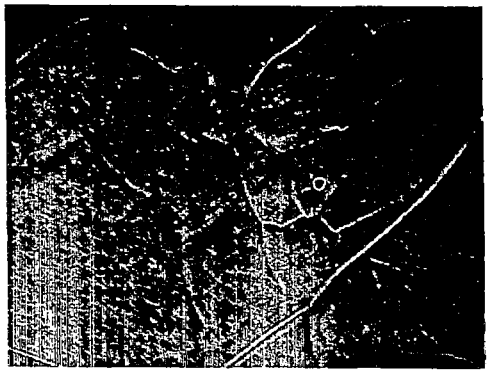

HAZ 1500X

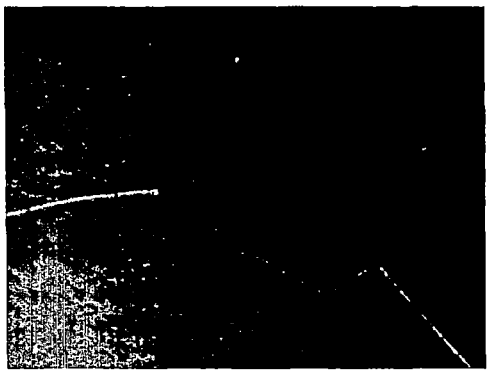

Base Metal 1500X

(a) Post Weld Annealed 1 Hour at 2200°F

Weld Zone 500X

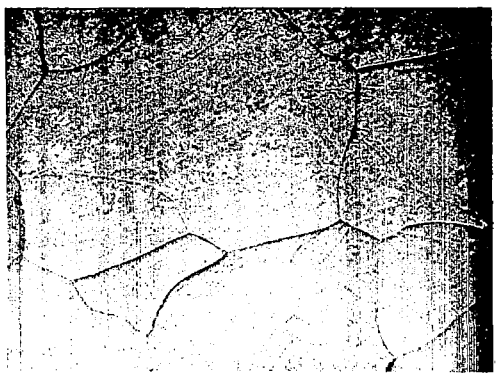

HAZ 500X

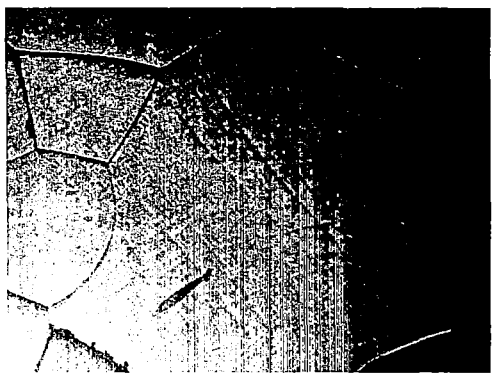

Base Metal 500X

(b) Post Weld Annealed 16 Hours at 2200°F

FIGURE 46 - Influence of Post Weld Annealing on the Microstructure of GTA Welded Ta-7W-1Re-0.7Hf-0.012C-0.012N Sheet

Weld Zone 1500X

HAZ 500X

Base Metal 500X

(c) Post Weld Annealed for 500 Hours at 2200°F

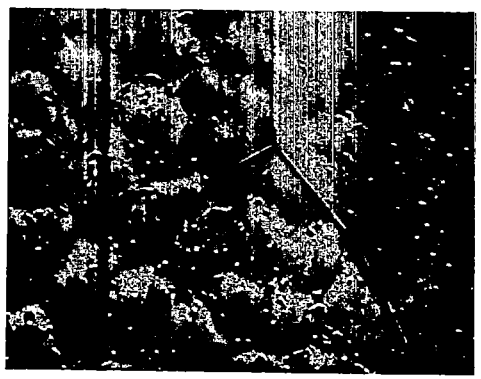

Weld Zone 1500X

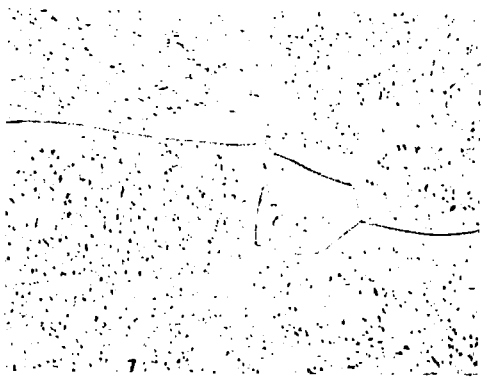

HAZ 500X

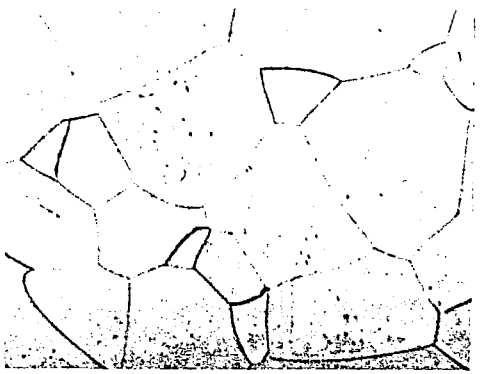

Base Metal 500X

(d) Post Weld Annealed for 1 Hour at 1800°F

FIGURE 46 (Continued) - Influence of Post Weld Annealing on the Microstructure of GTA Welded Ta-7W-1Re-0.7Hf-0.012C-0.012N Sheet

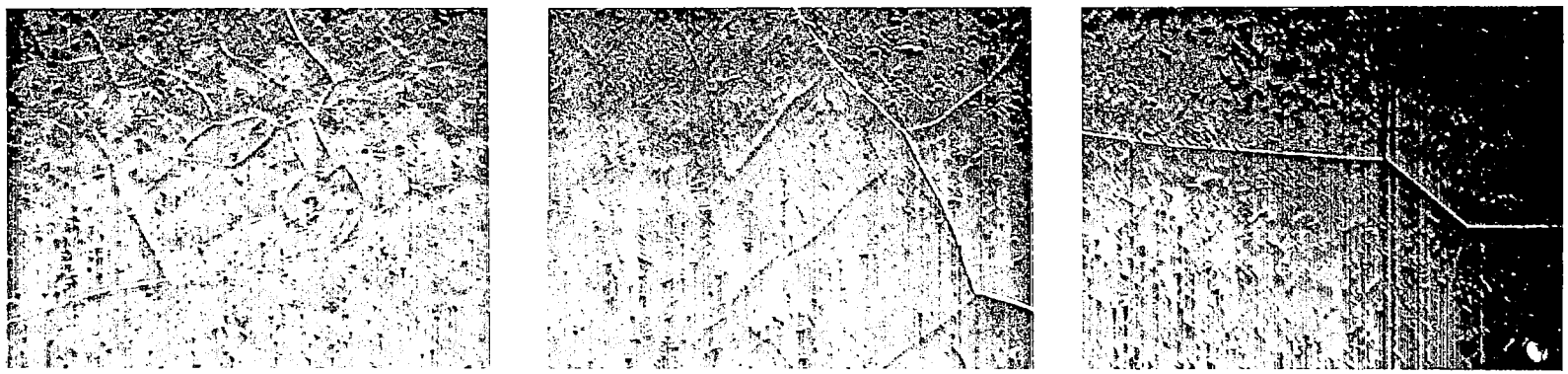

Weld Zone 1500X HAZ 1500X Base Metal 1500X

(e) Post Weld Annealed 1 Hour at 2600°F

FIGURE 46 (Continued) - Influence of Post Weld Annealing on the Microstructure of GTA Welded Ta-7W-1Re-0.7Hf-0.012C-0.012N Sheet

over the range of 1800°F to 2600°F resulted in a 245-260 DPH final hardness level. After 500 hours at 2200°F though the hardness had decreased to 220 DPH. The hardness level after the various exposures can be rationalized on the basis of the precipitating phase(s). After 1 hour exposure at 1800 - 2600°F, only the Ta_2C phase was detected as it was after 16 hours at 1800, and 2200°F. However, after 16 hours at 2600°F, a minor amount of a FCC phase (TaHf) $(CN)_{1-x}$ was also found. Only the FCC precipitate was detected after 500 hours at 2200°F. Thus the change in hardness as a result of the post weld annealing treatments can be explained on the basis of the nitrogen remaining in solid solution. Chemical analysis of weld metal verified that during GTA welding no carbon or nitrogen was lost or added.

The complex nature of the precipitation reactions occurring in the tantalum alloy precluded detailed study within the scope of this investigation. However, it is an area where more work will certainly have to be done to identify the causes for the change in fracture behavior of carbide and/or nitride strengthened tantalum alloys.

5. Mechanical Properties

(a) Creep Behavior. The primary strength criterion during this investigation was resistance to creep deformation. Thus most of the effort in mechanical property evaluation was directed toward determination of creep behavior. The creep properties of the three scale-up compositions are in Table 20 and compared with each other and T-111 by way of the parametric plot shown in Figure 47. The test data presented here is for 0.04 inch material annealed one hour as 3000°F prior to test. The as-recrystallized grain size after this treatment is nominally 0.02 to 0.03 mm. The dispersed phase makes its most effective contribution to creep resistance at test temperatures up to 2400°F. Above this temperature the dispersed phases do not appear to be as effective and the creep resistance is limited primarily by the contribution of the solid solution additions. This behavior is illustrated by the plot in Figure 47 where at the lower test temperatures the plot for the scale up compositions is diverging, with the solid solution alloy the lower boundary and the dispersed phase strengthened compositions the upper boundary. However, as the test temperature is increased above 2400°F, the creep properties of all three compositions are very similar and thus the plot is converging. Another interesting

TABLE 20 - CREEP TEST RESULTS FOR SCALE-UP COMPOSITIONS (0.04 INCH SHEET, ANNEALED 1 HOUR AT 3000°F PRIOR TO TEST)

Composition	Test Temperature (°F)	Stress (Psi)	Total Test Time (Hours)	Total Plastic Strain (%)	Time to Elongate 1% (Hours)
Ta-8W-1Re-0.7Hf-0.025C ASTAR-811C	2400	15,000	930	36.8	210
	2400	12,500	531	0.93	570
	2400	15,000	554	2.53	262
	2400	15,000	457	3.0	202
	2200	18,000	1,017	1.0	1,017
	2600	8,000	165	0.88	188
	2600	8,000	283	2.62	159
	2800	4,000	260	3.3	78
Ta-8W-1Re-1Hf	2200	15,000	1670	0.66	--
	2200	17,000	472	4.13	131
	2200	17,000	331	4.34	59
	2400	12,766	377	1.33	317
	2400	17,000	147	45.	6
	2400	12,500	357	2.22	207
	2400	15,000	165	4.6	54
	2600	6,000	712	1.97	440
Ta-7W-1Re-1Hf-0.012C-0.012N	2200	17,000	1,312	1.59	1,007
	2200	19,000	839	2.90	607
	2400	12,500	530	1.43	403
	2400	15,000	426	7.28	157
	2400	15,750	353	22.9	152
	2600	6,000	520	2.20	331
	2600	8,000	382	5.40	172

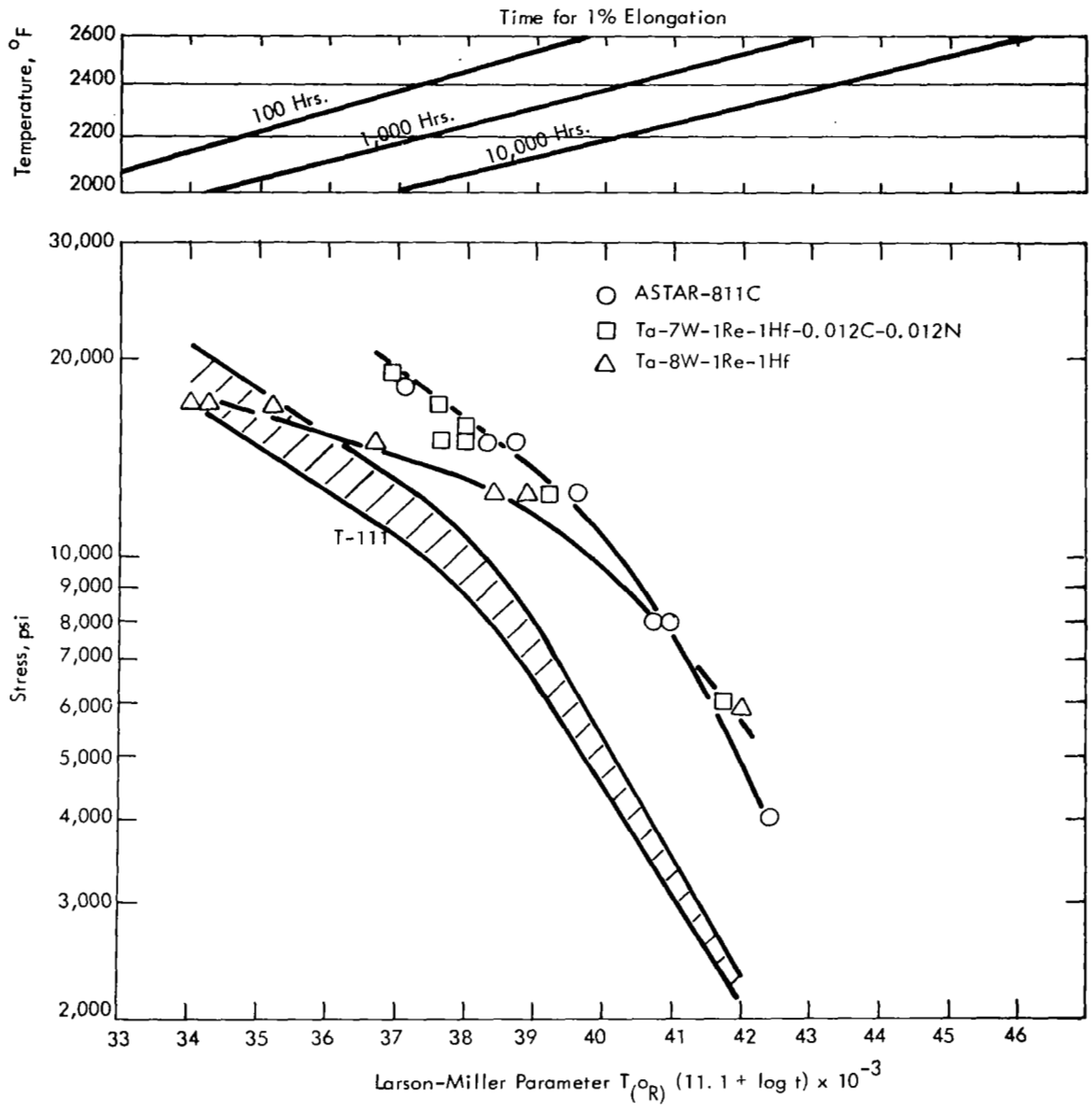

FIGURE 47 - Larson-Miller Plot Comparing Time to 1% Elongation for the Scale-Up Alloy Compositions

feature of the plot in Figure 47 is the position of the T-111 curve in relation to the Ta-8W-1Re-1Hf curve. At the lower test temperature, (2200°F) the strength of both are equivalent although the rhenium containing composition is decidedly superior at 2400°F and above. The reason for this behavior may be the combination of two effects: (1) the Ta-8W-1Re-1Hf alloy has half as much reactive metal addition which has been shown previously to have a deleterious effect on creep resistance and (2) small additions of rhenium have been shown to exert a significant effect on improving creep resistance. The creep strength of the rhenium containing alloy at 2400°F and above based on a stress to give an equivalent time to elongate 1% is at least 2 to 2-1/2 times stronger than T-111. This is truly a significant improvement considering the minor compositional variations between the alloys!

The effect of final annealing time and temperature on the creep behavior of the ASTAR-811C composition was studied in a limited evaluation. As discussed previously, time dependent deformation is sensitive to a number of factors which include grain size, annealing temperature, and metallurgical condition which is a function of the prior thermal-mechanical history. Specimens of ASTAR-811C were annealed over the temperature range of 3000°F to 3600°F for times up to 1 hour. The final resulting grain diameter range achieved was 0.03 to 0.2 mm. Since ASTAR-811C is a carbide containing composition, increasing the final annealing temperature also causes a change in the carbide morphology as well as the grain size. Specimens of the Ta-8W-1Re-1Hf solid solution alloy were also similarly treated to try and separate the individual grain size and carbide contributions to the creep strength. The data obtained are summarized in Table 21 and illustrated graphically in Figure 48. At a grain size of 0.03 mm, there is a slight increase in the creep resistance of ASTAR-811C as the annealing temperature was increased from 3000°F to 3630°F. And the same increment of improvement was also observed on the solid solution alloy, Ta-8W-1Re-1Hf, and amounted to an increase in the time to elongate 1% by about 30-40 hours. However, at a grain size of 0.07 mm, there was a distinct improvement in the creep behavior of ASTAR-811C with the time to elongate 1% increasing from 260 hours to 640 hours. Further examination of the data indicate that there may be an optimum grain size for creep resistance at the final annealing temperature

TABLE 21 - EFFECT OF HEAT TREATMENT ON THE CREEP BEHAVIOR OF ASTAR-811C and Ta-8W-1Re-1Hf at 2400°F and 15,000 psi

Composition	Annealing Conditions		Grain Size	Total Test Time	Total Elong	Time to 1% Elong	DPH	
	Time (minutes)	Temp °F	(mm)	(hours)	(%)	(hours)	Pre-Test	Post-Test
ASTAR-811C, Ta-8W-1Re-0.7Hf-0.025C	60	3000	0.03	554	2.53	262	257	221
	60	3000	0.02	457	2.0	202	249	229
	60	3270	0.06	507	2.0	290	249	226
	10	3270	0.03	472	2.58	235	283	222
	5	3450	0.03	497	2.12	278	279	224
	15	3450	0.07	424	2.33	200	280	224
	60	3450	0.09	257	0.95	270	244	221
	0.5	3630	0 03	523	2.18	290	293	221
	0.5	3630	0.03	534	2.57	288	284	223
	5	3630	0.07	1000	1.65	639	280	226
	60	3630	0.2	1003	2.10	474	260	231
	60(a)	3630	0.2	1047	16.8	310	251	247
Ta-8W-1Re-1Hf	60	3000	0.03	165	4.6	54	206	208
	5	3450	0.03	138	4.24	51	213	212
	30	3450	0.07	211	6.16	67	208	209
	0.5	3630	0.03	168	2.26	96	222	212
	60	3630	0.2	190	2.71	85	216	209

(a) Tested at 2600°F and 8,000 psi

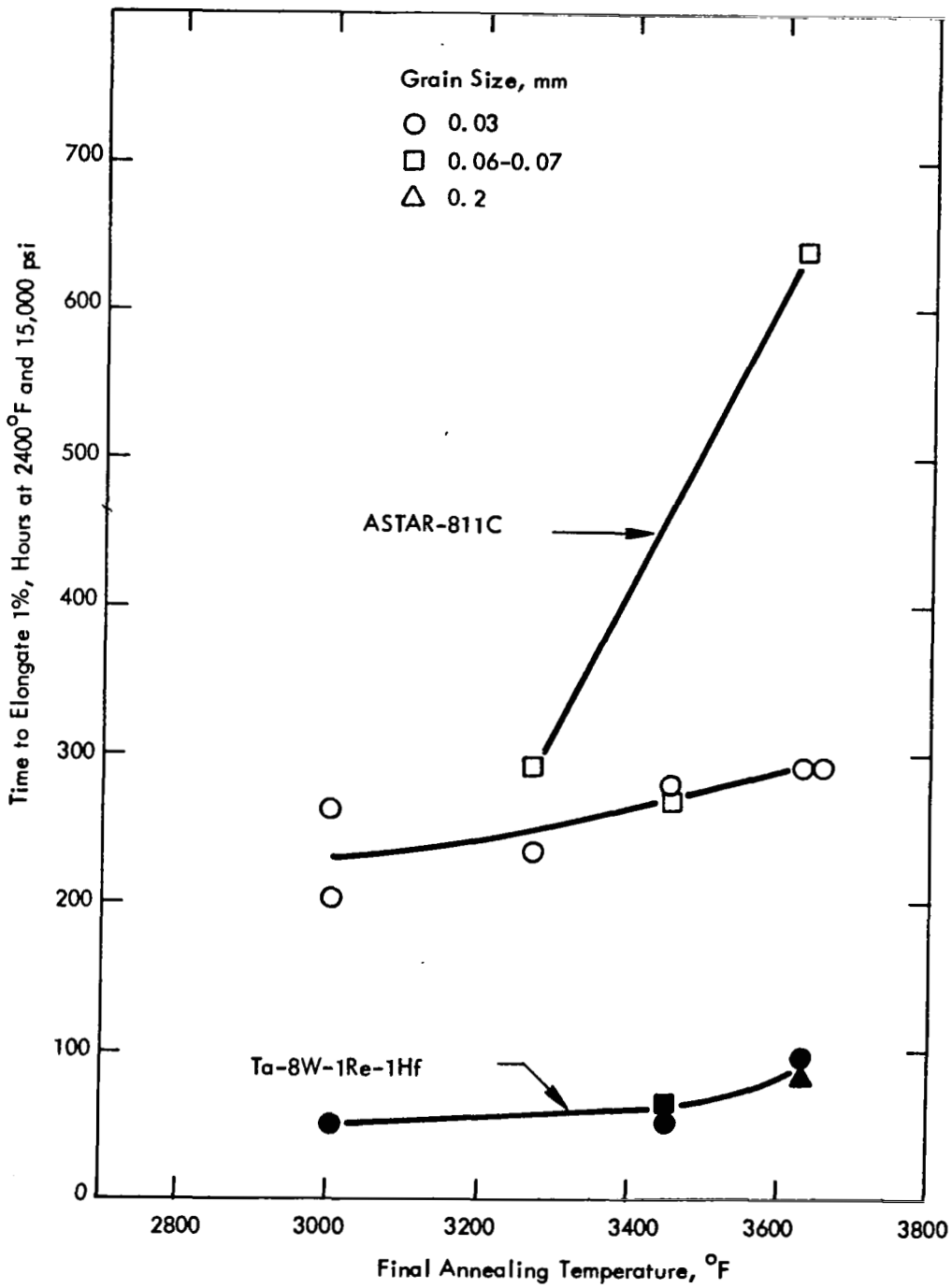

FIGURE 48 - Effect of Annealing Temperature and Grain Size on the Creep Properties of ASTAR-811C and Ta-8W-1Re-1Hf at 2400°F and 15,000 psi

of 3630°F (See Figure 49). An optimum grain size for creep resistance has been observed previously for a number of FCC materials.[47,48,49,50] Although fewer specimens of the solid solution alloy were investigated, the data obtained suggest that its creep behavior is little affected by grain size. Pre-test examination of the microstructure of the heat treated ASTAR-811C revealed a significant change in the amount of observable carbide phase as the annealing temperature was increased (See Figure 50). However, after testing at 2400°F and 15,000 psi to a total plastic strain of 2-1/2%, the microstructure of the tested specimens appeared identical (See Figure 51).

Room temperature hardness measurements before and after creep testing show that the final hardness level after testing at 2400°F was 220-230 DPH irrespective of the as-heat treated hardness (See Table 21). The time-extension plot for two ASTAR-811C specimens, one annealed 1 hour at 3000°F and the other at 3630°F, are shown in Figure 52. The creep rate of the specimen annealed 1 hour at 3000°F was 0.016% per hour at the termination of the test. The specimen annealed 1 hour at 3630°F had a constant creep rate of 0.002%/hour throughout the test duration. Thus, the low temperature properties as evaluated by hardness give little insight into the elevated temperature strength since the post test hardness of both of these specimens was similar (220-230 DPH).

Examination of the bulk extracted precipitate from several creep specimens revealed that there was a significant change in the morphology of the Ta_2C phase as the final pre-test annealing temperature was increased (See Figure 53). After 1 hour at 3630°F, ASTAR-811C appeared single phase when examined at 1500X, but transmission electron microscopy of thin films revealed the presence of a fine precipitate which exhibited coherency strain to some degree with the matrix (See Figure 54). Even though initially there appears to be coherency of the Ta_2C precipitate with the matrix, the kinetics of the precipitation reaction are so rapid that this condition is extremely short lived at elevated temperatures. However, the finely divided non-coherent Ta_2C does appear to offer obstacles to dislocations as illustrated in the electron transmission micrograph in Figure 55.

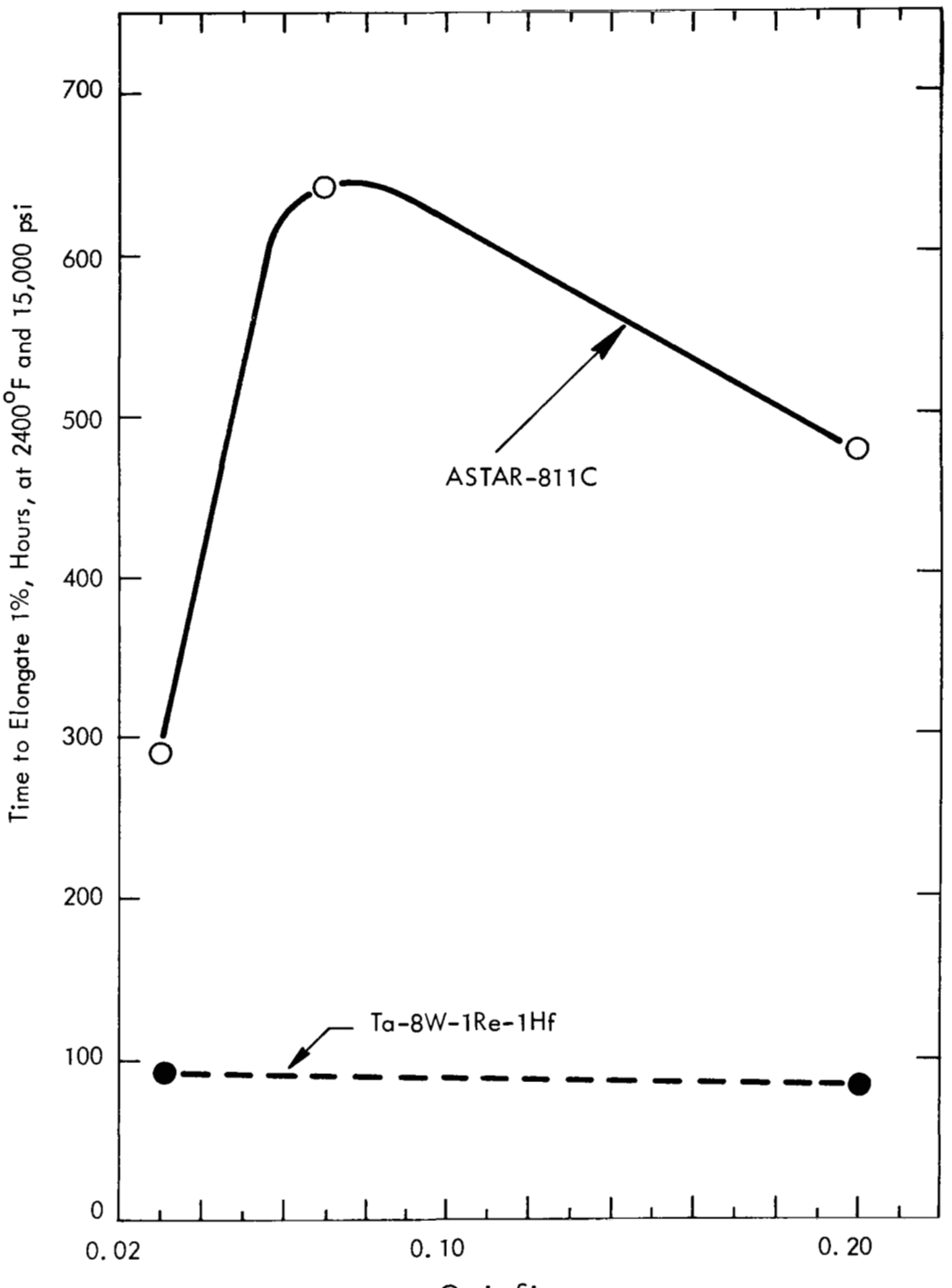

FIGURE 49 - Effect of Grain Size on the Creep Behavior of ASTAR-811C and Ta-8W-1Re-1Hf Sheet Annealed at 3630°F and Tested at 2400°F and 15,000 psi

(a) 500X

(b) 1500X

1 Hour at 3000°F

(c) 500X

(d) 1500X

5 Minutes at 3450°F

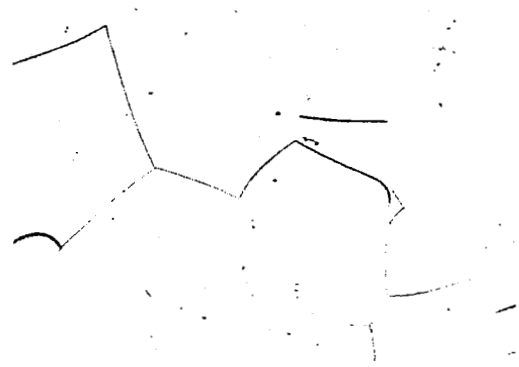

(e) 500X

(f) 1500X

30 Seconds at 3630°F

FIGURE 50 - Pre-Test Microstructure of ASTAR-811C Sheet

(a) 500X

(b) 1500X

FIGURE 51 - Microstructure of ASTAR-811C After Testing at 2400°F and 15,000 psi to a Total Elongation of 2-1/2% (Pre-Test Annealing Treatment, 30 Seconds at 3630°F)

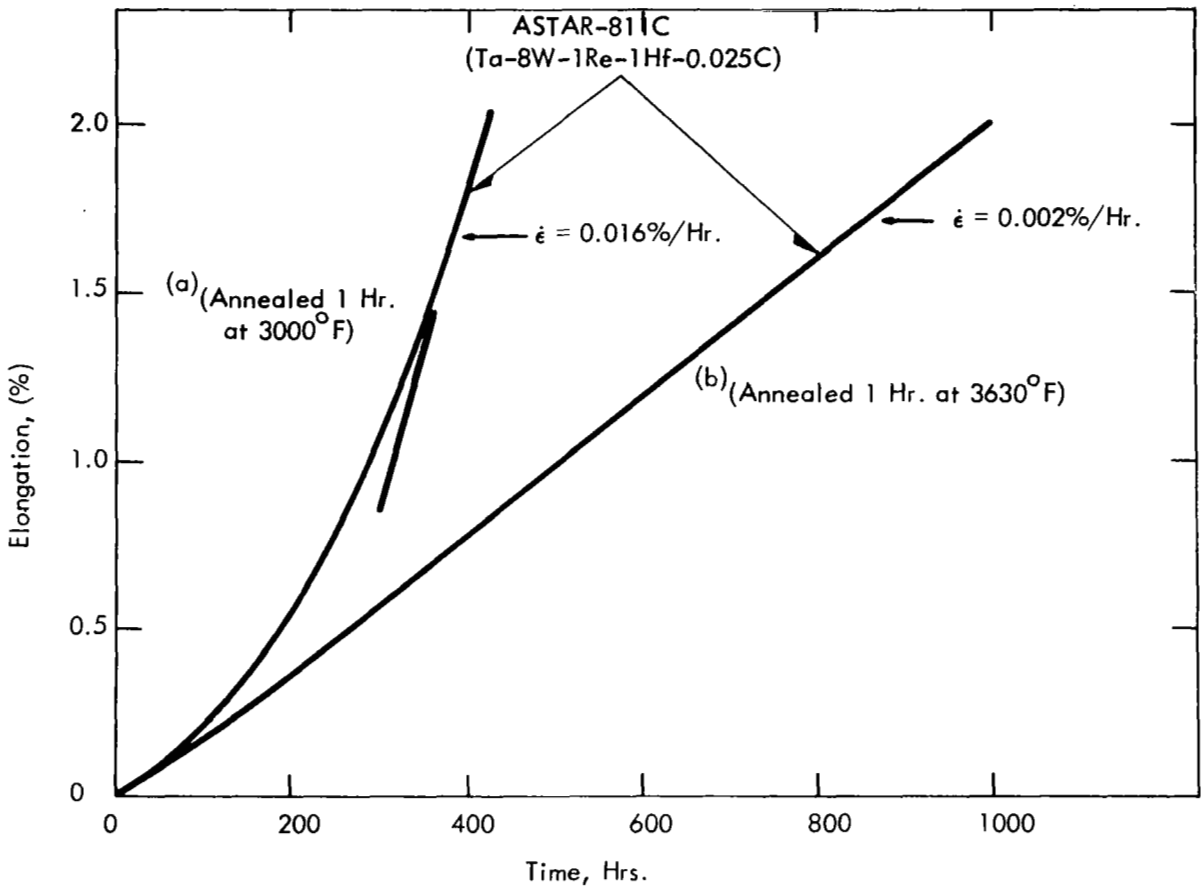

FIGURE 52 - Effect of Final Annealing Temperature on the Shape of the Creep Curve for ASTAR-811C Tested at 2400°F and 15,000 psi

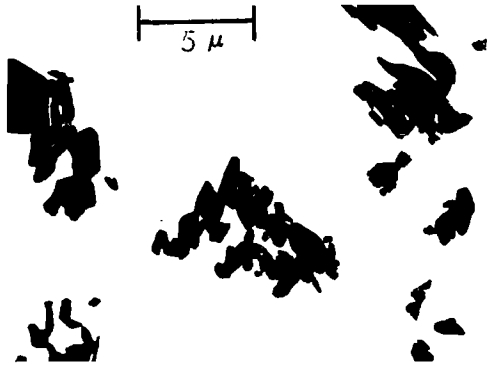

(a) 1 Hour at 3000°F then tested at 2400°F for 500 hours

(b) 1 Hour at 3280°F then tested at 2400°F for 500 hours

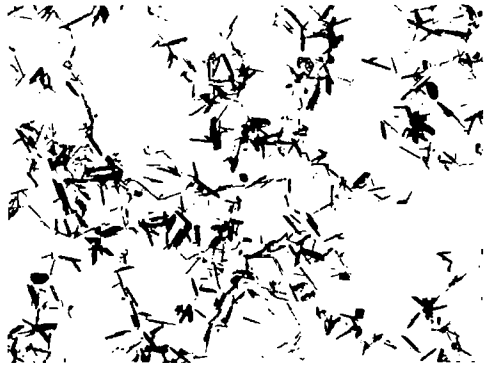

(c) 1 Hour at 3630°F then tested at 2400°F for 1000 hours

FIGURE 53 - Electron Micrographs of Tantalum Dimetal Carbide (Ta_2C) Precipitate Extracted from ASTAR-811C Specimens, Creep Tested at 2400°F and 15,000 psi

(a)

(b)

FIGURE 54 - Electron Transmission Micrographs of ASTAR-811C After Annealing for 1 Hour at 3630°F. (a) Interior of Grain (b) Grain Boundary

FIGURE 55 - Electron Transmission Photomicrograph of ASTAR-811C, Annealed 1 Hour at 3630°F, Then Tested at 2400°F and 15,000 psi. Test Duration 1000 Hours. Total Plastic Strain 2.5%.

From this limited study of heat treat response, it would appear that the potential strength limit of the ASTAR-811C composition has yet to be achieved. Identifying the strengthening mechanism and understanding the role of the carbide precipitate in the creep deformation process would also greatly aid in optimizing the thermal mechanical processing schedule to achieve the best combination of creep resistance and fabricability.

Generally, the creep tests were terminated when the total elongation reached 2-3%. However some specimens were tested to achieve a high total elongation or fracture in order to observe the fracture mode. At 2400°F, ASTAR-811C was strained 37% in 930 hours at a stress level of 15,000 psi. No grain boundary voids were observed with massive carbide precipitates forming on the boundaries perpendicular to the axis of the applied stress. Extensive sub-boundary formation also occurred. The precipitate particles which were distributed uniformly throughout the matrix in the as-annealed specimen prior to test (See Figure 50a) redistributed during test to the sub-boundary and transverse grain boundary areas (See Figure 56a). A Ta-7W-1Re-1Hf-0.012C-0.012N specimen tested also at 2400°F and 15,000 psi elongated 23% in 353 hours. The formation of grain boundary voids was observed in this specimen. The grain boundaries were generally found to be denuded of precipitates and the precipitates were distributed throughout the grain volume (See Figure 56b). The only precipitating phase in ASTAR-811C is the Ta_2C. However when nitrogen is substituted for a portion of the carbon the Ta_2C precipitate initially present transforms upon exposure to the FCC $(TaHf)(CN)_{1-x}$ phase. It would appear then that the grain boundary precipitate, as observed in ASTAR-811C is certainly beneficial in preventing grain boundary separation. This is another critical area where more investigation is needed.

A preliminary evaluation was also made on the effect of GTA welding on the creep behavior of ASTAR-811C. Bead-on-plate welds with 100% penetration were made on 0.05 inch thick material. Specimens 0.04 inch thick were prepared by surface grinding. The weld bead was parallel to the stress axis and occupied essentially the entire volume of the gage section. A total elongation of 6% occurred in 680 hours with the time to 1% elongation 171 hours. This compares with 210 to 260 hours to 1% for the base metal. Photomicrographs

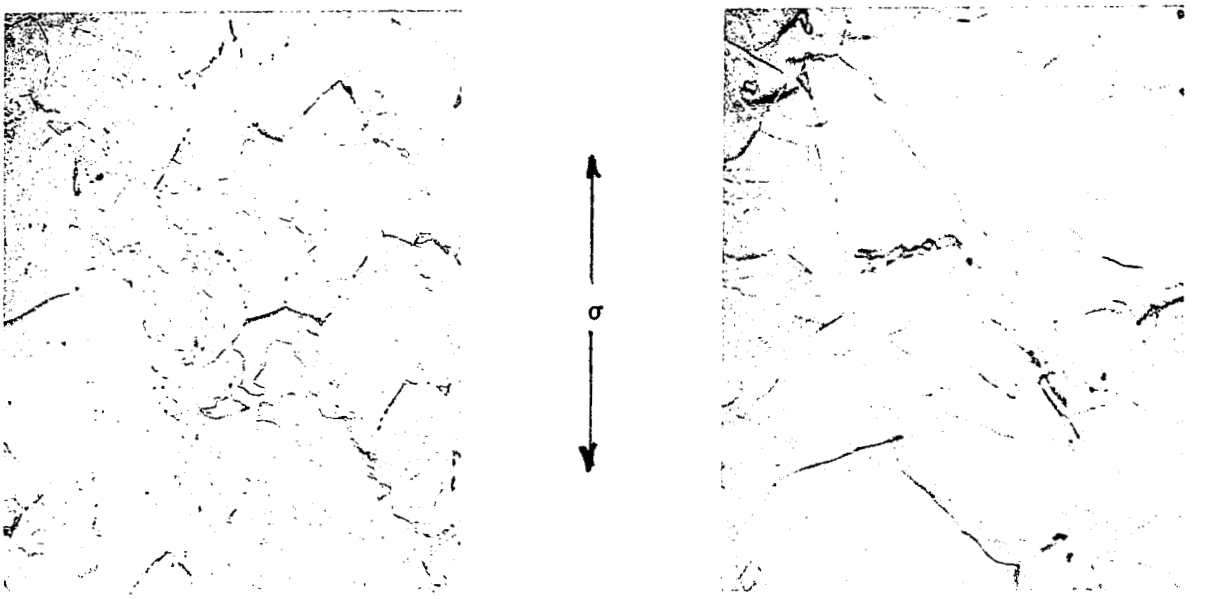

500X 1500X

(a) ASTAR-811C 2400°F and 15,000 psi - 37% Elongation in 903 Hrs. (Did not fracture)

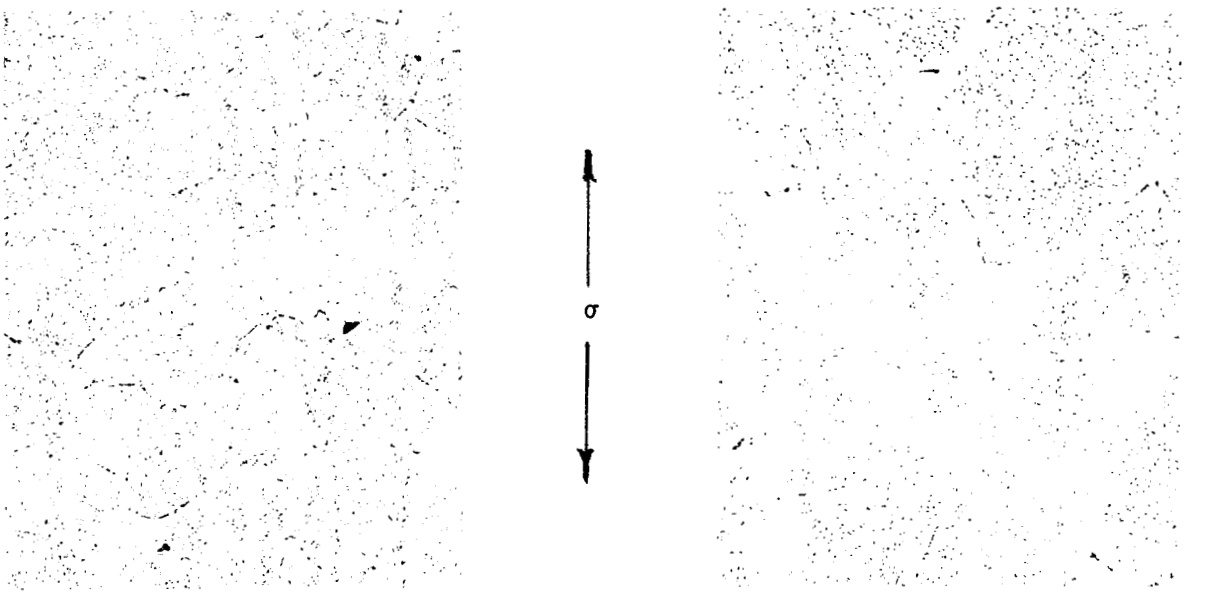

150X 500X

(b) Ta-7W-1Re-1Hf-0.012C-0.012N-2400°F, 1500 psi - 23% Elongation in 353 Hrs.

FIGURE 56 - Microstructure of ASTAR-811C and Ta-7W-1Re-1Hf-0.012C-0.012N After Creep Testing

taken from the head section and gage section are shown in Figure 57. Both massive grain boundary and a finely divided grain volume precipitate were observed. After testing there was more grain volume precipitate observed in the weldment than in the base metal specimen. However the solute redistribution which occurred during welding no doubt effects the precipitate reactions. From this very limited test data, one may conclude that GTA welding significantly altered the creep behavior of ASTAR-811C. For example, after welding, the fusion and heat affected zones are single phase with the carbon in solid solution. As shown previously, the creep properties of the base metal were significantly improved by solutioning of the carbon prior to testing. Thus base metal material so treated strained 1% in only 500-650 hours at 2400°F and 15,000 psi, as compared to only 171 hours for the GTA weldment. Again the effect of solute redistribution has not been accounted for and if hafnium rich areas are present, they would certainly tend to creep at a faster rate. Since the systems in which ASTAR-811C is intended will be fabricated by welding, more detailed understanding of the creep behavior of weldments will be needed before the most structurally efficient system design can be achieved.

The cleanliness of the ultra-high vacuum environment used for conducting the creep tests is shown by the chemical analysis data in Table 22 for ASTAR-811C creep specimens for the test duration. There was no significant change in oxygen or carbon content. The inertness of the tantalum alloy test specimen with the test environment is exceedingly critical if reliable long time creep data are to be generated.

(b) Tensile Properties. The tensile properties of all three scale-up compositions were determined over the range of -320 to 3000°F. Tensile behavior was determined on 0.04 inch sheet annealed 1 hour at 3000°F prior to test, as well as on as-GTA welded material. The tensile data are listed in Tables 23 and 24 while the yield strength as a function of temperature is plotted in Figure 58. Both carbon and nitrogen additions raise the

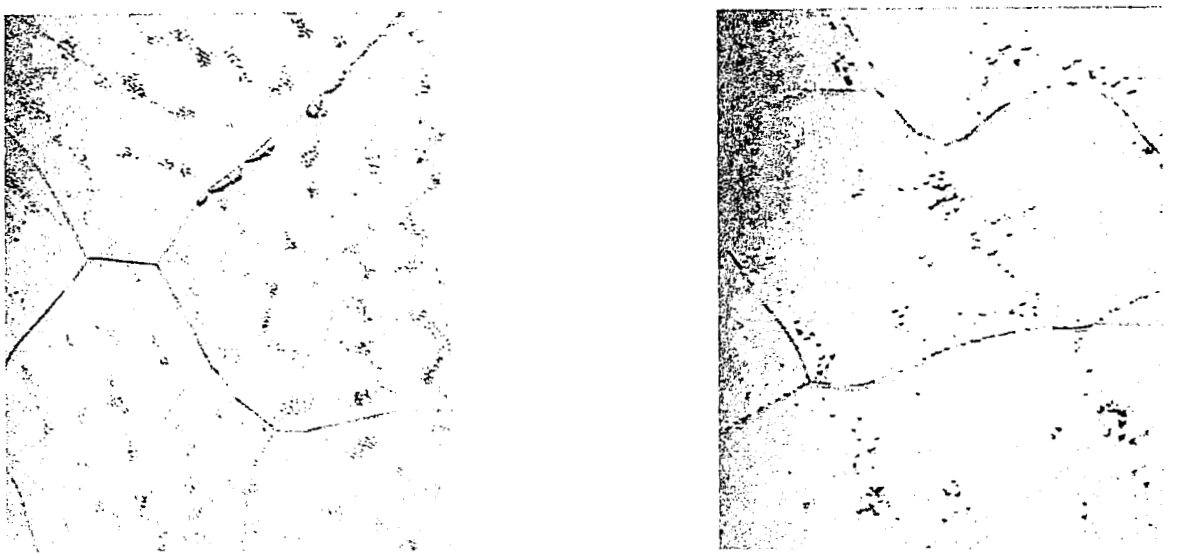

500X 1500X

(a) Head Section

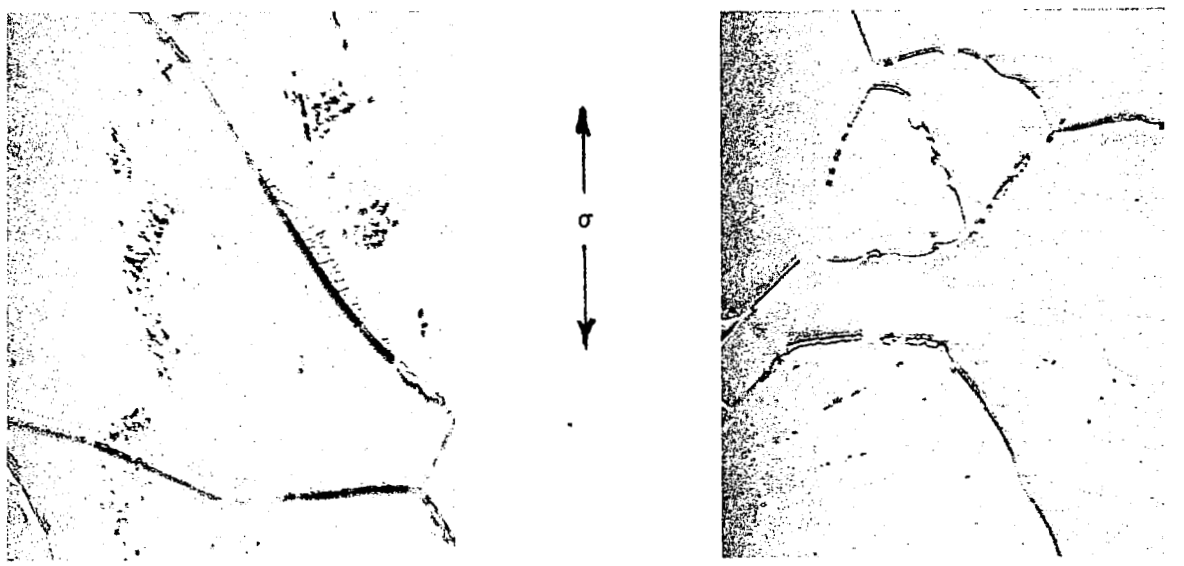

1500X 1500X

(b) Gage Section

FIGURE 57 - Microstructure of As-GTA Welded ASTAR-811C After Creep Testing at 2400°F and 15,000 psi for 670 Hours

TABLE 22 - POST TEST CHEMICAL ANALYSIS OF ASTAR-811C CREEP TEST SPECIMENS CREEP TESTED AT $\leq 1 \times 10^{-8}$ TORR

Test Conditions	Post Test Chemical Analysis,* Weight %	
	Carbon	Oxygen
642 hours at 2400°F	0.022	0.0012
500 hours at 2400°F	0.023	0.0010
1000 hours at 2400°F	0.023	0.0011

*Pre-test Chemical Analysis - 0.020C, 0.0013O_2

TABLE 23 - MECHANICAL PROPERTIES[a] OF SCALE-UP COMPOSITIONS

Composition	Test Temperature (°F)	0.2% Yield Strength[b] (ksi)	Ultimate Tensile Strength[b] (ksi)	Elongation		Reduction in Area (%)
				Uniform (%)	Total (%)	
Ta-8W-1Re-1Hf	-320	134.5	147.8	24.6	31.4	62.6
	-150	97.6	113.2	18.9	29.4	61.6
	-RT	76.0	88.0	19.3	33.4	66.2
	+600	42.2	55.0	18.1	28.1	51.3
	2200	38.7	40.4	----	30.3	----
	2400	22.6	33.7	----	28.9	----
	2600	21.8	28.7	----	28.6	----
	3000	22.1	22.9	----	10.9	----
Ta-8W-1Re-0.7Hf-0.025C (ASTAR-811C)	-320	147.7	165.3	22.1	26.3	42.0
	-150	111.0	130.3	20.1	28.5	46.3
	RT	85.0	105.4	17.0	25.9	50.0
	RT	85.3	103.5	15.5	26.6	48.4
	RT	82.8	104.6	16.4	27.6	49.3
	+600	53.7	75.5	15.3	24.5	47.9
	1500	41.3	79.6	----	18.8	----
	2000	35.0	60.9	----	24.0	----
	2200	31.6	49.9	----	28.8	----
	2400	30.4	40.9	----	35.0	----
	2600	29.5	35.3	----	34.8	----
	2800	23.0	28.4	----	49.5	----
Ta-7W-1Re-1Hf-0.012C-0.012N	-320	177.5	189.0	14.2	21.6	38.2
	-150	140.0	145.8	12.6	23.7	53.0
	RT	110.3	117.3	14.4	25.4	56.0
	+600	63.0	77.5	15.9	23.8	53.1
	2200	35.8	57.3	----	17.7	----
	2400	31.5	45.5	----	24.6	----
	2600	26.8	36.0	----	20.1	----
	3000	20.9	21.5	----	31.6	----

(a) Specimens annealed for 1 hour at 3000°F prior to test.
(b) Strain rate of 0.05 in/min throughout test.

TABLE 24 - TENSILE PROPERTIES OF SCALE-UP ALLOYS TESTED IN THE AS-WELDED CONDITION

Composition	Test Temp. (°F)	Weld Direction	0.2% Yield Strength (ksi)	Ultimate Tensile Strength (ksi)	% Elongation	
					Uniform	Total
Ta-8W-1Re-1Hf	-320	Longitudinal	134.6	152.3	17.50	22.15
	-320	Transverse	137.0	148.0	11.25	14.35
	RT	Longitudinal	77.6	92.3	14.60	19.15
	RT	Transverse	79.2	90.9	9.20	11.95
	1800	Longitudinal	36.2	57.6	---	18.1
	2000	Transverse	30.7	47.2	---	10.7
	2400	Longitudinal	27.8	32.2	---	6.6
	2600	Transverse	24.3	28.5	---	4.9
ASTAR-811C (Ta-8W-1Re-0.7Hf-0.025C)	-320	Longitudinal	157.3	184.6	16.7	24.2
	-320	Transverse	159.0	176.2	10.9	14.2
	RT	Longitudinal	109.8	115.3	15.0	28.5
	RT	Transverse	89.3	107.2	10.6	18.7
	1800	Longitudinal	44.0	67.1	---	18.7
	2400	Longitudinal	35.3	41.1	---	29.0
	2600	Longitudinal	32.5	36.0	---	26.7
TA-7W-1RE-1Hf-0.012C-0.012N	-320	Longitudinal*	162.0	188.0	4.85	5.50
	-320	Transverse*	158.4	189.8	3.70	5.90
	RT	Longitudinal	109.0	116.0	13.15	22.70
	RT	Transverse	110.0	114.0	3.65	5.95
	1800	Longitudinal	45.3	70.6	---	20.6
	2000	Transverse	40.0	65.0	---	16.4
	2400	Longitudinal	37.2	45.4	---	19.7
	2600	Transverse	31.0	35.9	---	21.5

*The stress-strain curves indicated that twinning may have occurred.

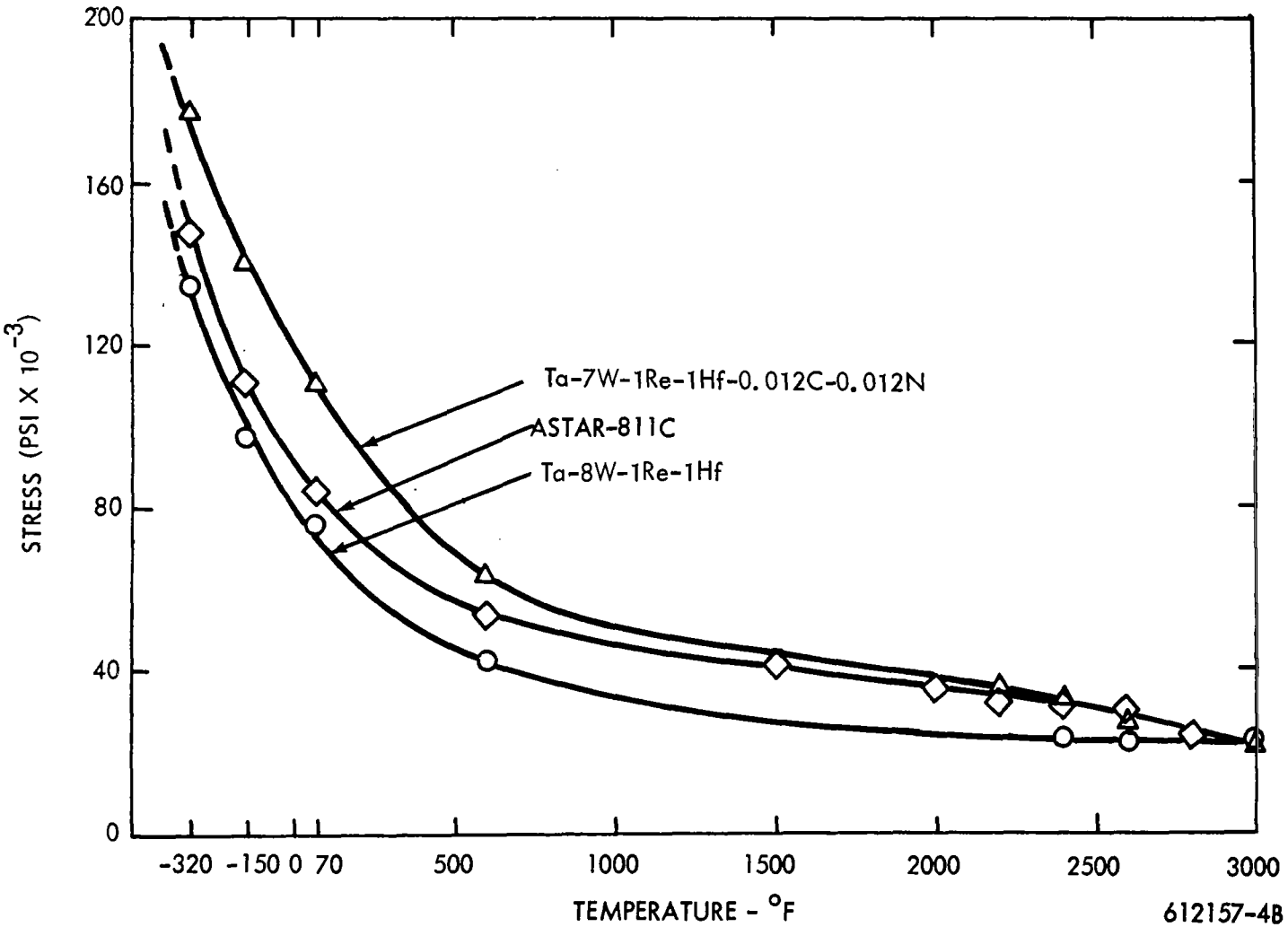

FIGURE 58 - Temperature Dependence of Yield Strength of Scale-Up Tantalum Alloy Compositions

tensile strength of the Ta-W-Re-Hf matrix over the range of -320 to 2600°F with the nitrogen as expected being the most potent. Above 2600°F, carbon and/or nitrogen contribute little to the elevated temperature strength. Excellent tensile ductility was exhibited by all three compositions at -320°F. However, the Ta-7W-1Re-1Hf-0.012C-0.012N composition twinned during testing at -320°F, indicating that the transition region to brittle fracture was being approached. Examples of these mechanical twins which exhibit serrated edges are shown in Figure 59. At -320°F, the solid solution Ta-8W-1Re-1Hf alloy failed by shear while both ASTAR-811C and the Ta-7W-1Re-1Hf-0.012C-0.012N alloy exhibited considerable intergranular separation. However, as the test temperature was raised to 2400°F, ASTAR-811C exhibited less intergranular separation than did either of the other two alloys. Thus the carbide phase is effectively strengthening the boundary (See Figure 60).

The tensile strength of as-GTA welded ASTAR-811C was significantly higher than the annealed base metal over the temperature range of -320 to 2600°F. This is expected since most or all of the carbon is taken in and retained in solution during welding. The GTA welded tensile strength of the other two alloys though was essentially identical to the annealed base metal. This is as expected for the solid solution alloy Ta-8W-1Re-1Hf and also for the Ta-7W-1Re-1Hf-0.012C-0.012N since after the 3000°F anneal, most or all of the carbon and all of the nitrogen is in solution.

During tensile testing of the GTA welded ASTAR-811C at -320°F, audible clicks were also heard, indicative of mechanical twinning. Mechanical twins having both smooth and irregular sides, similar to Neumann bonds in iron were observed. The twins were found only in the cast weld metal and were not detected in the annealed base metal specimens tested at -320°F. The tendency for twinning in the GTA welded ASTAR-811C was probably caused by the greater amount of carbon in solution than for the annealed base metal. Examples of the twins observed in the cast weld metal are illustrated in Figure 61.

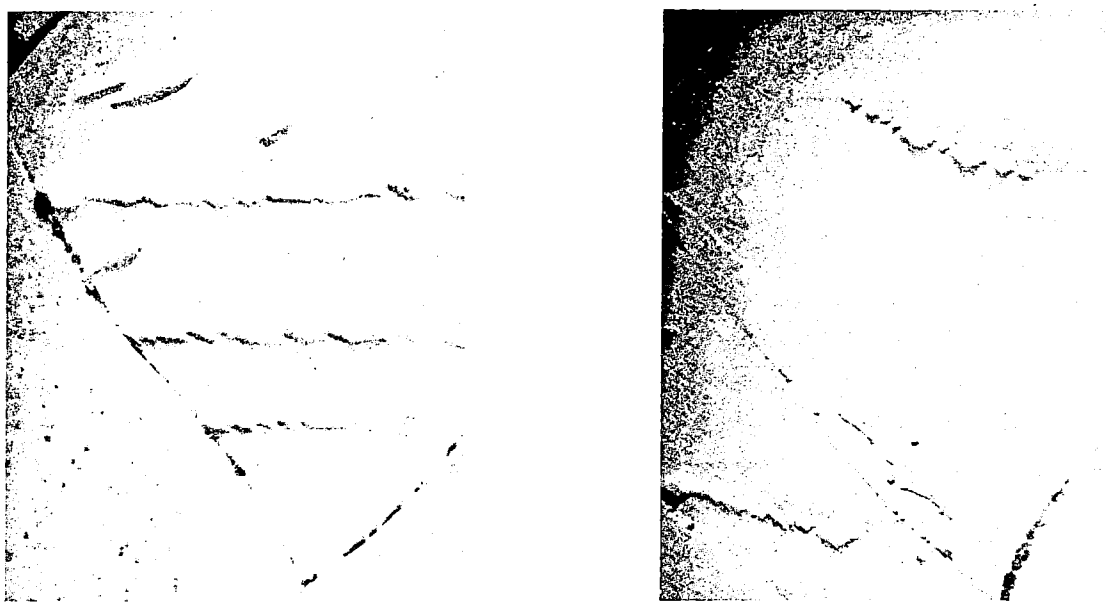

(a) 1500X (b) 1500X

FIGURE 59 - Microstructure of Ta-7W-1Re-1Hf-0.012C-0.012N Tested at -320°F

75X

Ta-8W-1Re-1Hf

150X

ASTAR-811C

(a) Tested at -320°F

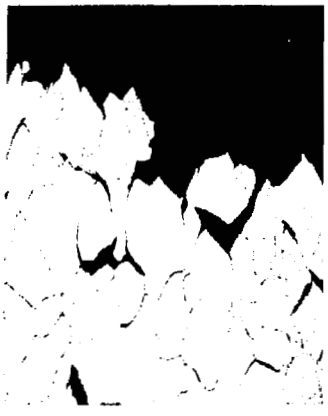

75X

150X

(b) Tested at 2400°F

FIGURE 60 - Tensile Fracture Observed in Scale-Up Alloy Compositions

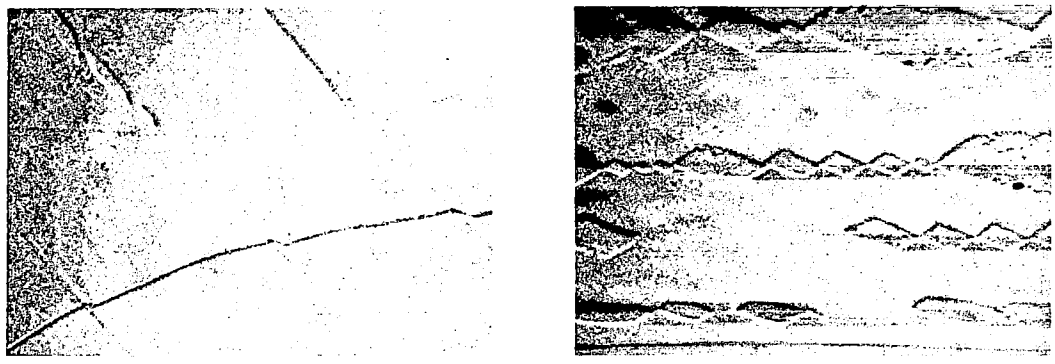

(a) (b)

FIGURE 61 - Microstructure of As-GTA Welded ASTAR-811C Sheet Tensile Tested at -320°F 1500X

As discussed under the previous section, increasing the final annealing temperature improved the resistance of ASTAR-811C to creep deformation at 2400°F. There was also an increase in the room temperature tensile properties as indicated by hardness testing results. The effect of annealing temperature on the tensile properties of ASTAR-811C is illustrated in Figure 62. Photomicrographs showing the resulting microstructure and fracture characteristics are in Figure 63. The sharp increase in yield strength as the annealing temperature was increased is caused most likely by the precipitation of a Ta_2C precipitate which has coherency with the lattice. This has been discussed previously. Another piece of evidence supporting this hypothesis is that the rate of work hardening goes essentially to zero as the annealing temperature was raised to 4000°F. This change in work hardening behavior is typically observed in systems which exhibit coherent precipitation hardening.[39]

The mode of fracture changes from shear for the specimen annealed at 3000°F to intergranular rupture for material annealed at 4000°F. This behavior is consistent with the fracture behavior of ASTAR-811C which has been previously discussed. However, excellent room temperature ductility was exhibited irrespective of the final annealing temperature.

6. Phase Relationships. The phase relationships exhibited by the scale-up compositions were those predicted from the observations made during the screening investigation. However, the major features will be briefly reviewed.

The only precipitating phase found in ASTAR-811C is the (Ta_2C) tantalum dimetal carbide. This phase has been found after heating for short times at temperatures up to 3600°F and after 1000 hours at 2400°F. The solvus for the 250 ppm carbon is estimated to be about 3600°F. However, cooling rates sufficiently fast to suppress precipitation of the carbide when cooling from 3600°F and above have not been achieved. Even though the matrix appears single phase after heat treatment, transmission electron microscopy reveals the presence of a submicron precipitate.

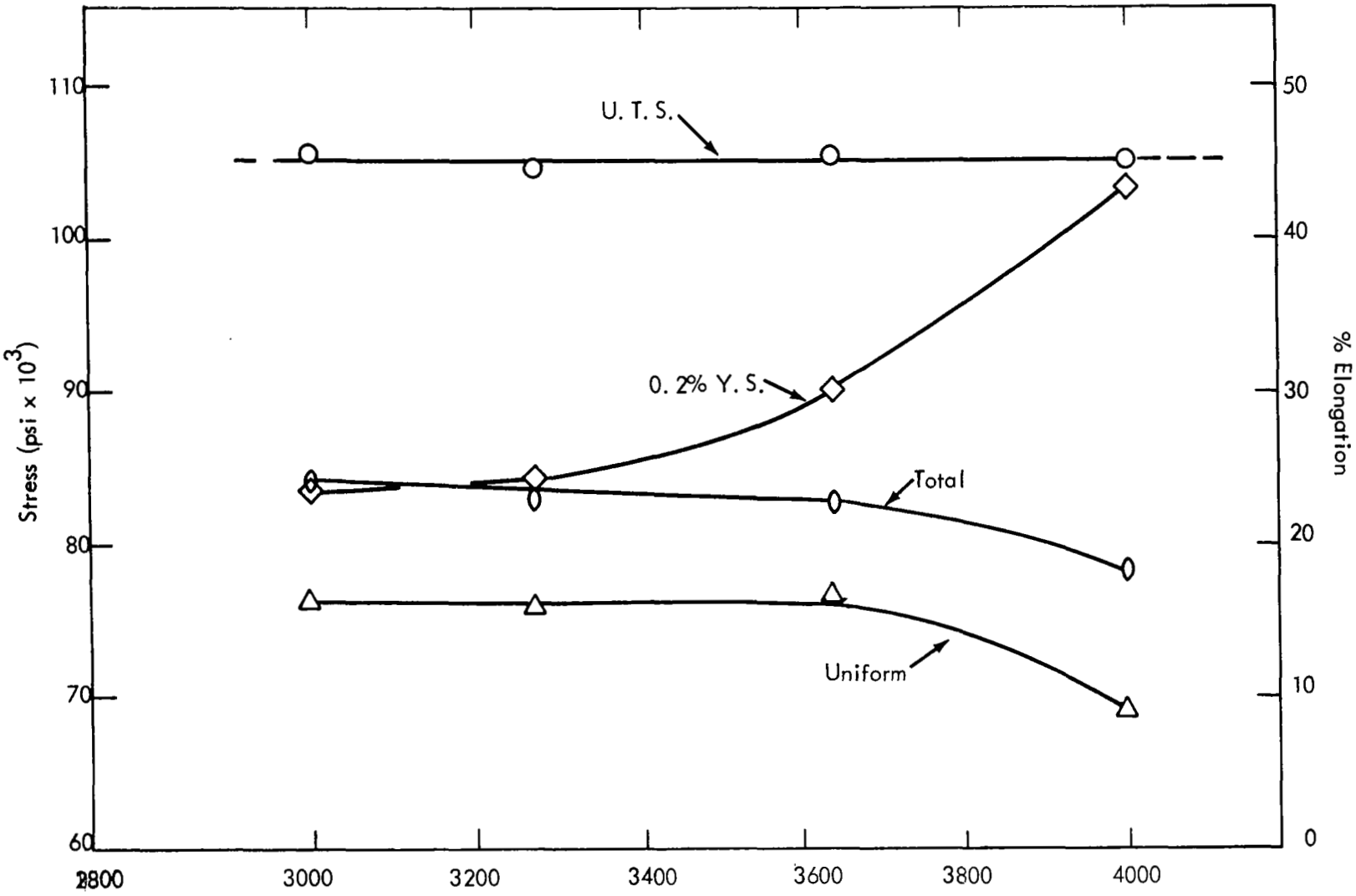

FIGURE 62 - Room Temperature Mechanical Properties of ASTAR-811C (Ta-8W-1Re-0.7Hf-0.025C) as a Function of Heat Treatment

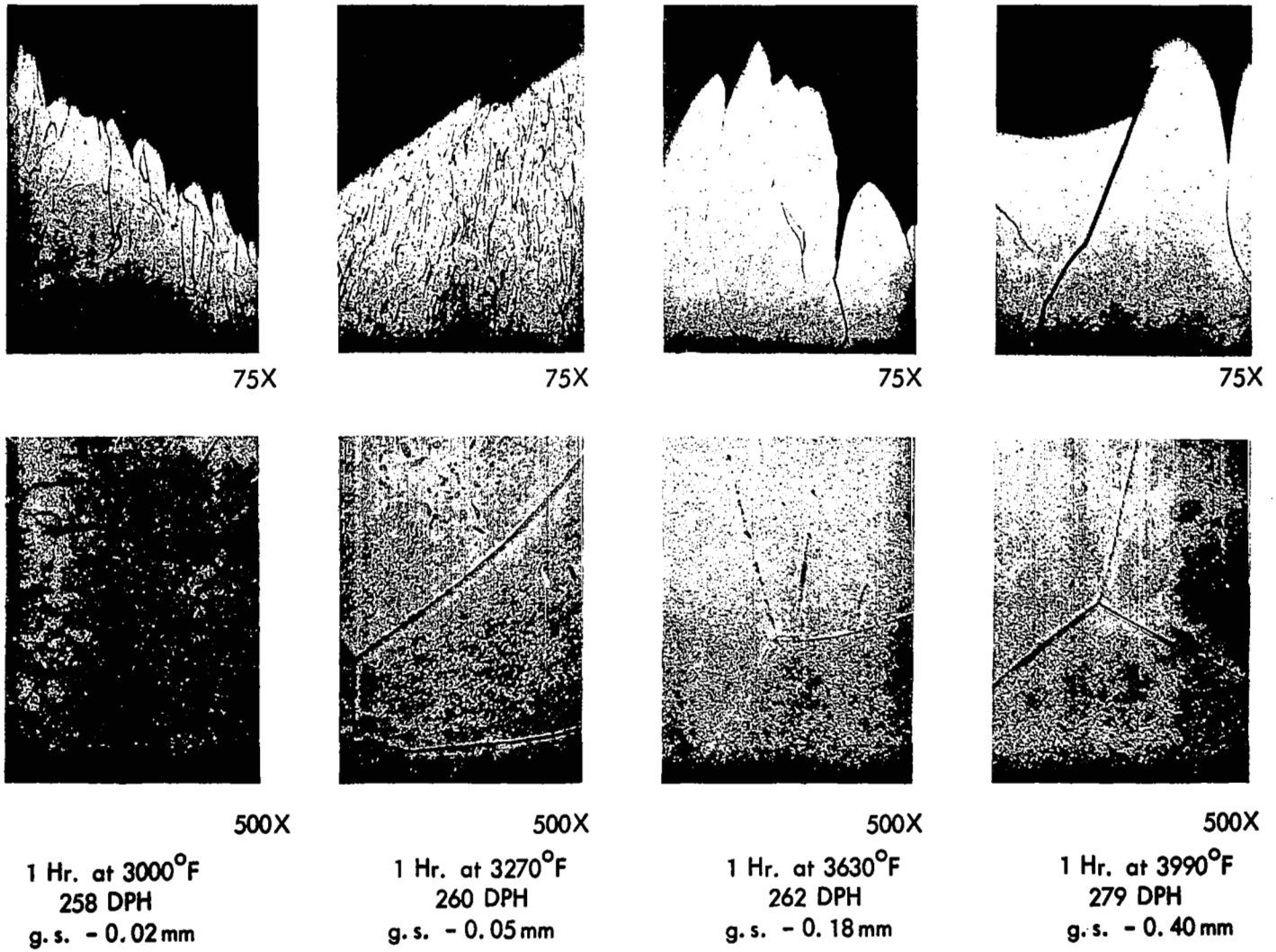

FIGURE 63 - Effect of Annealing Temperature on Microstructure and Room Temperature Fracture Behavior of ASTAR-811C

Two precipitating phases are found in the Ta-7W-1Re-1Hf-0.012C-0.012N alloy. Both the carbon and nitrogen are in solution when heating at 3000°F and above. However, on subsequent reheating at temperatures below 3000°F for 1 hour, the Ta_2C phase precipitates and after extended heating transforms eventually to the FCC $(TaHf)(CN)_{1-x}$ phase. This behavior is summarized in Table 25. Although this system offers ideally the best precipitation kinetics from the standpoint of creep strengthening, the control of nitrogen and the extreme sensitivity of the low temperature ductility to the nitrogen level does not make this system the most desirable for a sheet and tubing alloy. However the possibility of introduction of nitrogen into the tantalum alloy after fabrication of the final component by gas nitridation offers an area worthy of more study and evaluation.

TABLE 25 - PHASE RELATIONSHIPS IN THE Ta-7W-1Re-1Hf-0.012C-0.012N ALLOY

Thermal Treatment		Identification of Bulk Extracted Residue
Temperature (°F)	Time (Hrs.)	
2000	1	Ta_2C[a]
2200	1	Ta_2C
2400	1	Ta_2C
2600	1	Ta_2C
2000	16	Ta_2C
2200	16	Ta_2C
2400	16	Ta_2C
2600	16	Ta_2C+$(TaHf)(CN)_{1-x}$[b]
2200	840	$(TaHf)(CN)_{1-x}$
2400	165	$(TaHf)(CN)_{1-x}$
2400	426	$(TaHf)(CN)_{1-x}$
2400	907	$(TaHf)(CN)_{1-x}$

(a) Ta_2C is HCP with lattice parameters a_o = 3.10-3.11 Å and c_o = 4.94 Å c/a = 1.59

(b) FCC is $(TaHf)(CN)_{1-x}$ with a_o = 4.56-4.58 Å

IV. EFFECT OF OXYGEN CONTAMINATION ON THE WELDABILITY AND THERMAL STABILITY OF TANTALUM ALLOYS

Although ground testing of advanced Rankine liquid alkali metal systems will be done under ultra-high vacuum conditions ($\leq 1 \times 10^{-8}$ torr), a small but finite oxygen pick-up by the refractory alloy components will occur during testing. Oxygen will also be absorbed from the liquid metal fluids being used and local high areas of oxygen concentration can occur by mass transport within the system.[29] Also, accidental inleakage of air due to an uncontrolled leak such as a cracked sight port or a defective weld in the vacuum vessel can result in contamination. Thus the tolerance of the alloy to oxygen contamination and its effects on the weldability and subsequent long time thermal stability is of importance. Detailed investigations in this area have been conducted on T-111 and other commercially available tantalum and columbium base alloys.[60] A limited investigation of oxygen contamination and its effect on weldability and thermal stability was also conducted on selected experimental tantalum alloy sheet compositions developed during this investigation. The compositions selected for study included the following:

1. Ta-10W-1Re-0.5Hf
2. Ta-8W-1Re-0.7Hf-0.025C (ASTAR-811C)
3. Ta-5W-1Re-0.3Zr-0.025N
4. Ta-7.5W-1.5Re-0.5Hf-0.015C-0.015N

This represents tantalum alloy matrices strengthened by (1) substitutional solid solution additions only, (2) (1) plus a carbide dispersed phase, (3) (1) plus a nitride dispersed phase, and (4) (1) plus a carbide, nitride, and/or carbonitride dispersed phase. Weldability, oxygen contamination, and thermal stability tests were conducted on 0.035 inch thick sheet material annealed 1 hour at 3000°F prior to test. Prior to oxygen contamination the optimum welding parameters were developed for each alloy composition. The welding parameters used for each of the alloys studied and the weld bend DBTT in the as-GTA welded condition are listed in Table 26.

TABLE 26 - WELD PARAMETER AND BEND TRANSITION TEMPERATURE RESULTS

Composition	GTA Weld Parameters		Bend Ductile - Brittle[(a)] Transition Temperatures, °F
	Speed ipm	Currents amps	
Ta-10W-1Re-0.5Hf	30	158	-250
Ta-8W-1Re-0.7Hf-0.025C (ASTAR-811C)	15	80	<-250
Ta-5W-1Re-0.3Zr-0.025N	15	118	-250
Ta-7.5W-1.5Re-0.05Hf -0.015C-0.015N	30	124	< +100

(a) 1t bend radius at one ipm punch speed.

Annealed base metal of each of the four compositions was contaminated with nominally 150 and 350 ppm oxygen. Oxygen contamination was done by exposure of 3/4 inch x 6 inch x 0.035 inch test strips at 800-1100°F in a helium atmosphere contaminated with 500 ppm oxygen. An oxygen gage on the outlet side of the apparatus was used to monitor the rate of oxygen pick-up by the specimens. The oxygen contamination procedure has been described in detail by Stoner.[60] Gravimetric techniques were used to measure oxygen pick-up. Correlation with chemical analytical results confirmed the reliability of this method.[60] The oxygen rich layer formed on the surface during the low temperature contamination treatment is diffused inward by heating for 50 hours at 1800°F at $\leq 1 \times 10^{-7}$ torr. After the homogenization treatment, the specimens were GTA welded using the optimum set of welding parameters developed for each of the individual compositions.

The weld bend transition temperature of each composition increased significantly as a result of the prior oxygen contamination. The weld DBTT of each of the alloys studied was more sensitive to oxygen contamination than was T-111 as illustrated by the data in Table 27. An interesting feature of this data is that ASTAR-811C was not any more sensitive to the oxygen contamination than the solid solution alloy studied even though ASTAR-811C has an intentional carbon addition of 250 ppm. The carbonitride strengthened composition exhibited the least sensitiveness to the oxygen contamination in that when contaminated with 350 ppm oxygen the as-GTA welded DBTT increased by only +300F°. The remaining compositions exhibited at least a +550F° increase in DBTT as a result of the 350 ppm oxygen contamination.

GTA welded specimens contaminated with 350 ppm oxygen were exposed for 1000 hours at 1800°F and the bend DBTT was determined. Base metal and as-GTA welded uncontaminated material was also included for those compositions where sufficient material was available. The results of the bend ductile brittle transition temperature determinations are summarized in Table 28. The 1000 hour thermal exposure resulted in an increase in the bend DBTT of GTA welded material and oxygen contaminated material. Again, the reference standard T-111 weldments exhibits the least change in bend ductility after aging. After oxygen contamination and welding, a significant increase in bend DBTT is observed.[60]

TABLE 27 - EFFECT OF OXYGEN CONTAMINATION ON THE BEND TRANSITION TEMPERATURE OF AS-GTA WELDED MATERIAL

Composition	Ductile - Brittle Transition, °F, After GTA Welding Sheet Material Contaminated With Oxygen At A Level Of		
	None	125 - 180 ppm	205 - 370 ppm
T-111[60]	<-320	-275	-250
Ta-10W-1Re-0.5Hf	-250	+ 75	+300
Ta-8W-1Re-0.7Hf-0.025C (ASTAR-811C)	<-250	+ 75	+300
Ta-5W-1Re-0.3Zr-0.025N	-250	+ 75	+400
Ta-7.5W-1.5Re-0.5Hf -0.015C-0.015N	+100	+250	+400

TABLE 28 - EFFECT OF A 1000 HOUR EXPOSURE AT 1800°F ON THE BEND DUCTILITY OF OXYGEN CONTAMINATED GTA WELDS

Composition	Bend Ductile - Brittle Transition Temperature, °F					
	Base Metal	As-GTA Welded	0_2 Contam.[(a)] and TIG Welded	Base Metal Aged[(b)]	Welded and Aged[(b)]	0_2 Contam.[(a)] Welded and Aged[(b)]
T-111[(60)]	<-320	<-320	-250	<-320	<-320	0
Ta-10W-1Re-0.5Hf	<-320	-250	+300	-225	-150	+500
Ta-8W-1Re-0.7Hf -0.025C (ASTAR-811C)	<-320	<-250	+250	--	-100	+200
Ta-5W-1Re-0.3Zr -0.025N	<-320	-250	+400	-300	+300	>+800
Ta-7.5W-1.5Re-0.5Hf -0.012C-0.012N	-175	+100	+400	--	+200	+600

(a) Contaminated with nominally 350ppm 0_2

(b) 1000 hours at 1800°F

Room temperature hardness was measured on the transverse weld sections which were:

(a) GTA welded plus 1000 hours at 1800°F.

(b) Contaminated with 350 ppm O_2 then GTA welded.

(c) (b) plus 1000 hours at 1800°F.

The hardness traverse data are presented along with selected photomicrographs in Figures 64 through 71. The letter notations on the hardness traverse plots correspond to the area from which the photomicrographs were taken. Local hardness variations within the fusion zone are most likely due to grain orientation and constitutional segregation during freezing. The severe thermal disturbance, over a broad temperature spectrum, experienced in the adjacent heat affected zone no doubt may have triggered complex precipitation reactions. Although quantitative interpretation of the hardness data are difficult since the precipitation reactions occurring in the oxygen contaminated material have not been positively identified, the data obtained do permit a discussion of the probable precipitation reactions and their effect on the low temperature strength of the base metal.

The starting sheet material (0.035 inch thick) was annealed for 1 hour at 3000°F prior to oxygen contamination and/or welding. After 1000 hours at 1800°F, the hardness of each of the compositions has decreased significantly with the exception of the nitrogen bearing alloy, as shown by the data tabulated in Table 29.

During the final annealing treatment at 3000°F all or part of the carbon and/or nitrogen addition was taken into solution. During subsequent annealing at 1800°F, the carbon precipitates from the Ta-W-Re-0.5-1Hf solid solution matrix by the following reaction.

$$(Ta,W,Re,Hf)_{\text{solid solution}} + C_{\text{solid solution}} \rightleftharpoons Ta_2C(ppt) + (Matrix)_{SS}$$

TABLE 29 - EFFECT OF 1000 HOURS AT 1800°F ON THE HARDNESS OF TANTALUM ALLOY SHEET (ANNEALED 1 HOUR AT 3000°F PRIOR TO THE EXPOSURE)

Composition	As-Annealed 1 Hr. at 3000°F	Hardness, DPH Plus 1000 Hours at 1800°F	Δ DPH
Ta-10W-1Re-0.5Hf	230	195	-35
Ta-8W-1Re-7Hf-0.025C (ASTAR-811C)	255	188	-67
Ta-7.5W-1.5Re-0.5Hf-0.015C-0.015N	310	228	-82
Ta-5W-1Re-0.3Zr-0.025N	275	325	+50

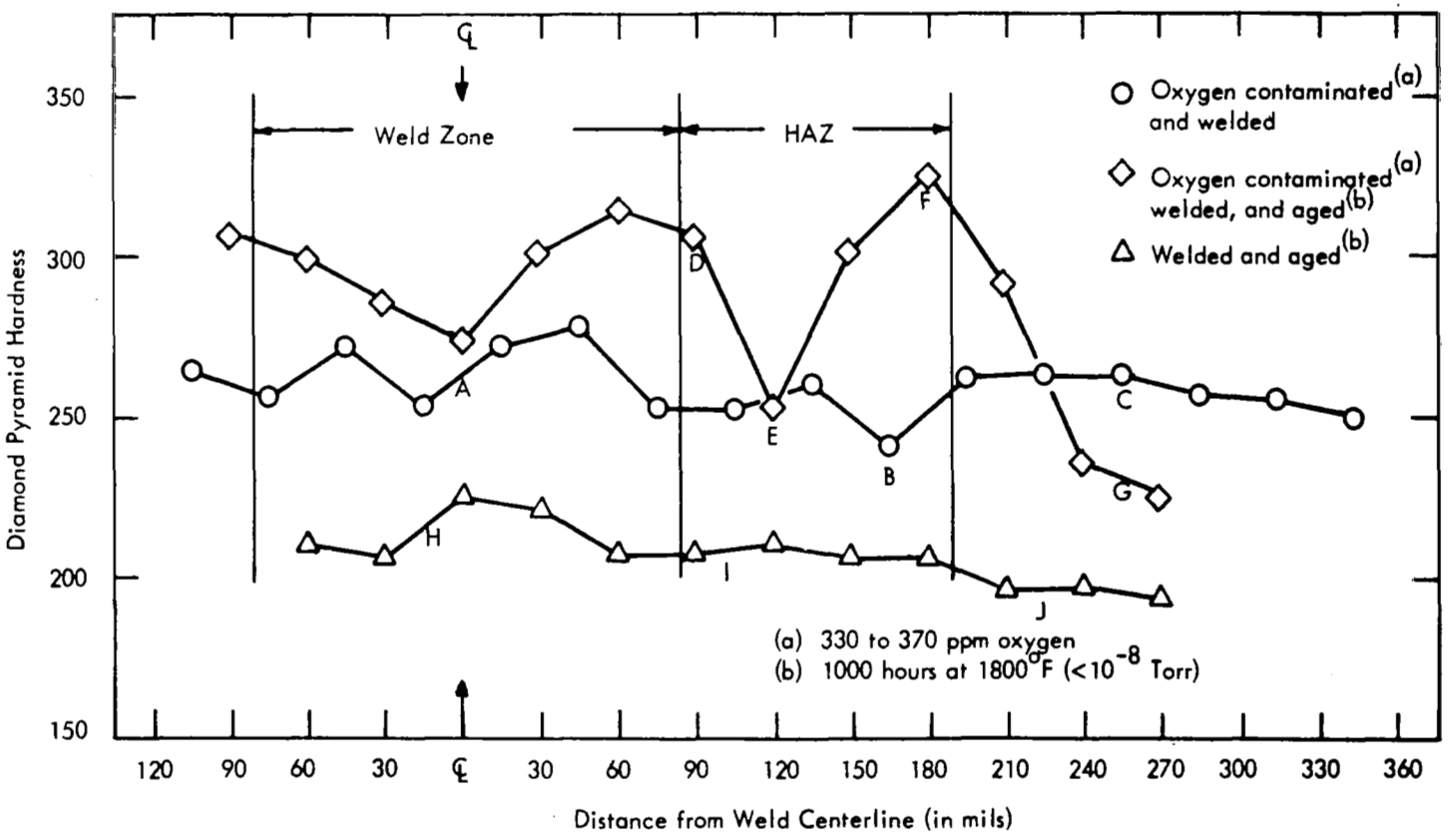

FIGURE 64 - Diamond Pyramid Hardness Traverses of Ta-10W-1Re-0.5Hf Weld Specimens

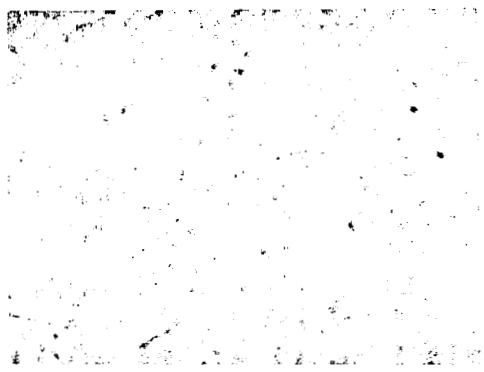

(a) Weld Zone (Point A in Fig. 64) 500X 268 DPH

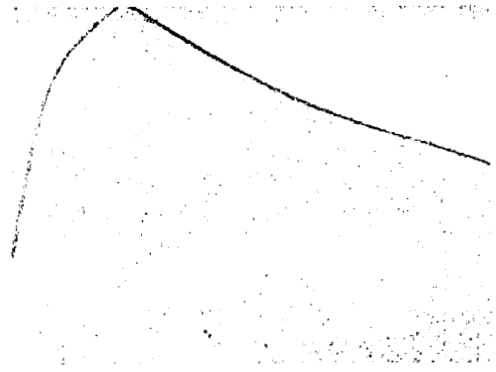

(b) HAZ (Point B in Fig. 64) 1500X 240 DPH

(c) Base Metal (Point C in Fig. 64) 1500X 263 DPH

Oxygen Contaminated and Welded Specimen

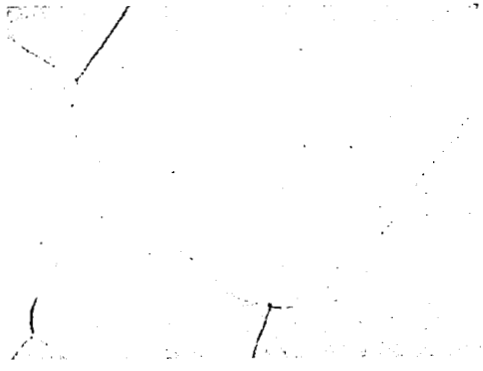

(d) HAZ (Point D in Fig. 64) 500X 307 DPH

(e) HAZ (Point E in Fig. 64) 1500X 252 DPH

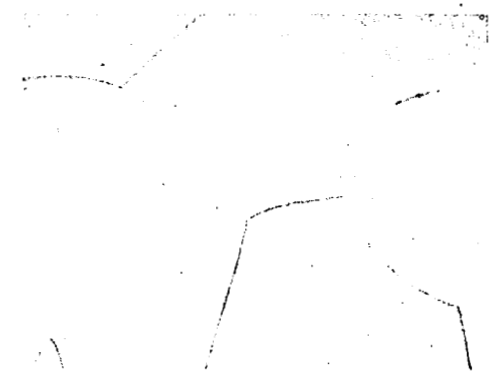

(f) Base Metal (Point G in Fig. 64) 500X 225 DPH

Oxygen Contaminated, Welded, and Aged[(a)] Specimen

(a) 1000 Hours at 1800°F ($<10^{-8}$ Torr)

FIGURE 65 - Microstructures of Ta-10W-1Re-0.5Hf Welded Specimens

(g) Weld Zone (Point H in Fig. 64) 1500X 212DPH

(h) HAZ (Point I in Fig. 64) 500X 208 DPH

(i) Base Metal (Point J in Fig. 64) 500X 197 DPH

Welded and Aged[(a)] Specimen

(a) 1000 Hours at 1800°F (<10^{-8} Torr)

FIGURE 65 (Continued) - Microstructures of Ta-10W-1Re-0.5Hf Welded Specimens

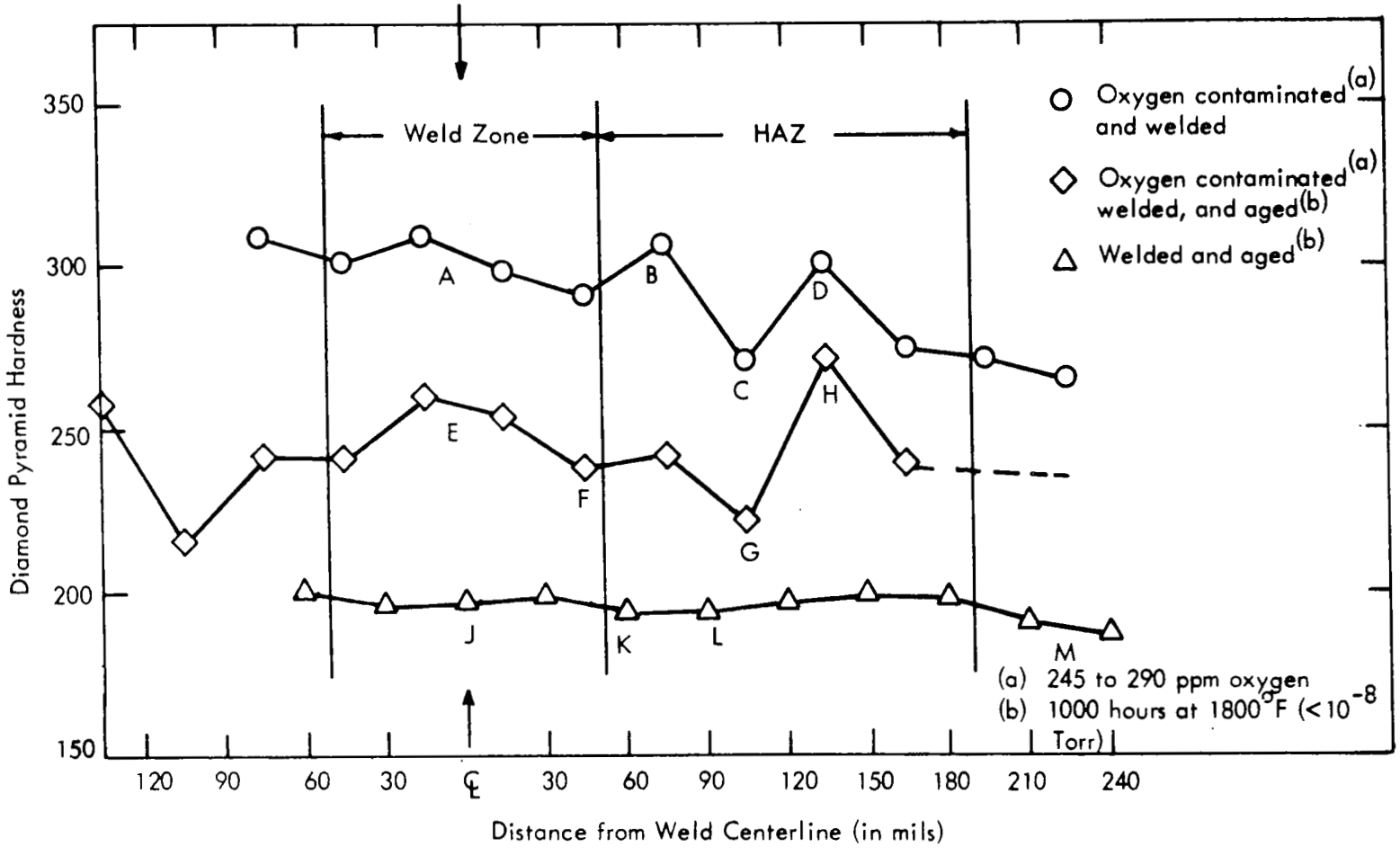

FIGURE 66 - Diamond Pyramid Hardness Traverses of ASTAR-811C (Ta-8W-1Re-0.7Hf-0.025C) Weld Specimens

(a) Weld Zone (Point A in Fig. 66) 1500X
305 DPH

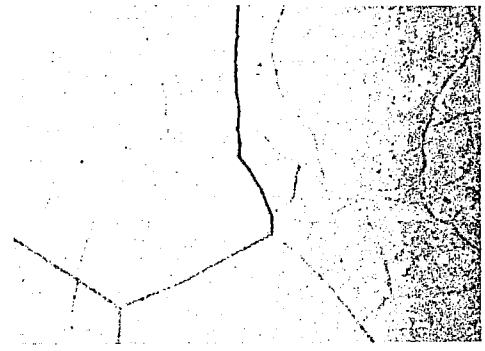

(b) HAZ (Point B in Fig. 66) 1500X
305 DPH

Oxygen Contaminated and Welded Specimen

(c) HAZ (Point C in Fig. 66) 1500X
270 DPH

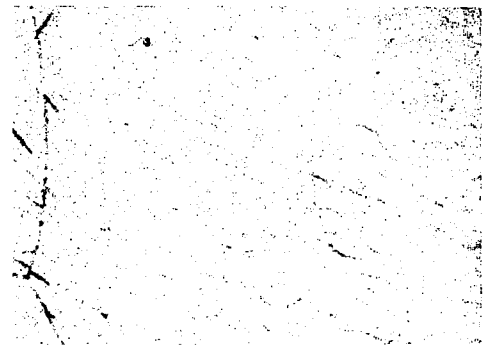

(d) HAZ (Point D in Fig. 66) 1500X
300 DPH

Oxygen Contaminated and Welded Specimen

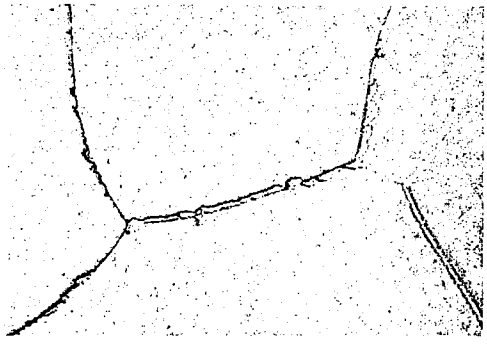

(e) Weld Zone (Point E in Fig. 66) 500X
255 DPH

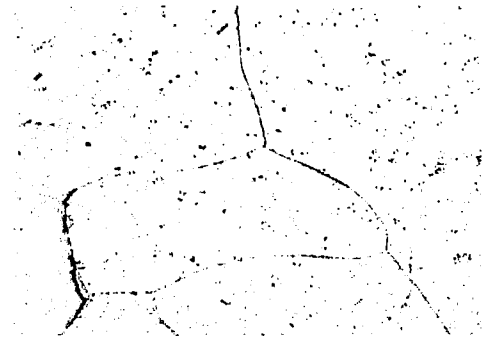

(f) Weld Zone (Point F in Fig. 66) 500X
262 DPH

Oxygen Contaminated, Welded, and Aged[a] Specimen

(a) 1000 Hours at 1800°F (<10^{-8} Torr)

FIGURE 67 - Microstructures of ASTAR-811C(Ta-8W-1Re-0.7Hf-0.025C) Welded Specimens

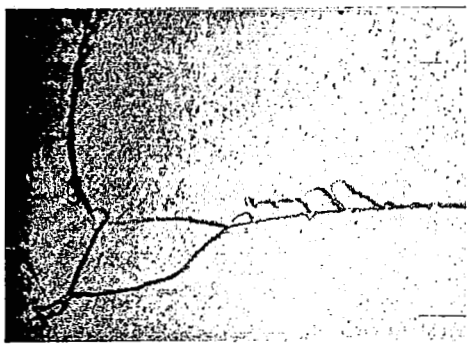

(g) HAZ (Point G in Fig. 66) 1500X
223 DPH

(h) Base Metal (Point I in Fig. 66) 500X
220 DPH

Oxygen Contaminated, Welded, and Aged[a] Specimen

(i) Weld Zone (Point J in Fig. 66) 500X
195 DPH

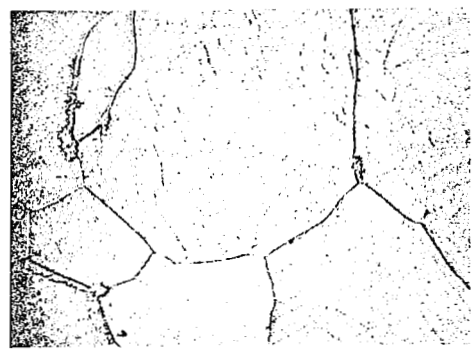

(j) HAZ (Point K in Fig. 66) 500X
190 DPH

Welded and Aged[a] Specimen

(k) HAZ (Point L in Fig. 66) 500X
190 DPH

(e) Base Metal (Point M in Fig. 66) 500X
188 DPH

Welded and Aged[a] Specimen

(a) 1000 Hours at 1800°F ($<10^{-8}$ Torr)

FIGURE 67 - (Continued) - Microstructures of ASTAR 811-C (Ta-8W-1Re-0.7Hf-0.025C) Welded Specimens

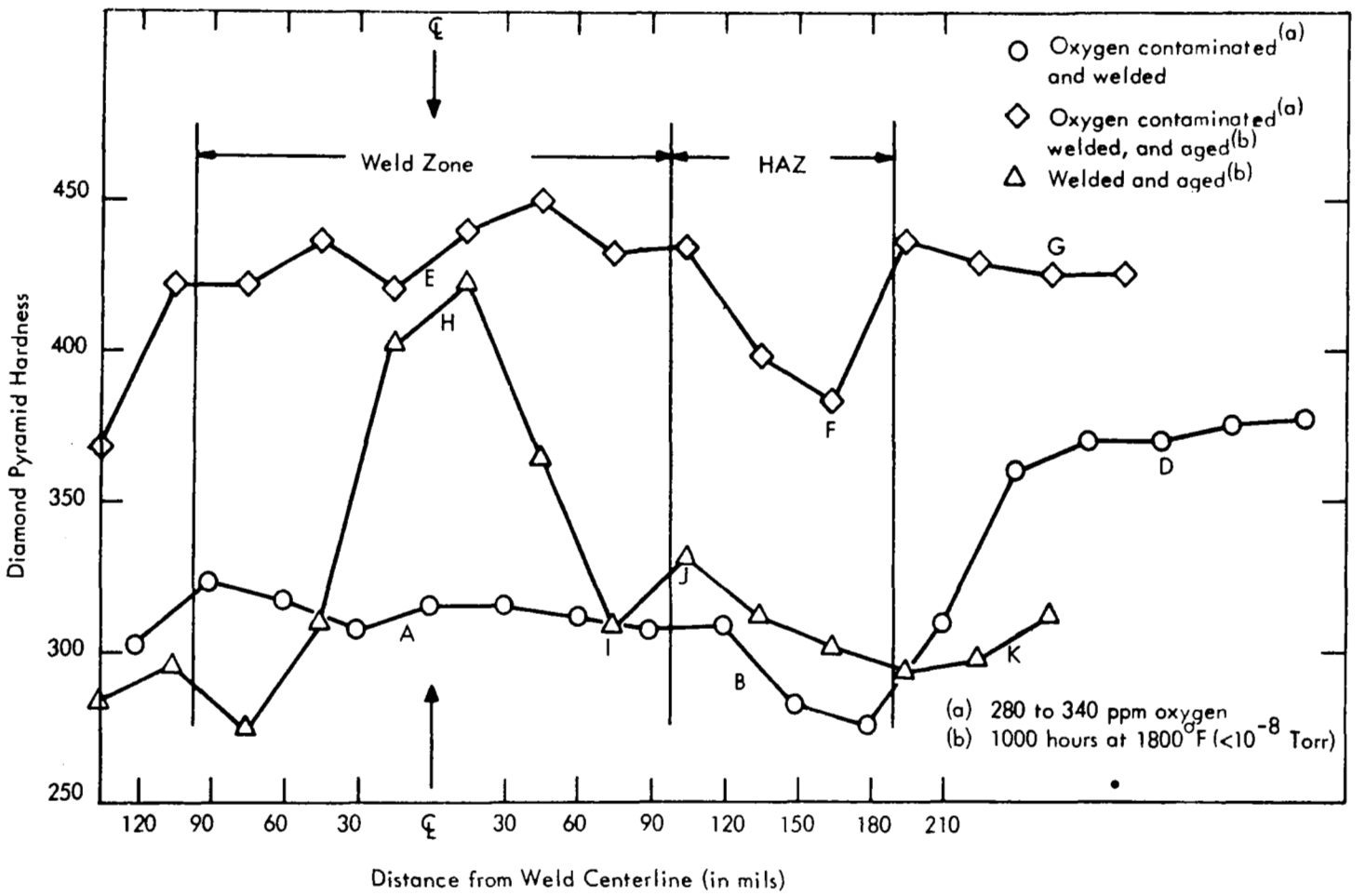

FIGURE 68 - Diamond Pyramid Hardness Traverses of Ta-5W-1Re-0.3Zr-0.025N Weld Specimens

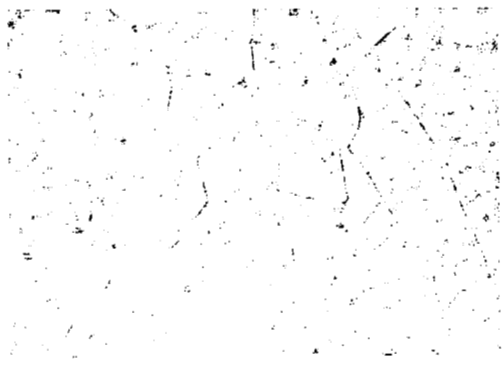

(a) Weld Zone (Point A in Fig. 68) 500X
315 DPH

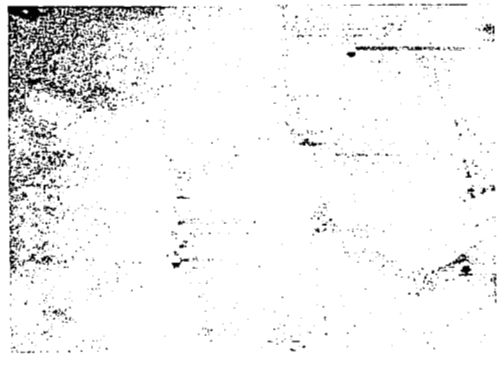

(b) Weld Zone (Point A in Fig. 68) 1500X
315 DPH

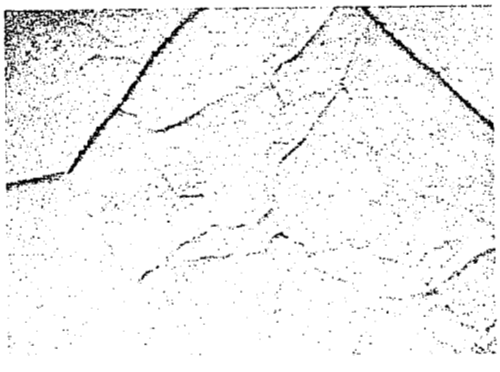

(c) HAZ (Point B in Fig. 68) 1500X
300 DPH

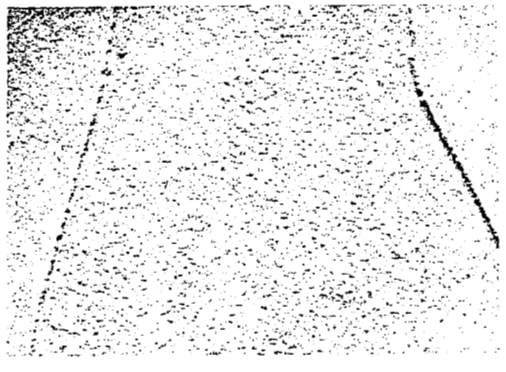

(d) HAZ (Point C in Fig. 68) 1500X
275 DPH

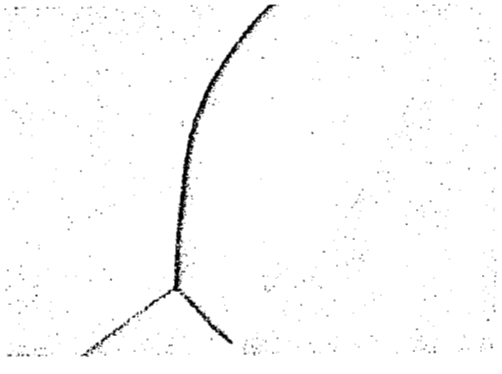

(e) Base Metal (Point D) in Fig. 68) 1500X
370 DPH

Oxygen Contaminated and Welded Specimens

FIGURE 69 - Microstructures of Ta-5W-1Re-0.3Zr-0.02N Welded Specimens

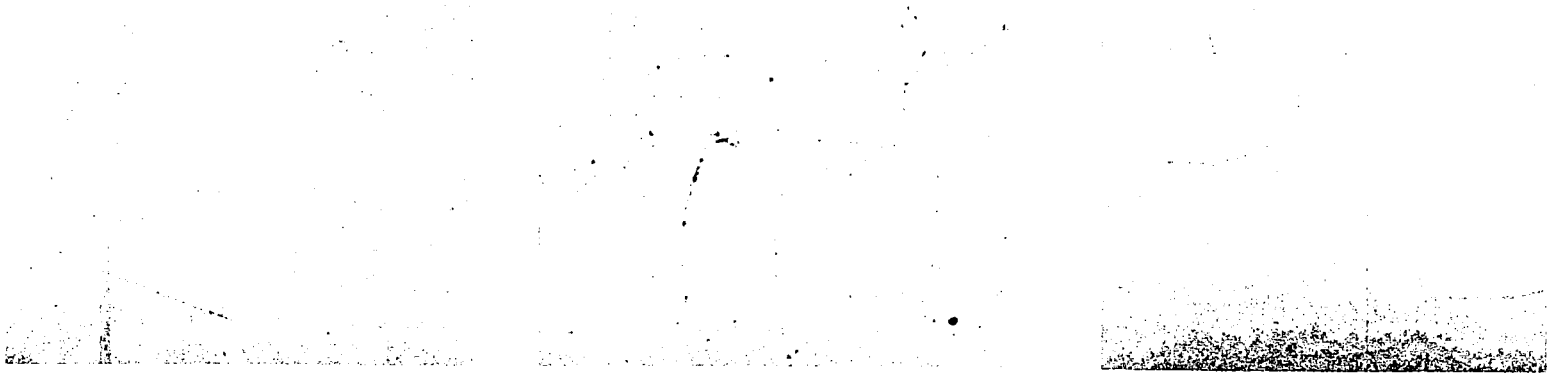

(f) Weld Zone (Point E in Fig. 68) 500X 430 DPH

(f) HAZ (Point F in Fig. 68) 500X 383 DPH

(h) Base Metal (Point G in Fig. 68) 500X 425 DPH

Oxygen Contaminated, Welded, and Aged[(a)] Specimen

(i) Weld Zone (Point H in Fig. 68) 500X 308 DPH

(j) HAZ (Point J in Fig. 68) 500X 332 DPH

(k) Base Metal (Point K in Fig. 68) 1500X 305 DPH

Welded and Aged[(a)] Specimen

(a) 1000 Hours at 1800°F ($<10^{-8}$ Torr)

FIGURE 69 (Continued) - Microstructures of Ta-5W-1Re-0.3Zr-0.02N Welded Specimens

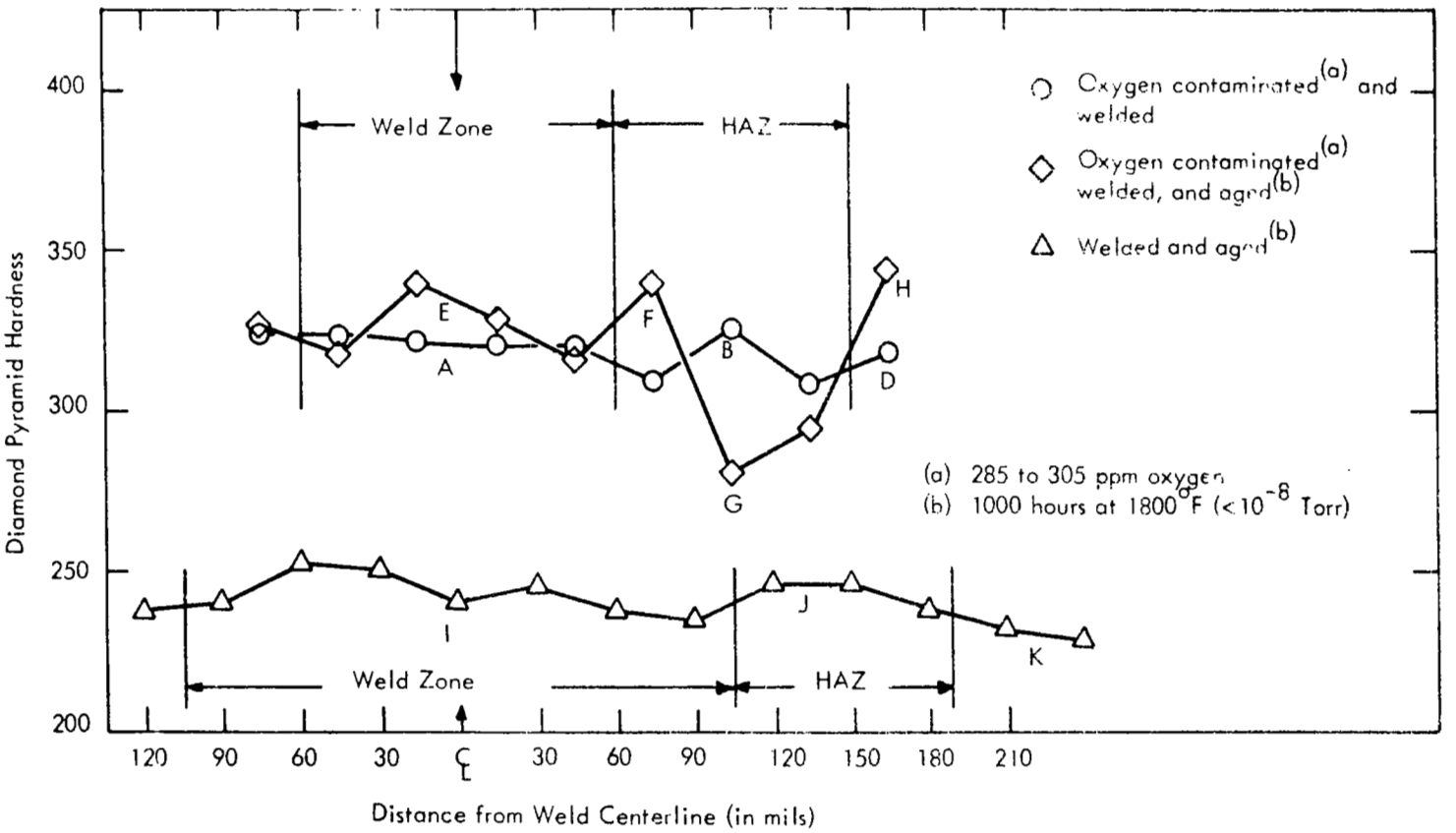

FIGURE 70 - Diamond Pyramid Hardness Traverses of Ta-7.5W-1.5Re-0.5Hf-0.015C-0.015N Weld Specimens

(a) Weld Zone (Point A in Fig. 70) 500X
320 DPH

(b) HAZ (Point B in Fig. 70) 500X
325 DPH

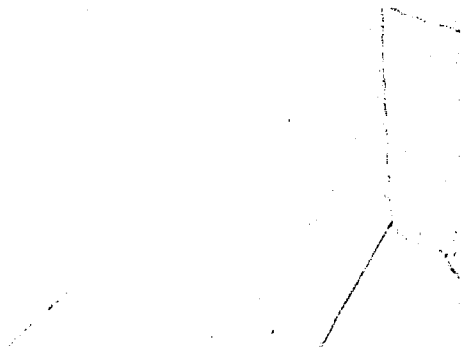

(c) HAZ (Point C in Fig. 70) 1500X
308 DPH

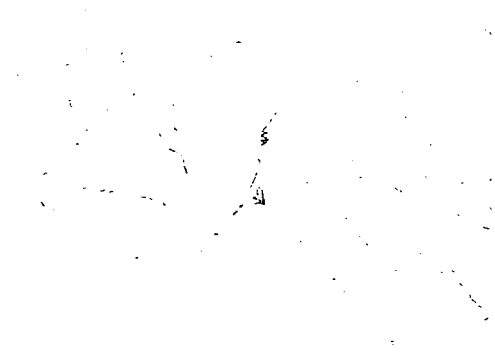

(d) Base Metal (Point D in Fig.70) 500X
318 DPH

Oxygen Contaminated and Welded Specimen

FIGURE 71 - Microstructures of Ta-7.5W-1.5Re-0.5Hf-0.015C-0.015N Welded Specimens

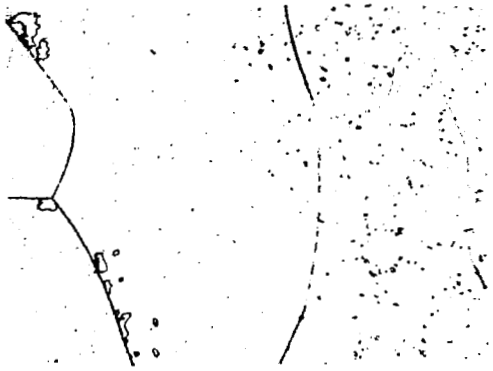

(e) Weld Zone (Point E in Fig. 70) 500X 335 DPH

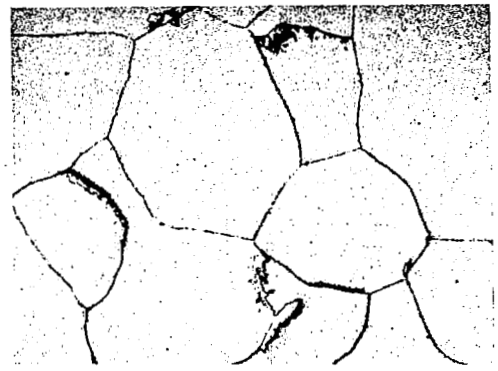

(f) HAZ (Point F in Fig. 70) 500X 340 DPH

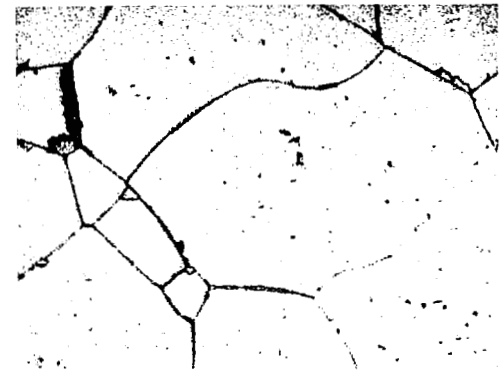

(g) Base Metal (Point H in Fig. 70) 500X 345 DPH

Oxygen Contaminated, Welded, and Aged[(a)] Specimen

(h) Weld Zone (Point I in Fig. 70) 500X 240 DPH

(i) HAZ (Point J in Fig. 70) 500X 245 DPH

(j) Base Metal (Point K in Fig. 70) 500X 230 DPH

Welded and Aged[(a)] Specimen

(a) 1000 Hours at 1800°F ($<10^{-8}$ Torr)

FIGURE 71 (Continued) - Microstructures of Ta-7W-1.5Re-0.5Hf-0.015C-0.015N Welded Specimens

The hardness of the matrix is lowered by this reaction since the dimetal carbide forms a discreet non-coherent second phase particle. The decrease in hardness observed for the solid solution composition Ta-10W-1Re-0.5Hf is atributed to precipitation of the residual carbon (~32 ppm) as Ta_2C. This data would indicate that the carbon solubility in the matrix is very low at 1800°F. The nitride strengthened composition Ta-5W-1Re-0.3Zr-0.025N showed, however, a 50 DPH increase in hardness as a result of the 1000 hour exposure at 1800°F. The hardness increase here is attributed to the coherent nitride precipitation reaction.

$$(Ta,W,Re,Hf,Zr)_{\text{solid solution}} + N_{\text{solid solution}} \rightleftharpoons (ZrHf)N \text{ (coherent ppt)} + (\text{Matrix})_{SS}$$

The kinetics of this reaction and the degree of strengthening are dependent on the aging temperature, aging time, and degree of supersaturation.

Thus in the carbonitride containing composition, Ta-7.5W-1.5Re-0.5Hf-0.015C-0.015N, both reactions may be occurring simultaneously. However, the hardness data in Table 30 suggest that the precipitation reaction resulted in the formation of a non-coherent phase. This indicates that the presence of carbon may alter the nitride precipitation reaction.

As discussed earlier, oxygen was added to the base metal by formation of an adherent oxide film at approximately 1100°F which was then subsequently diffused in by annealing for 50 hours at 1800°F. Introducing oxygen to the tantalum alloy matrix by low temperature oxidation results in an increase in the matrix room temperature hardness. (See Table 29). Rowcliffe, et al[61] have shown that a coherent oxide precipitate is formed when Cb-1Zr or Cb-1W-1Zr sheet is exposed to a low oxygen partial pressure at 1500-1800°F. The observed increase in both the low temperature and elevated temperature properties was attributed to a coherent ZrO_2 precipitate formed during the low oxygen partial pressure exposure.[61]

TABLE 30 - HARDNESS OF OXYGEN CONTAMINATED TANTALUM ALLOYS BEFORE AND AFTER EXPOSING FOR 1000 HOURS AT 1800°F

Composition	Initial[a] Condition DPH	Oxygen Contaminated					
		Oxygen Level Weight %	Atom %	A_s[b] Contaminated DPH	$\partial\Delta DPH/\partial C$[c]	O_2 Contaminated Plus 1000 Hrs. at 1800°F DPH	$\partial\Delta DPH/\partial C$[d]
Ta-10W-1Re-0.5Hf	230	0.021	0.24	255	104	225	125
Ta-8W-1Re-0.7Hf-0.025C (ASTAR-811C)	255	0.0295	0.33	265	30	235	143
Ta-7.5W-1.5Re-0.5Hf-0.015C-0.015N	310	0.029	0.33	318	24	340	340
Ta-5W-1Re-0.3Zr-0.025N	275	0.0335	0.38	375	263	425	263

(a) Annealed 1 hour at 1650°C (3000°F).

(b) Doped at 1100°F and then diffusion annealed 50 hours at 1800°F.

(c) $\partial\Delta DPH/\partial C$, change in hardness per atom percent oxygen added, $\Delta DPH = DPH_{\text{as doped}} - DPH_{\text{as annealed}}$

(d) $\Delta DPH = DPH_{\text{contaminated+1000 hours at 1800°F}} - DPH_{\text{annealed+1000 hours at 1800°F}}$

The strengthening of the tantalum alloy matrix by the oxygen contamination is assumed to be caused by a similar reaction. The strengthening effect of the oxygen addition was evaluated using room temperature hardness values. The change in hardness per atom percent oxygen ($\partial\Delta DPH/\partial C$) added are listed in Table 30. For material in the as-contaminated condition, values of $\partial\Delta DPH/\partial C$ of 24-30 were observed for the carbide and carbonitride strengthened compositions and 100-250 for the solid solution and nitride strengthened composition. The values of 24-30 for $\partial\Delta DPH/\partial C$ appear low. Adding oxygen to columbium and tantalum results in values for $\partial\Delta DPH/\partial C$ of 140 and 170 respectively[36] and are representative values for interstitial hardening in BCC metals.[62] This is in contrast to values of $\partial\Delta DPH/\partial C$ of 10-20 for substitutional solute strengthening additions (i. e., W,Re,Hf,Mo).[36,62] As contaminated (See Figure 65a), the microstructure is single phase when examined at 1500X, and as previously noted, it is assumed that the oxygen combines with the reactive metal (Hf) to form a coherent HfO_2 precipitate. The strengthening of the coherent precipitate ($\partial\Delta DPH/\partial C$) should be on the same order of magnitude as that observed for the interstitial solid solution strengthening. After exposing for 1000 hours at 1800°F, the $\partial\Delta DPH/\partial C$ values for the strengthening contribution of the oxygen addition are consistent. The low values of $\partial\Delta DPH/\partial C$ for ASTAR-811C and the Ta-7.5W-1.5Re-0.5Hf-0.015C-0.015N alloy in the as-contaminated condition most probably resulted from carbide precipitation during the 50 hour homogenizing treatment. The values of $\partial\Delta DPH/\partial C$ for the carbonitride and nitride strengthened alloys after the 1000 hour exposure are 2 to 3 times that for the solid solution Ta-10W-1Re-0.5Hf and carbide strengthened ASTAR-811C composition and no doubt reflects the additive contribution of the coherent nitride precipitation reaction.

The strengthening effects of the oxygen, nitrogen, and carbon on the tantalum alloy matrix are very complex. The interesting strength properties resulting from the various precipitation reactions will require much more investigation before they are understood, particularly their effect on elevated temperature strength.

The interactions of the oxide, nitride, and/or carbide precipitation reactions are complex. Though studied by many to determine their effects on mechanical properties, little has been done to identify the kinetics, and sequence of precipitation. Although it would appear that the oxide may even offer some elevated temperature strengthening possibilities, the oxide precipitate loses coherency with the matrix at 2000°F and above and thus is not effective for imparting high temperature strength.[61] As illustrated here, oxygen has a deleterious effect on weldability and thermal stability, at least at 1800°F, but it would be expected that by heating the contaminated material above 2200°F, precipitation of an innocuous HfO_2 or ZrO_2 would occur which would not impair ductility or strength.

The study described here is very preliminary in nature and will have to be expanded upon before an understanding of the inter-relation between the interstitial compounds and strength, fabricability and weldability of the tantalum alloy matrix is understood.

V. CONCLUSIONS

This was the first refractory metal alloy development program where primary emphasis was on optimizing long time creep properties. A significant advance has been made in tantalum technology with the development of ASTAR-811C, Ta-8W-1Re-0.7Hf-0.025C, a carbide dispersion strengthened tantalum alloy which has significantly better creep resistance than any commercially available tantalum alloy, and yet good fabricating and welding characteristics were retained.

A number of important conclusions which can be made from the results of this investigation are:

1. Carbides and nitrides are both effective creep strengtheners of tantalum alloy matrices.

2. From weldability and fabricability limitations, the carbon content should not exceed 300 ppm and from creep strength considerations should not be less than 200 ppm in an alloy containing 8-10% W+Re+Hf.

3. The (Ta+W)-Hf-C phase relationships have been defined and show that the Ta_2C is an effective dispersed phase for improving long time creep properties.

4. The amount of rhenium and hafnium are both critical. Optimum creep resistance is achieved with rhenium present in the amount of 0.5 to 1.5% and hafnium 0.5 to 1%.

5. The creep behavior can be significantly altered by changing the morphology of the Ta_2C precipitate by controlling final annealing practice.

6. Nitrides are more effective strengtheners than carbides below 2400°F since it has been shown that the reactive metal nitride precipitate has coherency with the tantalum alloy matrix.

VI. REFERENCES

1. R. W. Buckman, Jr., and R. C. Goodspeed, "Precipitation Strengthened Tantalum Base Alloy ASTAR-811C," Topical Summary, WANL-PR-(Q)-016, Westinghouse Astronuclear Laboratory, Pittsburgh, Pa. (NASA CR-1641, 1970).

2. R. L. Orr, O. D. Sherby, and J. E. Dorn, Trans. AIME, Vol. 200, p. 70, 1954.

3. J. E. Dorn, "Symposium on Creep and Fracture of Metals at High Temperature," p. 89, Her Majesty's Stationery Office, London, 1956.

4. O. D. Sherby, Acta Met. Vol. 10, p. 135, 1962.

5. P. Shaninion and J. R. Lane, Trans. ASM, Vol. 45, p. 177, 1953.

6. J. Weertman, Appl. Physics, Vol. 28, p. 362, 1957.

7. G. S. Ansell, "Mechanical Properties of Two-Phase Materials", International Symposium on High Temperature Technology, Asilomar Conference Grounds, California, September 8-11, 1963.

8. A. L. Field Jr., R. L. Ammon, A. I. Lewis, and L. S. Richardson, "Research and Development of Tantalum and Tungsten Base Alloys", Final Report Prepared under Navy, Bureau of Naval Weapons, Contract NOas 58-852-C, May 26, 1961.

9. R. L. Ammon and R. T. Begley, "Pilot Production and Evaluation of Tantalum Alloy Sheet", Summary Phase Report, WANL-PR-M-004, June 15, 1963, Prepared under Navy, Bureau of Naval Weapons, Contract NOw 62-0656-d.

10. F. F. Schmidt, et al, "Investigation of Tantalum and its Alloys", ASD-TDR-62-594, October, 1962.

11. F. F. Schmidt, E. S. Bartlett, and H. R. Ogden, "Investigation of Tantalum and its Alloys", ASD-TRD-62-594, Part II.

12. R. L. Ammon and R. T. Begley, "Pilot Production and Evaluation of Tantalum Alloy Sheet", Summary Phase Report, Part II, Prepared under Navy Contract N600(19)59762, July 1, 1964, (WANL-PR-M-009).

13. R. T. Begley, R. W. Buckman, J. L. Godshall, and R. Stickler, "Development of Columbium-Base Alloys", WADC-TR-57344, Part VII, April, 1963.

14. W. C. Chang, "A Study of the Influence of Heat Treatment to Microstructures and Properties of Refractory Alloys", Technical Report, ASD-TR-211, April, 1962.

15. P. Schwarzkopf and R. Kieffer "Refractory Hard Metals" McMillan, New York, 1953.

16. E. K. Storms, "A Critical Review of Refractories", Part I Selected Properties of Group 4a, 5a, and 6a Carbides, LAMS-2674, March 15, 1962.

17. Breuer, Bromoly, Tofgreen,"Thermodynamic and Physical Properties of Nitrides and Carbides" Page 4 in Chemistry and Metallurgy, Miscellaneous Material Thermodynamics, L. L. Quill, Editor, National Nuclear Energy Series.

18. W. H. Chang, "The Effect of Heat Treatment on Strength Properties of Molybdenum Base Alloys", ASM Transactions Quarterly, March 1963.

19. R. T. Begley, R. L. Ammon, and R. Stickler, "Development of Niobium Base Alloys", Technical Report WADC-TR-57-344, Part VI, February, 1963.

20. D. R. Stoner and G. G. Lessmann, "Measurement and Control of Weld Chamber Atmospheres" Welding Journal Research Supplement, August 1965.

21. Anon: "Evaluation Test Methods for Refractory Metal Sheet Materials", Material Advisory Board, Report 176M.

22. Anon: "Evaluation Test Methods for Refractory Metal Sheet Materials", Material Advisory Board, Report 192M.

23. R. W. Buckman, Jr., and J.S. Hetherington "Apparatus for Determining Creep Behavior Under Conditions of Ultra High Vacuum" Review of Scientific Instruments Vol. 37, No. 8, pp 999-1003, August 1966.

24. J. C. Sawyer and E. A. Steigerwald "Generation of Long Time Creep Data on Refractory Alloys at Elevated Temperature - Final Report - No ER-7203, TRW, Inc., Cleveland, Ohio, June 6, 1967.

25. R. W. Hall and R. H. Titran, "Creep Properties of Columbium Alloys in Very High Vacuum", NASA-Lewis Research Center Technical Reprint 15-63, Presented at Symposium on Application of Refractory Metals, Los Angeles, California.

26. R. W. Buckman, Jr., "Operation of Ultra High Vacuum Creep Testing Laboratory" Transactions Vacuum Metallurgy Conference, 1966, pp 25-37.

27. H. Inouye, "The Contamination of Refractory Metals in Vacua Below 10^{-6} Torr", ORNL, Presented at Symposium on Application of Refractory Metals, Los Angeles, California (December 9-10, 1963).

28. T. K. Roche, "The Effect of Degree of Vacuum on the Slow Bend Creep Behavior of Columbium-0.6% Zirconium at 1832°F", ORNL, Presented at Symposium on Application of Refractory Metals, Los Angeles, California (December 9-10, 1963).

29. Anon: "Space Power Systems Advanced Technology Conference" Lewis Research Center, August 23-24, 1966 - NASA SP-131, pp 169-199.

30. J. R. DiStefano and E. E. Hoffman "Corrosion Mechanism in Refractory Metal - Alkali Metal Systems" The Science and Technology of Tungsten, Tantalum, Molybdenum, Niobium and their Alloy. Based on AGARD Conference, Oslo University Center, Oslo-Blendern, Norway 23-26 June 1963 Pergamon Press, 1964, pages 257-285.

31. M. L. Pochon, et al, "The Solubility and Structure of Carbide Phases in Tantalum and Columbium", Vol. 2 Reactive Metals, Interscience Publications, pp 327-347.

32. H. R. Ogden, et al "The Solubility of Carbon in Tantalum, "Trans AIME, Vol. 227 p 1458-1460, Dec. 1963.

33. H. D. Seghezzi, "New Investigations of the Tantalum-Nitrogen System", 3rd Plansee Seminar, Reute, Austria, 1958.

34. P. Bunn and C. Wert "Solubility of Nitrogen in Tantalum" Trans. of Met. Soc. AIME, Vol. 230, June 1964, p. 937.

35. Schmidt, F. F., et al "Investigation of the Properties of Tantalum and its Alloys," Battelle Memorial Institute, WADD TR No. 59-13 (December 31, 1959).

36. L. Seigle, "Solid Solution Strengthening of Refractory Metals" AGARD Conference on Refractory Metals, Oslo University Centre, Oslo-Blindern, Norway, June 23-26, 1963.

37. F. F. Schmidt et al "Investigation of Tantalum and its Alloy" Technical Documentary Report No. ASD-TDR-62-544, Part II, May 1963.

38. R. T. Begley, et al "Precipitation Hardening Columbium-Hafnium Nitrogen Alloys" 5th Plansee Seminar, June 22-26, 1964, Reutte, Austria.

39. A. Kelley and R. B. Nicholson, "Precipitation Hardening", pp286-287, Progress in Materials Science, Vol. 10, No. 3, 1963.

40. W. H. Chang "A Study of the Influence of Heat Treatment on Microstructure and Properties of Refractory Alloys" ASD-TDR-62-211, Part III.

41. R. L. Ammon and D. L. Harrod "Strengthening Effects in Ta-W-Hf Alloys" AIME Symposium on the Physical Metallurgy of Refractory Metals, French Link, Indiana, Oct 3-5, 1965.

42. E. L. W. Perryman, "Recovery of Mechanical Properties", Creep and Recovery, ASM, Page 134.

43. R. H. Titran and R. W. Hall, "High Temperature Creep Behavior of a Columbium Alloy, FS-85" NASA-TND-2885, June, 1965.

44. R. H. Titran and R. W. Hall, "Ultra High Vacuum Creep Behavior of Columbium and Tantalum Alloys at 2000°F and 2200°F for Twines Greater than 1000 Hours" NASA-TND-3222.

45. J. W. Clark, "Recent Developments in Columbium Base Alloys" General Electric Co., Brochure, February 10, 1965.

46. J. W. Clark, E. J. Jones "U.S. Patent No. 3,243,290, Tantalum Base Alloy, March 29, 1966.

47. D. Hanson, "The Creep of Metals", Trans. AIME. Vol. 133, 1939, p. 15.

48. C. Crussard, "The Influence of Grain Size on Creep Rate", Comptes rendus, Vol. 219, 1944, p. 681.

49. P. Shahinian and J. R. Lane, "Influence of Grain Size on High Temperature Properties of Monel", Trans. ASM, Vol. 45, 1953.

50. D. Garafalo, "Fundamentals of Creep and Creep-Rupture in Metals", MacMillan Series in Materials Science, 1965.

51. P. Feltham and J. D. Meakin, Acta Met, 7, 614, 1959.

52. J. McKeown, J. Inst. Metals, 60, 201, 1937.

53. R. T. Begley and J. Cornie, and R. C. Goodspeed, "Development of Columbium Base Alloys" Final Technical Report, AFML-TR-67-116, November 1967, pp 122-132.

54. R. Resnick and L. S. Castleman, Trans. AIME, p 218, 307, 1960.

55. J. Weertman, "Theory of Steady State Creep Based on Dislocation Climb" J. of Appl. Physics. Vol. 26, No. 10, p 1213, 1955.

56. J. E. Dorn "A Survey of Recent Results on Experimental Determinations of Activation Energies for Creep" Presented at Fourth Sugamore Ordnance Materials Research Conference, Racquette Lake, New York, Aug 21-23, 1957.

57. E. Rudy and H. Nowotny, "Untersuchen in System Hafnium-Tantal-Kohlenstoff", Mh Chem., 94, 1963, p. 507.

58. D. Turnbull, "Grain Boundary and Surface Diffusion" ATOM Movements - ASM, 1951, pp 129-152.

59. J. E. Burke "The Migration of Grain Boundaries" ATOM Movements, ASM, 1951 pp 220-221.

60. D. R. Stoner, "Welding Behavior of Oxygen Contaminated Refractory Metal Alloys", Presented at AWS Spring Meeting, April 25, 1967, Detroit, Michigan (Report NASA-CR-72390).

61. D. Rowcliffe, et al, "Strengthening of Niobium-Zirconium Alloys by Internal Oxidation", Presented at Conference on Oxide Dispersion Strengthening, Bolton Landing, New York, June 27-29, 1966.

62. R. L. Fleischer and W. R. Hibbard, Jr., "Solution Hardening", p. 261, The Relation Between the Structure and Mechanical Properties of Metals, Vol. 1, Symposium No. 15, London, Her Majesty's Stationery Office.

TABLE 1-1. 1-3/4 LBS. NON-CONSUMABLE ELECTRODE MELTED COMPOSITIONS

HEAT No.	W a/o	W w/o	Mo a/o	Mo w/o	Re a/o	Re w/o	Hf a/o	Hf w/o	Zr a/o	Zr w/o	C a/o	C w/o	N a/o	N w/o	W-Mo+Re -Zr+Hf a/o	W-Mo+Re -Zr+Hf w/o	(W-Mo-Re) (Hf+Zr) (atom ratio)	(C-N) (Hf+Zr) (atom ratio)
NAS-1	14.77	14.9	----	----	----	----	1.78	1.80	----	----	----	----	----	----	16	16.4	8	0
NAS-2	14.77	14.9	----	----	----	----	1.78	1.80	----	----	0.44	0.03	----	----	16	16.4	8	0.25
NAS-3	14.77	14.9	----	----	----	----	1.78	1.80	----	----	0.89	0.06	----	----	16	16.4	8	0.5
NAS-4	14.77	14.9	----	----	----	----	1.78	1.80	----	----	1.78	0.12	----	----	16	16.4	8	1.0
NAS-5	14.77	14.9	----	----	----	----	1.78	1.80	----	----	2.22	0.15	----	----	16	16.4	8	1.25
NAS-6	8.0	8.2	----	----	----	----	1.0	1.0	----	----	0.5	0.035	----	----	9	9.2	8	0.5
NAS-7	8.0	8.2	----	----	----	----	1.0	1.0	----	----	1.0	0.07	----	----	9	9.2	8	1.0
NAS-8	8.0	8.2	----	----	----	----	1.0	1.0	----	----	1.5	0.1	----	----	9	9.2	8	1.5
NAS-9	14.77	15.2	----	----	----	----	1.23	1.23	----	----	0.62	0.04	----	----	16	16.43	12	0.5
NAS-10	14.77	15.2	----	----	----	----	1.23	1.23	----	----	1.23	0.08	----	----	16	16.43	12	1.0
NAS-12	15.07	15.4	----	----	----	----	0.93	0.93	----	----	0.93	0.06	----	----	16	16.33	16	1.0
NAS-13	10.67	11.0	----	----	----	----	1.33	1.33	----	----	0.66	0.045	----	----	12	12.33	8	0.5
NAS-14	10.67	11.0	----	----	----	----	1.33	1.33	----	----	1.33	0.090	----	----	12	12.33	8	1.0
NAS-16	11.08	11.3	----	----	----	----	0.92	0.92	----	----	0.92	0.06	----	----	12	12.22	12	1.0
NAS-18	11.3	11.5	----	----	----	----	0.70	0.70	----	----	0.70	0.05	----	----	12	12.2	16	1.0
NAS-20	8.31	8.5	----	----	----	----	0.69	0.70	----	----	0.69	0.045	----	----	9	9.2	12	1.0
NAS-21	8.47	8.6	----	----	----	----	0.53	0.53	----	----	0.26	0.02	----	----	9	9.13	16	0.5
NAS-22	8.47	8.6	----	----	----	----	0.53	0.53	----	----	0.53	0.035	----	----	9	9.13	16	1.0
NAS-23	8.47	8.6	----	----	----	----	0.53	0.53	----	----	0.79	0.050	----	----	9	9.13	16	1.5
NAS-24	8.31	8.5	----	----	----	----	0.69	0.70	----	----	1.14	0.07	----	----	9	9.2	12	1.5
NAS-25	11.08	11.3	----	----	----	----	0.92	0.92	----	----	1.38	0.09	----	----	12	12.22	12	1.5
NAS-26	15.07	15.4	----	----	----	----	0.93	0.93	----	----	1.39	0.095	----	----	16	16.33	16	1.5
NAS-27	4.5	4.6	----	----	----	----	1.5	1.5	----	----	0.75	0.05	----	----	6	6.1	3	0.5
NAS-28	4.5	4.6	----	----	----	----	1.5	1.5	----	----	1.50	0.10	----	----	6	6.1	3	1.0

TABLE 1-1. 1-3/4 LBS. NON-CONSUMABLE ELECTRODE MELTED COMPOSITIONS (CONTINUED)

HEAT No.	W a/o	W w/o	Mo a/o	Mo w/o	Re a/o	Re w/o	Hf a/o	Hf w/o	Zr a/o	Zr w/o	C a/o	C w/o	N a/o	N w/o	W+Mo+Re +Zr+Hf a/o	W+Mo+Re +Zr+Hf w/o	(W+Mo+Re) (Hf+Zr) (atom ratio)	(C+N) (Hf+Zr) (atom ratio)
NAS-29	4.5	4.6	----		----		1.5	1.5	----		2.25	0.15	----		6	6.1	3	1.5
NAS-30	4.0	4.1	----		----		2.0	2.0	----		1.0	0.067	----		6	6.1	2	0.5
NAS-31	4.0	4.1	----		----		2.0	2.0	----		2.0	0.134	----		6	6.1	2	1.0
NAS-32	3.0	3.1	----		----		3.0	3.0	----		1.5	0.10	----		6	6.1	1	0.5
NAS-33	3.0	3.1	----		----		3.0	3.0	----		3.0	0.204	----		6	6.1	1	1.0
NAS-34	6.8	7.0	1.7	0.85	0	--	0.25	0.25	0.25	0.13	0	---	0.5	0.04	9	8.23	16	1.0
NAS-35	6.8	7.0	1.7	0.85	0	--	0	--	0.50	0.26	0	--	0.25	0.02	9	8.35	16	0.5
NAS-36	5.6	5.7	1.4	0.7	1.5	1.56	0.25	0.25	0.25	0.13	0.25	0.017	0.25	0.02	9	8.34	16	1.0
NAS-37	5.6	5.7	1.4	0.7	1.5	1.56	0	--	0.50	0.26	0.125	0.008	0.125	0.01	9	8.22	16	0.5
NAS-38	7.0	7.1	0	--	1.5	1.56	0	--	0.50	0.26	0	--	0.25	0.02	9	8.92	16	0.5
NAS-39	7.0	7.1	0	--	1.5	1.56	0.25	0.25	0.25	0.13	0	--	0.50	0.04	9	9.04	16	1.0
NAS-40	8.5	8.7	0	--	0	--	0	--	0.50	0.26	0.125	0.008	0.125	0.01	9	8.96	16	0.5
NAS-41	8.5	8.7	0	--	0	--	0.25	0.25	0.25	0.13	0.25	0.017	0.25	0.02	9	9.08	16	1.0
NAS-42	5.2	5.3	1.3	0.65	1.5	1.56	0	--	1.0	0.52	0	--	1.0	0.08	9	8.03	8	1.0
NAS-43	5.2	5.3	1.3	0.65	1.5	1.56	0.5	0.5	0.5	0.26	0	--	0.5	0.04	9	8.27	8	0.5
NAS-44	6.4	6.5	1.6	0.8	0	--	0.5	0.5	0.5	0.26	0.25	0.017	0.25	0.02	9	8.06	8	0.5
NAS-45	6.4	6.5	1.6	0.8	0	--	0	--	1.0	0.52	0.50	0.034	0.50	0.04	9	7.82	8	1.0
NAS-46	6.5	6.6	0	--	1.5	1.56	0	--	1.0	0.52	0.50	0.034	0.50	0.04	9	8.68	8	1.0
NAS-47	6.5	6.6	0	--	1.5	1.56	0.5	0.5	0.5	0.26	0.25	0.017	0.25	0.02	9	8.92	8	0.5
NAS-48	8.0	8.1	0	--	0	--	0.5	0.5	0.5	0.26	0	--	0.50	0.04	9	8.68	8	0.5
NAS-49	8.0	8.1	0	--	0	--	0	--	1.0	0.52	0	--	1.0	0.08	9	8.62	8	1.0
NAS-56	7.9	8.0	----		1.0	1.0	0.7	0.7	----		0.45	0.025	----		9.6	9.7	12.7	0.64
NAS-57	7.9	8.0	----		1.0	1.0	0.7	0.7	----		0.45	0.025	----		9.6	9.7	12.7	0.64

TABLE I-2. TWO INCH DIAMETER INGOT - CONSUMABLE ELECTRODE MELTED COMPOSITIONS

HEAT NO.	W a/o	W w/o	Mo a/o	Mo w/o	Re a/o	Re w/o	Hf a/o	Hf w/o	Zr a/o	Zr w/o	C a/o	C w/o	N a/o	N w/o	W+Mo+Re +Zr+Hf a/o	W+Mo+Re +Zr+Hf w/o	(W+Mo+Re) (Hf+Zr) (atom ratio)	(C+N) (Hf+Zr) (atom ratio)
NASV-1	7.8	8.0	----		----		2.0	2.0	----		----		----		9.8	10	3.9	0
NASV-2	7.8	8.0	----		----		2.0	2.0	----		0.8	0.05	----		9.8	10	3.9	0.4
NASV-3	7.8	8.0	----		----		3.5	3.5	----		1.5	0.10	----		11.3	11.5	2.2	0.4
NASV-4	7.8	8.0	----		----		2.7	2.7	0.8	0.47	0.8	0.05	----		11.2	11.1	2.2	0.2
NASV-5	9.4	9.6	----		----		3.2	3.2	----		0.8	0.05	----		12.6	12.8	2.9	0.3
NASV-6	9.3	9.6	----		----		3.9	3.9	----		1.5	0.10	----		13.2	13.5	2.4	0.4
NASV-7	5.6	5.7	1.3	0.70	1.5	1.56	0.25	0.25	0.25	0.13	0.21	0.015	0.19	0.015	8.9	8.34	17	0.8
NASV-8	5.6	5.7	1.3	0.70	1.5	1.56	0.75	0.75	0.25	0.13	0.21	0.015	0.19	0.015	9.4	8.84	8.4	0.4
NASV-9	8.8	9.0	----		----		1.0	1.0	----		0.45	0.030	----		9.8	10.0	8.8	0.45
NASV-10	7.0	7.1	----		1.5	1.56	0.25	0.25	0.25	0.13	----		0.39	0.03	9.0	9.0	17	0.8
NASV-11	8.8	9.0	----		1.45	1.5	1.0	1.0	----		0.21	0.015	0.19	0.015	11.25	11.5	10	0.4
NASV-12	7.4	7.5	----		1.45	1.5	0.5	0.5	----		0.21	0.015	0.19	0.015	9.35	9.5	18	0.8
NASV-13	6.4	6.5	----		2.44	2.5	0.3	0.3	----		0.15	0.010	0.13	0.010	9.14	9.3	29	0.9
NASV-14	3.9	4.0	1.9	1.0	1.95	2.0	----		0.6	0.3	0.21	0.015	0.19	0.015	8.35	7.3	13	0.7
NASV-15	8.9	9.0	----		1.45	1.5	1.0	1.0	----		----		0.77	0.06	11.35	11.5	10	0.8
NASV-16	9.4	9.5	----		0.5	0.5	----		0.5	0.25	0.30	0.02	0.13	0.01	10.40	10.25	20	0.9
NASV-17	3.9	4.0	----		2.9	3.0	0.75	0.75	----		0.15	0.01	0.26	0.02	7.55	7.75	9	0.5
NASV-18	4.9	5.0	----		1.0	1.0	----		0.06	0.03	----		0.52	0.04	6.50	6.3	10	0.9
NASV-19	8.4	8.5	----		1.45	1.5	1.0	1.0	----		----		----		10.85	11.0	10	--
NASV-21	9.9	10.0	----		1.0	1.0	0.5	0.5	----		----		----		11.40	11.5	22	--

TABLE 1-3. CHEMICAL ANALYSIS 1-3/4 LBS. NON-CONSUMABLE ELECTRODE MELTED INGOTS

Heat Number (Composition, w/o)	Analysis, Weight Percent													
	As-Cast			As-Cast + 1 Hr. at 2300°C			As-Rolled 0.040 Inch Sheet							
	C	O	N	C	O	N	W	Mo	Re	Hf	Zr	C	O	N
NAS-2 (Ta-14.6W-1.8Hf-0.03C)	0.031	--	--	--	--	--	--	--	--	--	--	--	--	--
NAS-5 (Ta-14.6W-1.8Hf-0.15C)	0.0135	--	--	--	--	--	--	--	--	--	--	--	--	--
NAS-6 (Ta-8.2W-1.0Hf-0.035C)	--	--	--	--	--	--	8.0	--	--	1.00	--	0.032	0.0039	--
NAS-14 (Ta-11W-1.33Hf-0.09C)	0.073	--	--	--	--	--	--	--	--	--	--	--	--	
NAS-21 (Ta-8.6W-0.53Hf-0.02C)	--	--	--	--	--	--	8.2	--	--	0.51	--	0.021	--	--
NAS-27 (Ta-4.6W-1.5Hf-0.05C)	--	--	--	--	--	--	4.4	--	--	1.60	--	0.027	0.0017	--
NAS-28 (Ta-4.6W-1.5Hf-0.1C)	--	--	--	--	--	--	4 4	--	--	1.56	--	0.10	--	--
NAS-34 (Ta-7W-0.85Mo-0.25Hf-0.13Zr -0.04N	--	--	0.034	--	--	0.018	--	--	--	--	--	--	--	--
NAS-35 (Ta-7W-0.8Mo-0.26Zr-0.02N)	--	--	0.022	--	--	0.013	7.1	0.83	--	--	0.24	--	--	--
NAS-36 (Ta-5.7W-1.56Re-0.7Mo-0.25Hf -0.13Zr-0.017C-0.02N	0.016	--	0.017	0.013	--	0.012	5.6	0.65	1.65	--	0.24	0.0096	0.0024	0.015
NAS-37 (Ta-5.7W-1.56Re-0.7Mo-0.26Zr -0.008C-0.01N)	--	--	--	0.0066	--	0.012	--	--	--	--	--	--	--	--
NAS-38 (Ta-7.1W-1.56Re-0.26Zr-0.02N)	--	--	--	--	0.0018	0.012	7.0	--	1.60	--	0.23	0.0023	--	0.016
NAS-39 (Ta-7.1W-1.56Re-0.25Hf-0.13Zr -0.04N)	--	--	0.032	--	0.0053	0.015	--	--	--	--	--	--	--	0.031
NAS-40 (Ta-9.7W-0.26W-0.008C-0.01N)	0.010	--	0.010	--	--	--	8.4	--	--	--	0.24	0.0086	0.0029	0.010
NAS-42 (Ta-5.3W-1.56Re-0 65Mo-0.52Zr -0.08N)	--	--	0.079	--	0.0026	0.026	--	--	--	--	--	--	--	0.049
NAS-44 (Ta-6.5W-0.8Mo-0.5Hf-0.26Zr -0.17C-0.02N)	--	--	--	--	--	--	6.2	0.68	--	0.54	0.25	0.018	0.0024	0 018

TABLE 1-4. CHEMICAL ANALYSIS, TWO INCH DIAMETER DOUBLE VACUUM ARC MELTED INGOT

Heat Number, (Composition)	Ingot Position	Analysis (Weight Percent) W	Mo	Re	Hf	Zr	C	O	N
NASV-1 (Ta-8W-2Hf)(T-111)	Top	7.3	--	--	1.72	--	0.0016	0.0053	0.003
	Bottom	7.5	--	--	1.87	--	--	0.0050	0.002
NASV-2 (Ta-8W-2Hf-0.05C)	Top	7.7	--	--	1.74	--	0.054	--	0.002
	Bottom	7.8	--	--	1.83	--	0.051	--	0.002
NASV-3 (Ta-8W-3.5Hf-0.10C)	Top	7.6	--	--	3.35	--	0.098	0.0095	0.002
	Bottom	7.4	--	--	2.98	--	0.095	0.0089	0.003
NASV-4 (Ta-8W-2.7Hf-0.47Zr-0.05C)	Top	7.5	--	--	2.56	--	0.054	0.0038	0.003
	Bottom	7.3	--	--	2.59	--	0.048	0.0053	0.003
NASV-5 (Ta-9.6W-3.15Hf-0.05C)	Top	9.2	--	--	3.03	--	0.054	0.0032	0.003
	Bottom	8.6	--	--	2.69	--	0.049	0.0021	0.003
NASV-6 (Ta-9.6W-3.9Hf-0.10C)	Top	8.8	--	--	3.64	--	0.10	--	0.003
	Bottom	8.7	--	--	3.52	--	0.093	0.0059	0.003
NASV-7 (Ta-5.7W-0.7Mo-1.56Re-0.25Hf-0.13Zr-0.015C-0.015N)	Top	5.7	0.66	1.58	0.25	0.14	0.015	--	0.011
	Bottom	6.2	0.63	1.50	0.26	0.13	0.014	0.0057	0.012
NASV-8 (Ta-5.7W-0.7Mo-1.56Re-0.75Hf-0.13Zr-0.015C-0.015N)	Top	6.4	0.65	1.61	0.76	0.12	0.016	0.0043	0.013
	Bottom	6.2	0.65	1.58	0.80	0.12	0.016	0.0045	0.015
NASV-9 (Ta-9W-1Hf-0.03C)	Top	8.9	--	--	0.95	--	0.025	0.0024	0.002
	Bottom	9.0	--	--	1.00	--	0.025	0.0032	0.001
NASV-10 (Ta-7.1W-1.56 Re-0.025Hf--0.013Zr-03N	Bottom	7.3	--	1.63	0.28	0.12	0.0029	0.002	0.024
NASV-11 (Ta-9W-1.5Re-1Hf-0.015C-0.015N	Bottom	9.7	--	1.62	0.92	--	0.016	0.006	0.013
NASV-12(Ta-7.5W-1.5Re-0.5Hf-0.015C-0.015N	Bottom	7.9	--	1.52	0.5	--	0.019	--	0.011
NASV-13(Ta-6.5W-25Re-0.3Hf-0.01C-0.01N)	Bottom	6.3	--	2.57	0.3	--	0.011	--	0.012
NASV-14(Ta-4W-1Mo-2Re-0.3Zr-0.015C 0.015N	Bottom	4.0	1.01	2.05	--	0.3	0.016	--	0.013
NASV-16(Ta-9.5W-0.5Re-0.25Zr-0.026-0-01N)	Bottom	9.8	--	0.46	--	0.26	--	--	--
NASV-17(Ta-4W-3Re-0.75Hf-0.016-0.02N	Bottom	4.4	--	2.74	0.71				
NASV-18(Ta-5W-1Re-0.3Zr-0.04N)	Top	4.9	--	1.09	--	0.25	--	--	0.025
NASV-19(Ta-8.5W-1.5Re-1Hf	Bottom	8.8	--	1.42	0.97	--	0.0013	--	0.0005
NASV-21(Ta-10W-1Re-0.5Hf)	Bottom	10.0	--	1.03	0.57	--	0.0007	-	0.0003

APPENDIX II

PROCEDURE FOR APPLYING Al-12Si ALLOY COATING

Billet to be coated should be clean, free of oil, dirt, and scale or oxide. Use container large enough to permit complete immersion of billet being coated. Melt Al-12Si alloy in clay graphite container. Maintain temperature of bath at 1750°F ± 50°F. Just prior to immersion of billet, cover surface of Al-12Si alloy melt with 1/4" (min-thick) layer of flux (composition in weight percent).

46% KCl
35% NaCl
6% AlF_3
13% $NaAlF_3$

CAUTION - Provide adequate ventillation - Fluoride fumes released from flux when heated.

As soon as continuous layer of molten flux is formed slowly immerse billet through flux into bath until billet is completely immersed. Soak billet in bath for 20 minutes, then remove.

Table III-1

Summary of One Hour Recrystallization Results on 0.06 Inch Sheet, Ta-W-Hf-C Alloys

Composition	Prior Reduction Percent	DPH and Microstructure After 1 Hour at Temperature, °F								
		As Rolled	2190	2370	2550	2730	2910	3090	3270	3630
Ta-8W-2Hf (T-111)	85	337 W	283 RB	---	213 R	211 R	214 R	206 R	206 R	200 R
Ta-8W-2Hf-0.05C	85	375 W	334 W	---	262 R	276 R	271 R	269 R	266 R	278 R
Ta-8W-3.5Hf-0.1C	85	388 W	332 W	---	296 W	---	295 R	---	302 R	308 R
Ta-8W-2.7Hf-0.4Zr-0.05C	85	405 W	345 W	---	268 R	296 R	307 R	292 R	290 R	297 R
Ta-9.6W-3.2Hf-0.05C	85	423 W	362 W	---	281 RP	292 R	322 R	---	316 R	307 R
8.2W-1.0Hf-0.035C	76	357 W	328 W	280 W	237 RB	255 RP	250 R	247 R	252 R	249 R
8.2W-1.0Hf-0.070C	75	371 W	343 W	301 W	239 RB	249 RP	257 RP	249 R	249 R	256 R
8.2W-1.0Hf-0.100C	77	390 W	344 W	305 W	243 RB	256 RP	243 RP	260 R	252 R	260 R
8.5W-0.7Hf-0.045C	76	363 W	323 W	292 RP	232 R	250 R	248 R	239 R	248 R	247 R
8.5W-0.7Hf-0.070C	74	375 W	305 W	265 R	230 R	237 R	247 R	242 R	249 R	253 R

Table III-1 (Continued)

Composition	Prior Reduction Percent	DPH and Microstructure After 1 Hour at Temperature, °F								
		As Rolled	2190	2370	2550	2730	2910	3090	3270	3630
8.6W-0.53Hf-0.020C	73	337 W	306 W	259 RP	226 R	240 R	239 R	246 R	243 R	249 R
8.6W-0.53Hf-0.035C	76	352 W	323 W	247 RB	232 R	240 R	238 R	236 R	244 R	243 R
8.6W-0.53Hf-0.050C	71	347 W	318 W	255 RB	223 R	228 R	237 R	237 R	240 R	241 R
11.3W-0.92Hf-0.06C	72	431 W	356 W	---	272 RP	---	300 R	---	295 R	290 R
4.6W-1.5Hf-0.05C	72	296 W	222 RB	---	186 R	---	196 R	198 R	213 R	209 R
4.6W-1.5Hf-0.10C	68	314 W	210 RB	---	197 R	---	196 R	208 R	211 R	211 R
4.6W-1.5Hf-0.15C	68	324 W	214 RB	---	205 R	---	199 R	205 R	208 R	219 R
4.1W-2.0Hf-0.067C	75	311 W	203 RB	---	192 R	---	194 R	200 R	204 R	209 R
4.1W-2.0Hf-0.134C	68	318 W	214 RB	---	203 R	---	205 R	207 R	208 R	218 R

Table III-1 (Continued)

Composition	Prior Reduction Percent	DPH and Microstructure After 1 Hour at Temperature, °F								
		As Rolled	2190	2370	2550	2730	2910	3090	3270	3630
3.1W-3.0Hf-0.102C	74	310 W	241 W	---	194 R	---	196 R	196 R	203 R	214 R
3.1W-3.0Hf-0.204C	72	329 W	250 W	---	209 R	---	206 R	207 R	210 R	217 R

Remarks:
- W - Wrought
- RB - Formation of equiaxed grains<50%
- RP - Formation of equiaxed grains >50%
- R - Formation of equiaxed grains 98%
- S - Single Phase

APPENDIX IV

OPTICAL AND ELECTRON MICROSCOPE METALLOGRAPHIC PROCEDURES

A. METALLOGRAPHIC PREPARATION OF TANTALUM BASE ALLOYS CONTAINING CARBIDES

The standard method of metallographically preparing tantalum base alloys containing carbides for light and electron microscopy consists of mechanical polishing and etching, per the following:

Mechanical Polishing: In mechanical polishing the specimen shall be ground in the usual manner on 240, 400, and 600 grit silicon carbide papers. The scratches from the last paper shall then be removed by polishing with 30, 15 and 6 micron diamond abrasives for short times on a hard-finish cloth (i.e., unbleached muslin, Premier suede drill cloth, etc.). The mechanical polish shall be continued with very light pressure on a short-pile cloth (i.e., Buehler Microcloth) charged with a thick slurry of Linde B alumina abrasive and water. Finally, the specimen shall be acid polished, by addition of a 2 to 4% chromic acid solution to the polishing cloth, while still charged with the Linde B abrasive.

Etching: The specimen shall be etched in a solution consisting of 1 part of concentrated nitric acid, 1 part of 48% hydrofluoric acid, and 2 parts of glycerine. The etching time shall be kept to a minimum required to fully reveal the microstructure.

B. METALLOGRAPHIC PREPARATION OF TANTALUM BASE ALLOYS CONTAINING NITRIDES

The standard method of metallographically preparing specimens of tantalum base alloys containing nitrides for light and electron microscopy shall consist of mechanical polishing and cathodic vacuum etching, per the following:

Mechanical Polishing: In mechanical polishing the specimen shall be ground in the usual manner on 240, 400, and 600 grit silicon carbide papers. The scratches from the last paper shall then be removed by polishing with 30, 15 and 6 micron diamond abrasives for short times on a hard-finish cloth (i.e., unbleached muslin, Premier suede drill cloth, etc.). The mechanical polish shall be completed with very light pressure on a short-pile cloth (i.e., Buehler Microcloth) charged with a thick slurry of Linde alumina abrasive and water.

Cathodic Vacuum Etching: The specimen shall then be cathodic vacuum etched, using 1500 volts at a pressure of 300 microns of argon. The etching shall be done in 30 second intervals, each interval followed by a 30 to 60 second cooling period, until the microstructure is fully revealed. The total etching time will vary from specimen to specimen, but should be within the range of 3 to 10 minutes.

Alloys containing both carbon and nitrogen were prepared by the procedure developed for carbide containing alloys.

C. ELECTRON MICROSCOPE PROCEDURES

1. Surface Replicas - Surface replicas were obtained using the standard two-stage carbon technique. These replicas were shadowed with chromium to provide the required contrast.

2. Chemical Extraction and Examination of Dispersed Second Phases - The bulk extracted residue was obtained by dissolving the matrix of the sample in a solution which consists of 10 grams tartaric acid-10 ml bromine-90 ml methanol. Platinum wire was wrapped around the sample being dissolved to catalyze the reaction. The resulting residue was then carefully washed with methanol and dried in vacuo. Identification of the phases comprising the residues was made by x-ray analysis, using the standard Debye-Scherrer technique. A semi-quantitative analysis of the metallic components of the compound(s) was obtained utilizing X-ray fluorescence. A Siemens Crystalloflex IV x-ray diffraction unit was used for the x-ray diffraction and fluorescence analysis.

The residue was also studied by electron microscopy. This was accomplished by ultrasonically dispersing the residue in amyl acetate which was then flooded on a clean glass slide and allowed to dry in air. Replicas containing the extracted and dispersed particles were then made by the two-stage carbon replica process. Transmission electron microscopy and selected area electron diffraction of the phased dispersed on these replicas, referred to as dispersed phase replicas, were used to better define their size, shape, and structure than can be done on bulk specimens. Aluminum, deposited on part of each replica, was used as a standard for calibrating diffraction patterns.

3. Preparation of Thin Foils for Transmission - Thin foils were prepared and studied by transmission electron microscopy. The thinning procedure consisted of mechanical thinning of specimens to a thickness of 3 to 5 mils by grinding on silicon carbide papers. The specimens were then electro-polished between two stainless steel cathodes in a continuously stirred electrolyte of 85% H_2SO_4 and 15% Hf, which was maintained at room temperature. A current density of 25 ma/cm^2 resulted in optimum polishing. All electron microscopy was done using a JEM 6-A electron microscope equipped with a tilting and rotating stage. Accelerating voltages of 80 KV and 100 KV were used for surface replicas and transmission electron microscopy (including dispersed phase replicas as well as thin foils) respectively.